AFIT/GNE/ENP/01M-06

Assessment of the Effects of Entrainment and Wind Shear on Nuclear Cloud Rise Modeling

Thesis

Presented to the Faculty of the Graduate School of Engineering and Management

of the Air Force Institute of Technology

Air University

Air Education and Training Command

In Partial Fulfillment of the Requirements for the

Degree of Master of Science

Daniel E. Zalewski, B.S., M.S.

Major, USA

March 2001

The views expressed in this thesis are those of the author and do not reflect the official policy or position of the United States Air Force, Department of Defense, or the U.S. Government.

AFIT/GNE/ENP/01M-06

Assessment of the Effects of Entrainment and Wind Shear on Nuclear Cloud Rise Modeling

Daniel E. Zalewski
Major, USA

Approved:

Vincent J. Jodoin (Chairman)	date
Michael P. Susalla (Member)	date
Jim Petrosky (Member)	date

Acknowledgments

I would like to give recognition to all those who assisted me in the preparation of my thesis. I thank the Lord, for his grace and for walking with me every step of the way. To my wife and family their support and understanding allowed me to dedicate much of my time and efforts to my work. To my advisor, Major Vince Jodoin, who kept me focused and provided expertise throughout the process. To Commander Susalla and LTC Petrosky, who provided support both as committee members and technical advisors. Finally, to my classmates; Will, Tim, Rich, Tom, and Fred, their contributions can only be realized by those who endure the process.

Daniel E. Zalewski

Table of Contents

Page

List of Figures

Page

Page

Page

List of Tables

Page

Page

List of Symbols

C_p = specific heat of gas at constant pressure $\left(\text{J}/\text{kg K}\right)$

$\bar{C}_p$ = average specific heat $\left(\text{J}/\text{kg K}\right)$

E_k = turbulent kinetic energy per unit mass $\left(\text{J}/\text{kg}\right)$

H_c = vertical radius (m)

k_3, k_6 = dimensionless empirical constants

L = latent heat of vaporization of water or ice $\left(\text{J}/\text{kg}\right)$

m = mass of the cloud (kg)

N = number of shots compared

P = pressure $\left(\text{Pa}\right)$

R_a = gas constant of air $\left(287\ \text{J}/\text{kg K}\right)$

R_c = horizontal radius (m)

s = dry condensed mass in cloud per dry air mass

S = surface area of the spherical cloud (m^2)

t = time (s)

T = temperature $\left(\text{K}\right)$

T^* = virtual temperature $\left(\text{K}\right)$

T_e^* = virtual ambient temperature $\left(\text{K}\right)$

u = velocity of the cloud $\left(\text{m}/\text{s}\right)$

$\text{v} = \sqrt{u^2 + 2E_k}$ = characteristic velocity of the cloud $\left(\text{m}/\text{s}\right)$

V = volume of the spherical cloud (m^3)

w = liquid and solid water mass per unit dry air mass

W = yield (kilotons)

x = mixing ratio (water vapor mass per unit dry air mass)

z = cloud center height (m)

z_{rel}^{calc} = calculated relative cloud top height (m)

z_{rel}^{obs} = observed relative cloud top height (m)

$\beta' = \dfrac{1+x}{1+x+s+w}$ = ratio of cloud gas density to total density of cloud

ε = turbulent kinetic energy dissipation rate per unit mass $\left(\frac{\text{J}}{\text{kg s}}\right)$

$\gamma = \dfrac{C_p}{C_v}$ is the specific heat ratio

μ = entrainment parameter

ρ = density of the cloud $\left(\frac{\text{kg}}{\text{m}^3}\right)$

ρ_e = ambient air density $\left(\frac{\text{kg}}{\text{m}^3}\right)$

ξ = ratio of molecular weights of water and air $\frac{18}{29}$

Abstract

Accurate modeling of nuclear cloud rise is critical in hazard prediction following a nuclear detonation. This thesis recommends improvements to the model currently used by DOD. It considers a single-term versus a three-term entrainment equation, the value of the entrainment and eddy viscous drag parameters, as well as the effect of wind shear in the cloud rise following a nuclear detonation. It examines departures from the 1979 version of the Department of Defense Land Fallout Interpretive Code (DELFIC) with the current code used in the Hazard Prediction and Assessment Capability (HPAC) code version 3.2.

The recommendation for a single-term entrainment equation, with constant value parameters, without wind shear corrections, and without cloud oscillations is based on both a statistical analysis using 67 U.S. nuclear atmospheric test shots and the physical representation of the modeling. The statistical analysis optimized the parameter values of interest for four cases: the three-term entrainment equation with wind shear and without wind shear as well as the single-term entrainment equation with and without wind shear. The thesis then examines the effect of cloud oscillations as a significant departure in the code. Modifications to user input atmospheric tables are identified as a potential problem in the calculation of stabilized cloud dimensions in HPAC.

Assessment of the Effects of Entrainment and Wind Shear on Nuclear Cloud Rise Modeling

I - Introduction

A. Motivation

With the end of nuclear weapons testing, an increase in nuclear weapons states, and concern for collateral effects of precision weapons, the need for the most accurate nuclear weapons effects tool becomes more pronounced. In order to provide an accurate model of fallout after a nuclear detonation, we must first have a model that accurately predicts the cloud dimensions at stabilization. This stabilized cloud can then be handed off to a transport model that predicts the fallout pattern on the ground or in the air at designated points of time.

The development of an accurate model to predict the stabilized cloud is the motivation behind this research. The Department of Defense Land Fallout Interpretive Code (DELFIC) is the model currently in use and is based on both physics and empirical results. DELFIC has been the model to which other codes have been compared and is currently an option for computing cloud rise in the Hazard Prediction and Assessment Capability (HPAC) program maintained by the Defense Threat Reduction Agency. An attempt to limit uncertainty in both the modeled results and modeling of physical laws will be the focus of this research.

It will help to first gain a very basic understanding of what occurs during a nuclear detonation and the principles associated with the rise of the nuclear cloud.

B. Background

The detonation of a nuclear weapon results in the formation of a fireball due to ionization of the atmosphere and debris. The fireball starts to rise and expand. As the fireball rises, cooler air is entrained and heated. If the fireball touches the ground, soil and surface debris are also entrained and distributed throughout the volume through turbulent mixing. The point in time at which the pressure in the fireball reaches equilibrium with the ambient atmosphere will be the initial condition for the modeling of the nuclear cloud rise. The cloud will continue to rise buoyantly, cooling through entrainment and radiation. Radiative cooling and the drag of the air through which the cloud is rising cause the cloud to take on a toroidal shape with interior violent circulatory motion. This circulatory motion entrains more ambient air through the bottom of the cloud contributing to the dissipation of its energy. As the cloud rises, potential energy within the cloud is transferred to kinetic energy and turbulence, which affects cloud height. Depending upon the yield and atmospheric conditions at the time of detonation, the cloud may overshoot the point of neutral buoyancy and at some point begin to fall. Neutral buoyancy is defined as the point where the downward force on a parcel of air equals the upward force. In relation to densities, once the density of the cloud is in equilibrium with the density of the surrounding air, the parcel will reach neutral buoyancy. This overshooting and falling can result in the cloud oscillating before reaching neutral buoyancy. Once the cloud meets the termination criteria of the cloud rise module, the distribution of the radioactivity in the stabilized cloud is handed off to the transport model to track fallout. It will be important to clearly define what the termination criteria are and what is meant by the stabilized cloud or more specifically the

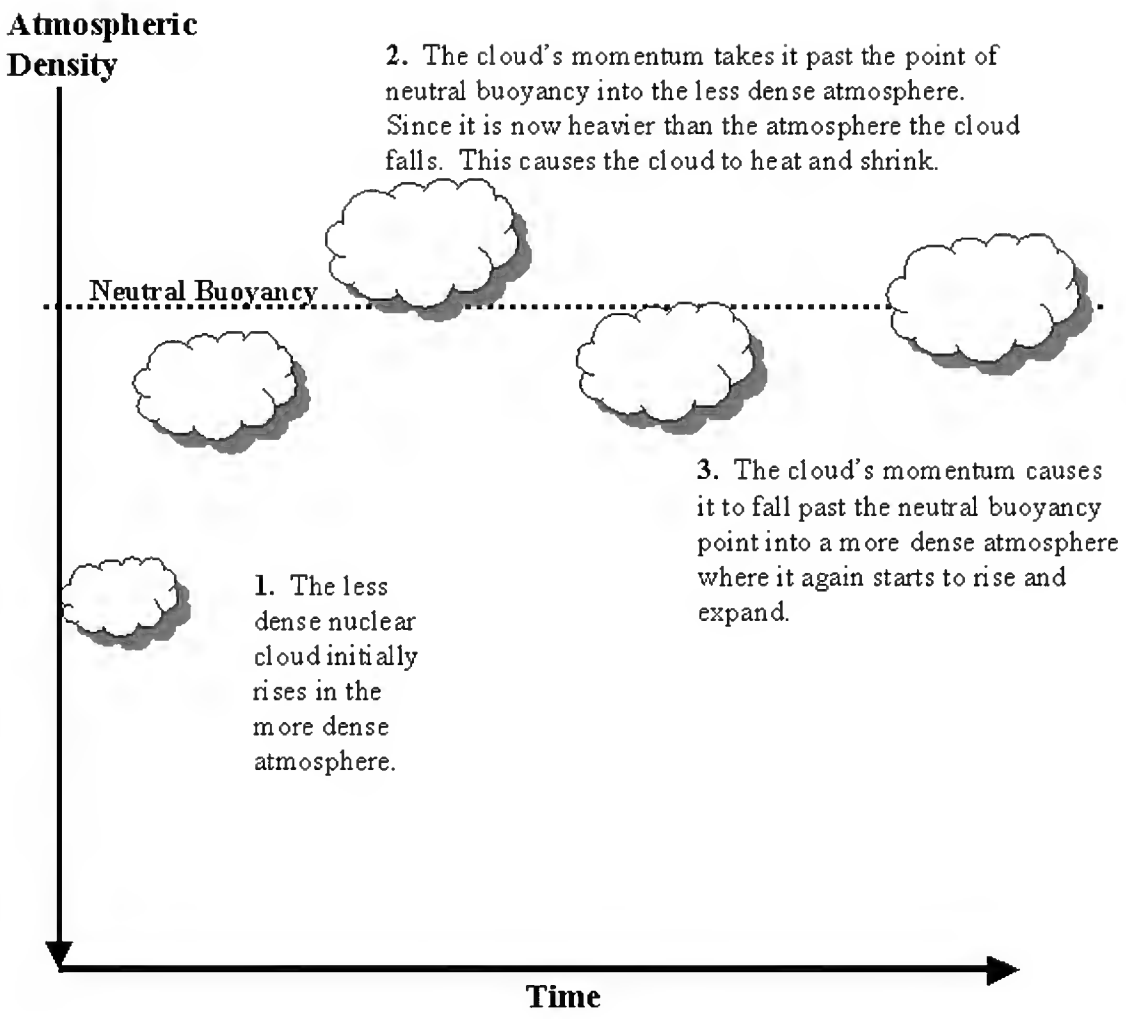

Figure 1. Cloud oscillation

stabilized cloud dimensions. This will be clearly defined in Chapter II.

Some of the early codes to predict atomic cloud rise were empirical in nature. Codes such as NEWFALL and the K Division Nuclear Fallout Code (KDFOC3) developed empirical equations that would predict the height of the cloud top based on measured data from various nuclear detonations or simulations. These empirical equations would then be used to predict cloud dimensions for future detonations. The most significant limitation in these models was the absence of effects from the atmospheric conditions. Atmospheric conditions play a role in reducing the mean

temperature of the fireball by producing an expansion of the atomic cloud as it rises, providing cooler air to entrain into the atomic cloud, and determining the rate at which the atmosphere reduces its buoyancy. (1:14) These conditions in turn affect the rise of the atomic cloud. This atmospheric affect varies from shot to shot based on different conditions in temperature, pressure and humidity. In particular, the presence of inversions in the atmosphere will have a significant impact on the cloud as it rises in the atmosphere. An atmospheric inversion can be defined as a warming of the ambient air with increasing altitude.

Huebsch developed the first model that accounted for these conditions and attempted to model the cloud using conservation laws in 1964, for water-surface-bursts. He defined the water-surface burst as "a nuclear explosion centered so close to the water surface that the fireball intersects the air-water interface, and the nuclear cloud initially contains both air and vaporized water." (6:1) His model included a combination of theory and empirical parameters. A strictly theoretical model would be computationally intensive. This model was later modified for use in land surface bursts and became the computational model for DELFIC. This is now one of three methods currently available in HPAC for computing cloud rise. The other two are NEWFALL and KDFOC3. Both provide an empirical fit without regard to atmospheric conditions; however, KDFOC3 is specifically designed for surface, near surface, and subsurface bursts.

In order to appreciate the development of these models, a more complete review of the literature is in order.

C. Review of the Literature

In 1945, G.I. Taylor first published his work on the *Dynamics of a Mass of Hot Gas Rising in Air*. Taylor equates the rising mass of hot gas to that of a bubble rising in water. He indicated that the rise was dependent upon the drag coefficient of the rising bubble, which was approximately 0.7 for a bubble in water, and entrainment. He represents the rate of entrainment by αu, where α is the entrainment parameter, which he took to be 0.2, and u is the speed of the rising bubble.

O.G. Sutton then published his work in 1947 on *The Atomic Bomb Trail as an Experiment in Convection*, where he presented a theory on the rise of the atomic cloud that was based on his diffusion theory between the cloud and the environment. This was also the first theory that incorporated meteorological principles in predicting cloud height. In 1950, Lester Machta published *Entrainment and the Maximum Height of an Atomic Cloud* that offered a different approach to Sutton's theory by considering entrainment of the environment as oppose to diffusion.

In 1955, the Armed Forces Special Weapons Project published *Operation Teapot, an Atomic Cloud Growth Study*. This study would collect complete and accurate cloud data and then correlate this data with yield, height of burst, and meteorological information to derive empirical relations for the evaluation of an atomic cloud.

In 1964, I.O. Huebsch published *The Development of a Water-Surface-Burst Fallout Model: The Rise and Expansion of the Atomic Cloud*. This was the first development of an analytic model coupled with empirical parameters to represent the atomic cloud rise history. The model would predict physical characteristics and cloud dimensions as a function of time given the explosion energy, the height of burst, and

atmospheric conditions as a function of altitude. Huebsch modified his model in 1965 to expand the capabilities to a land surface burst in his publication, *Development of a Land Surface Burst Cloud Rise Model*. His final modification to the model came in 1966, when he published *Turbulence, Toroidal Circulation and Dispersion of Fallout Particles from the Rising Nuclear Cloud*. The combination of this research allowed Huebsch to publish *The Department of Defense Land Fallout Prediction System. Volume III. Cloud Rise*, in 1967. This was the initial development of DELFIC.

In 1970, H.G. Norment published *The Department of Defense Land Fallout Prediction System. Volume III. Cloud Rise. Revised*. Some of Norment's more significant changes included removing particle growth capability and the development of the three-term entrainment equation. The latter of these changes is one of the focuses of this thesis.

Huebsch conducted a validation study on the revised model in 1975. Huebsch showed that the revised equations actually violated the conservation of energy. He made several additional suggestions to include returning to a single-term entrainment equation.

In 1977, Norment published his *Validation and Refinement of the DELFIC Cloud Rise Module*. Although Norment fixed the equations to no longer violate the conservation of energy, he elected to keep the three-term entrainment equation arguing a better representation of the physics and observed cloud data. He published his final revisions in 1979 in *DELFIC: Department of Defense Fallout Prediction System. Volume I – Fundamentals*.

Since then, research and validation studies have been done to improve the physics and results of DELFIC. Of concern are: the *Critique of DELFIC's Cloud Rise Model* by Jodoin in 1993, where several errors were identified in the development of the cloud rise

equations, the *Nuclear Cloud Rise and Growth Dissertation* by Jodoin in 1994, which considered the yield dependent representation of the entrainment and eddy viscous drag parameters, as well as the particle rise dynamics in the cloud, and the *Performance Evaluation of the Nuclear Weapon (NWPN) Source Model for the Hazard Prediction and Assessment Capability (HPAC) Code* by Lamarche in 1999, which evaluated the performance of DELFIC against DOD's new code HPAC.

Continuing with the validation efforts, a closer look is needed at the incorporation of DELFIC's cloud rise capabilities into the expanded hazard prediction capabilities of HPAC, to ensure that neither the physics nor accuracy of the results have been lost. Also, more consideration is given to the one-term versus three-term entrainment equation. While Jodoin showed better performance with a single-term entrainment equation using constant entrainment and eddy viscous drag parameter values, he did not investigate the performance of constant parameter values with the three-term equation. The significance of wind shear is another focus of this thesis, specifically, the impact on the parameter values, the impact on final cloud top height calculations, and its physical representation in the model.

D. Problem

This research examines the mass entrainment equation, wind shear effects, and the modification of two physical parameters used in the cloud rise model in an attempt to provide the best fit of calculated stabilized cloud dimensions to measured data.

In Huebsch's development of the water-surface-burst model he proposed a single term mass entrainment equation that represents the cloud as a bubble rising in water. In 1970, Norment refined the equation in the *Department of Defense Land Fallout*

Prediction System. Volume III. Cloud Rise. Revised, using the ideal gas law and came up with a three-term mass entrainment equation that he directly related to the equation of Huebsch. Although Norment claims to have shown the validity of his revision to the mass entrainment equation, there is skepticism to the validity of the additional terms, which will be explored in more detail in Chapter II, and to whether it more accurately models and ultimately predicts the cloud dimensions. Some of the uncertainty lies in assumed parameters used in the development of the additional terms.

In 1969, Huebsch published his work on the effects wind shear has on the rising atomic cloud in *Wind Shear, Turbulence and Interface Criteria for Nuclear-Explosion Cloud, Debris and Fallout Models*. (10) He relates the effects of wind shear to an increase in mass entrainment and an increase in the final cloud diameter. He then takes a cursory look at the affect on cloud height and whether it is significant.

Two parameters identified as having a large impact on the stabilized cloud dimensions are the entrainment parameter that is part of the mass equation and the eddy viscous drag parameter that appears in the momentum and turbulent kinetic energy density equations. Currently both parameters are calculated as functions of yield, however, research by Huebsch and later by Jodoin has shown that both parameters could be held as constant with a value in the range of 0.07 to 0.34. (6:14) This range of uncertainty is a result of the unique conditions associated with an atomic cloud, such as, the temperature and rise velocity of the cloud. It is also dependent on the theory used to model the cloud rise. Cloud rise has been modeled using plumes, jets, and thermals, each having their own characteristics.

E. Assumptions and Limitations

Although my research was primarily concerned with the entrainment and eddy viscous drag parameters, several parameters are used throughout the cloud rise module (CRM). The turbulent kinetic energy density equation contains a dimensionless constant to match observed data. The wind shear equation contains a dimensionless parameter, taken to be unity, that can be used to modify the affect wind shear has on the rising cloud. The cloud shape parameter affects the eccentricity of the oblate spheroid. This parameter has undergone changes over the years and currently a shape factor of 0.66 is used which corresponds to an eccentricity of 0.75. The fraction of yield used to heat the cloud is another dimensionless parameter used to partition the yield. McGahan has indicated some variation may be necessary in this parameter due to the affects of solar heating. It has been proposed that solar heating may influence the clouds with a low albedo, or very dark clouds, that may result from surface bursts. McGahan admits that the calculations are crude and for the cases he tested there was not a consistent improvement in calculated cloud top heights. (2:3) There are also a number of physical parameters, such as the constant for gravity, specific heats, and densities to name just a few. While some of these parameters are well known, others are merely best guesses based on observations and testing. For the purposes of this study, the two primary parameters of interest, entrainment and eddy viscous drag, will be varied. Once these two parameters are optimized to observed data, the wind shear parameter will be optimized as well.

This model is limited by its approximation of the cloud volume as a point. Atmospheric properties associated with the cloud are considered constant throughout the volume of the cloud. This clearly is an approximation since a cloud can achieve

dimensions of several kilometers with the final size largely dependent on yield. Higher yields tend to rise to a much greater altitude than lower yields, often reaching the tropopause. The inversion at the tropopause severely limits the rise and essentially fixes the vertical thickness of the cloud while the horizontal dimension continues to expand.

There is also uncertainty in the observed cloud dimensional data. Cloud top measurements were taken both from the air and from the ground. No standard method was used for all of the shots considered in this study. For measurements taken from the ground, depending on the shape of the cloud, the actual top may not have even been visible. An examination of observed cloud top heights for the test shots in a given operation may give some indication to the accuracy of the measurements. For the operations listed in Table 1 an assertion was made based on the recorded cloud top heights in DASA 1251 (16). An error of half the smallest increment is assumed, for example, in operation Teapot, observed cloud top heights to the nearest 100 feet are recorded, therefore an error of 50 feet is assumed.

Table 1. Observed cloud top error assumed from recorded values

Operation	Measured Increment (ft)	Error (ft)
Upshot-Knothole	100	± 50
Plumbbob	1000	± 500
Hardtack II	1000	± 500
Teapot	100	± 50
Castle	1000	± 500

Based on the large number of empirical fits and approximations, both in the development of the model and the measured data, there should be no expectation of developing a model which matches the observed data precisely, nor would that necessarily be meaningful. What is desired is a model that matches observed behavior

and reasonably predicts observed data. A comparison of plume dispersion models and environmental measurements concluded that model accuracy is limited to about a factor of two. At some point, incorporating more physically realistic complexity while adding more computing time adds little, if any, accuracy. (3:81)

F. General Approach

The first phase of this research was to determine which of the needed corrections were made in the 1979 version of DELFIC that is used in the current version of HPAC. This involved an analysis of the NEWTRANS component of HPAC to see if the corrections identified by Jodoin in the *Critique of DELFIC's Cloud Rise Module* (15) had been incorporated. In addition to determining what corrections had been implemented there was an investigation of all departures from the 1979 version of DELFIC when incorporating it into the current version of HPAC. This involved a comparison of the source code for both the 1979 version of DELFIC and the current source code for HPAC.

The next phase of research was to determine the best values or forms for the entrainment and eddy viscous drag parameters as they relate to nuclear cloud rise and to validate them in a comparison study using U.S. atmospheric nuclear test data. This comparison study not only encompassed an expanded number of test cases from the study conducted by Jodoin in 1994, but looked at both the three-term and single-term entrainment equation. An iterative routine was set up to vary the constant parameter values for entrainment and eddy viscous drag using both a single-term and three-term entrainment equation to determine the values which best predict observed stabilized cloud top heights in each case. The determination of the selected range of values will be

discussed in Chapter II of the thesis, as well as a complete discussion of the terms associated with the entrainment equation.

The final phase of this research will be the determination of the affect of eliminating wind shear in the cloud rise dynamics from the 1979 version of DELFIC when incorporating it into the current version of HPAC. Other departures from the 79 version of DELFIC examined during this phase, include, cloud oscillations and modified atmospheric files.

The final optimized parameter recommendations are based on a complete analysis of all phases of the research.

G. Sequence of Presentation

The next chapter will define the stabilized cloud. This will then define the dimensions to which all comparisons will be made. The chapter will then present the development of the entrainment equation to include how the equation is modified to include the affect of wind shear. The primary parameters of interest, that is, entrainment and eddy viscous drag, are introduced. Finally, the chapter will outline the figures of merit used in the data analysis.

The data analysis chapter considers four comparison cases to the 1979 corrected version of DELFIC, a three term entrainment equation with constant parameter values and wind shear, a three term entrainment equation with constant parameter values and no wind shear, a single-term entrainment equation with constant parameter values and wind shear, and a single-term entrainment equation with constant parameter values and no wind shear. The chapter then considers the affect of each modification from the 1979

corrected version of DELFIC to the current HPAC source code provided by the Defense Threat Reduction Agency. Particular attention is paid to the HPAC weather file.

The summary and conclusions chapter will first make a recommendation on the use of constant versus yield dependent parameters. Next, it considers the single versus the three-term entrainment equation, followed by a recommendation on whether a wind shear correction should be included in the calculations. Finally, the impacts of modifications to the code identified in the previous chapter are considered in making a recommendation on the final form of the entrainment equation.

II - Theory

It was pointed out in the review of the literature section that a lot of research has gone into the development of a cloud rise model that could not only accurately predict the cloud dimensions at the time of stabilization, but also have a physical basis. The one equation that has received the most attention and undergone the most modifications over the years is the mass entrainment equation.

This chapter will first present the criterion that defines the stabilized cloud, that is, it will define the conditions that must be met before the cloud is passed off to the transport model. Second, a close look at the development of the entrainment equation will be made, paying particular attention to the modifications presented by Norment in 1970 and then the validation study by Huebsch in 1975. Third, it will consider the affect wind shear has on the entrainment of the cloud and how this affect can be accounted for in our physical model. Chapter IV will examine the entrainment and eddy viscous drag parameters both from a historical and a physical perspective. This will be used to reinforce the position of whether the parameters should be constant over the entire range of yields or yield dependent. Finally, the figures of merit that will be used to conduct the follow on analysis will be defined.

A. Stabilized Cloud

Before any analysis can be conducted, it is important to have an understanding of what is meant by the stabilized cloud and the dimensions associated with the cloud at the time of stabilization. Glasstone states that the cloud is "stabilized" after about ten minutes when it reaches its maximum height. (4:32) The stabilized dimensions for a given yield are largely dependent upon the atmospheric conditions and the height of

burst. The mass of debris lifted up due to a land surface burst will limit the maximum cloud height.

For the purposes of this research the stabilized cloud is what is passed off to the transport model of DELFIC or HPAC. The termination criteria for DELFIC was modified slightly in Norment's 1979 validation to account for problems that were observed in low and high yield shots. (5, 16-17) The normal termination occurred when the following relation was satisfied.

$$\frac{|\Delta R_c|}{\Delta t} \leq \frac{R_c W^{0.014778}}{1153} \qquad (1)$$

where

R_c = Horizontal Radius (m)
t = Time (s)
W = Yield (kilotons)

This condition was referred to as the radius expansion rate or R-Rate switch. This termination occurs if the radius expansion rate falls below a threshold, which is defined as the difference between two consecutive cloud radii in the solution time step of the eight ordinary differential equations that are used to model the cloud rise.

Although this condition worked for most shots, problems arose with high and low yield shots. The problem with high yield shots was that they tend to oscillate slowly, which could cause the radial expansion rate to fall below the set limit. In order to correct this problem, an additional condition for termination was added that also required the rise velocity to be less than or equal to zero. For low yield shots a condition was added to terminate cloud rise when the turbulent kinetic energy density fell below a threshold defined by the following conditions.

$$\begin{cases} E_k < 10 & , W \le 0.0359Kt \\ E_k < 23 + 9\log_{10} W & , 0.0359Kt \le W \le 12{,}915Kt \\ E_k < 60 & , 12{,}915Kt \le W \end{cases} \quad (2)$$

where

E_k = turbulent kinetic energy per unit mass $\left(\text{J}/\text{kg}\right)$

It turns out that most of the low yield shots are terminated by the turbulent kinetic energy density condition, while the R-Rate switch terminates most of the high yield shots.

HPAC no longer has a condition to terminate when the rise velocity becomes less than or equal to zero. The calculated rise velocity is allowed to go negative which may occur due to the oscillations as shown in Figure 1. After the detonation, the atmospheric pressure on the bottom of the cloud is larger than the pressure on top. The rise velocity becomes much greater than the expansion rate and the cloud overshoots into an area where the density of the ambient air is lower than the density of the cloud. When this occurs, the cloud will fall. The momentum of the cloud causes it to fall to a region where the ambient density is greater than the cloud density. The cloud then shrinks and heats bringing it back to the rise conditions. This action of rising and falling produces the oscillations before actually stabilizing. This oscillatory behavior was observed in high yield U.S. atmospheric tests.

B. Entrainment Equation

The development of the CRM from the initial theories presented by Taylor, Machta, and Sutton, to the model used in the current version of HPAC is best described by Norment.

> The DELFIC CRM is a dynamic, one-dimensional, entrainment bubble model of nuclear cloud rise. It consists of a set of coupled ordinary differential equations that represent conservation of momentum, mass, heat and turbulent kinetic energy. The nuclear cloud is defined in terms of: vertical coordinate of its center (the cloud is in some respects treated as a point), cloud volume, average temperature, average turbulent energy density, and the masses of its constituents: air, soil, weapon debris, water vapor and condensed water. Cloud properties and contents are taken to be uniform over the cloud volume.
>
> Initial conditions are specified at approximately the time the fireball reaches pressure equilibrium with the atmosphere. Atmospheric conditions (vertical profiles of pressure, temperature and relative humidity) are accepted by the CRM in tabular form. (5:8)

Although I will not present a detailed derivation of all the equations used in the model, it is important for this research that a connection be made to the impact of the entrainment and eddy viscous drag parameters on the equations, the development of Norment's three-term entrainment equation and how it relates to the equation first presented by Huebsch and later supported by Jodoin, and the development of the wind shear equation and how it impacts on the set of equations. The complete set of coupled ordinary differential equations, currently in use in DELFIC and HPAC, along with their derivation can be found in the *Department of Defense Land Fallout Prediction System, Volume III Cloud Rise Revised* by Norment. The same set of equations has been reproduced in Appendix A.

Huebsch's development of the mass entrainment equation was primarily based on the theory proposed by Taylor that states the rate of increase in cloud mass due to entrainment is given by

$$\frac{dm}{dt} = S\mu|u|\rho_e . \tag{3}$$

where

m = mass of the cloud (kg)

S = surface area of the spherical cloud (m^2)

μ = entrainment parameter

u = velocity of the cloud $\left(\frac{m}{s}\right)$

ρ_e = ambient air density $\left(\frac{kg}{m^3}\right)$

As stated by Huebsch, "Averaging over the surface of the cloud, the ambient air of density ρ_e flows onto or into the cloud at a rate proportional to the absolute value of the cloud rise by a factor of μ."(6:13) Huebsch's modification to this equation accounts for the fact that the nuclear cloud is about ten times as hot and only about one tenth as dense as ambient air. He therefore proposes that the entrainment rate is also proportional to the density ratio of the cloud and ambient air.

$$\frac{dm}{dt} = S\mu\frac{\rho}{\rho_e}|\mathrm{v}|\rho_e = \frac{S}{V}m\mu|\mathrm{v}| \tag{4}$$

where

ρ = density of the cloud $\left(\frac{kg}{m^3}\right)$

V = volume of the spherical cloud (m^3)

$\mathrm{v} = \sqrt{u^2 + 2E_k}$ = characteristic velocity of the cloud $\left(\frac{m}{s}\right)$

E_k = turbulent kinetic energy $\left(\frac{J}{kg}\right)$

From the definition of the characteristic velocity, v, and equation (4) we note that the cloud continues to entrain surrounding air even after it has stopped rising. This further entrainment is a direct result of the horizontal expansion where $u = 0$ and $\mathrm{v} = \sqrt{2E_k}$. By redefining the characteristic velocity to be

$$v = \max\left(|u|, \sqrt{2E_k}\right) \tag{5}$$

we can account for the turbulence-induced mixing during the later stages of cloud rise when the cloud slows down.(6:21)

In 1970, Norment expressed the mass via entrainment in terms of the cloud growth behavior that is obtained from observations of nuclear clouds, the temperature of the cloud and the pressure of the cloud. (7:13)

$$\left.\frac{dm}{dt}\right|_{ent} = \frac{\beta' m}{V}\frac{dV}{dt} - \frac{\beta' m}{T}\frac{dT}{dt} + \frac{\beta' m}{P}\frac{dP}{dt} \tag{6}$$

where

$\beta' = \dfrac{1+x}{1+x+s+w}$ = ratio of cloud gas density to total density of cloud

x = mixing ratio (water vapor mass per unit dry air mass)

s = dry condensed mass in cloud per unit dry air mass

w = liquid and solid water mass per unit dry air mass

V = volume of the cloud $\left(\mathrm{m}^3\right)$

P = pressure $\left(\mathrm{Pa}\right)$

T = temperature $\left(\mathrm{K}\right)$

This three-term equation was developed to more accurately represent the cloud rise, particularly at early times. The first term corresponds to the single-term entrainment equation presented by Huebsch. Norment explains that the third term, or pressure term is small at all times compared to the other two, so neglecting this term would have little affect. In considering the second term, "when $T >> T_e$, the temperature of the cloud is much greater than ambient temperature, the cooling rate is indeed drastically in error."(7:38) Clearly at early times when the cloud is around 3000 K this second term will have a significant affect.

Norment's development of the three-term entrainment equation is presented to provide relevance to each of the terms and to show the relationship to the equation proposed by Huebsch. The following development will assume an air burst in a dry air environment at low altitude; therefore the β' term can be neglected.

Equation (6) is derived from the equations that describe the rate of change of temperature and volume for an ideal gas, hot bubble rising through an ideal gas in a hydrostatic atmosphere.

$$\frac{1}{T}\frac{dT}{dt} = -\left(1 - \frac{\rho}{\rho_e}\right)\frac{1}{m}\frac{dm}{dt} + \frac{1}{P}\frac{dP}{dt}\frac{R_a}{C_p} \tag{7}$$

$$\frac{1}{V}\frac{dV}{dt} = \frac{1}{m}\frac{dm}{dt} + \frac{1}{T}\frac{dT}{dt} - \frac{1}{P}\frac{dP}{dt} \tag{8}$$

where

C_p = specific heat of gas at constant pressure $\left(\text{J}/\text{kg K}\right)$

R_a = gas constant of air $\left(287\ \text{J}/\text{kg K}\right)$

By solving equation (8) for $\frac{dm}{dt}$ we get the form of the entrainment equation (6).

$$\frac{dm}{dt} = \frac{m}{V}\frac{dV}{dt} - \frac{m}{T}\frac{dT}{dt} + \frac{m}{P}\frac{dP}{dt} = \rho\frac{dV}{dt} - \frac{m}{T}\frac{dT}{dt} + \frac{m}{P}\frac{dP}{dt} \tag{9}$$

Norment then assumes an oblate spheroid for the shape of the cloud, which is supported by observations, $V = \frac{4}{3}\pi R_c^2 H_c$, where R_c represents the horizontal radius and H_c represents the vertical radius. Differentiating V with respect to t and multiplying through by $\frac{1}{V}$ yields:

$$\frac{1}{V}\frac{dV}{dt}=\frac{1}{V}\frac{dV}{dR_c}\frac{dR_c}{dt}+\frac{1}{V}\frac{dV}{dH_c}\frac{dH_c}{dt}$$

$$\frac{1}{V}\frac{dV}{dt}=\frac{2}{R_c}\frac{dR_c}{dt}+\frac{1}{H_c}\frac{dH_c}{dt}. \tag{10}$$

Norment notes that from observed nuclear detonations, the following hold until the cloud rise velocity is less than or equal to zero.

$$R_c=\lambda\left(z-z_1\right) \tag{11}$$

$$z-z_1=kt^n, \text{ and} \tag{12}$$

$$H_c=\mu\left(z-z_2\right) \tag{13}$$

where

z = cloud center height (m)
$\lambda, \mu, z_1, z_2, k,$ and n = constants determined from cinefilms for particular shots

Combining equations (11) and (12) gives

$$R_c=\lambda kt^n. \tag{14}$$

Substituting equation (12) into equation (13) gives

$$H_c=\mu\left[\left(kt^n+z_1\right)-z_2\right]=\mu kt^n+\mu\left(z_1-z_2\right). \tag{15}$$

These equations for R_c and H_c can now be substituted back into equation (10).

$$\frac{1}{V}\frac{dV}{dt}=\frac{2n}{t}+\frac{nkt^{n-1}}{kt^n+z_1-z_2} \tag{16}$$

We now differentiate equation (12) to get a function of velocity.

$$\frac{d\left(z-z_1\right)}{dt}=\frac{d}{dt}kt^n=nkt^{n-1}=n\frac{kt^n}{t}=\frac{n\left(z-z_1\right)}{t}$$

$$u = \frac{n(z - z_1)}{t} \tag{17}$$

Next we solve the velocity equation for n and substitute it back into equation (16).

$$\frac{1}{V}\frac{dV}{dt} = \frac{u}{z - z_1}\left(2 + \frac{kt^n}{kt^n + z_1 - z_2}\right) \tag{18}$$

Substituting $z - z_1$ for kt^n, see equation (12), into equation (18) and multiplying through by V yields;

$$\frac{dV}{dt} = \frac{Vu}{z - z_1}\left(2 + \frac{1}{1 + \frac{z_1 - z_2}{z - z_1}}\right) \tag{19}$$

Equation (19) can now be substituted into equation (9) to get the basic three-term entrainment equation derived from equation (8) and observed behaviors of nuclear clouds.

$$\frac{dm}{dt} = \frac{\rho u V}{z - z_1}\left(2 + \frac{1}{1 + \frac{z_1 - z_2}{z - z_1}}\right) - \frac{m}{T}\frac{dT}{dt} + \frac{m}{P}\frac{dP}{dt} \tag{20}$$

Norment notes in a classified document, z_1 is frequently equal to z_2 and in virtually all cases $\left|\frac{z_1 - z_2}{z - z_1}\right| << 1$ and therefore can be neglected. (7:37) With this simplification and recalling our definitions for V and H_c, where we assume $z_1 \approx z_2$, we can see a direct relationship between the mass entrainment equation above and the one proposed by Huebsch, equation (4).

$$\frac{dm}{dt} = \frac{3\rho u\left(\frac{4}{3}\pi R_c^2 H_c\right)}{\frac{H_c}{\mu}} - \frac{m}{T}\frac{dT}{dt} + \frac{m}{P}\frac{dP}{dt}$$

$$\frac{dm}{dt} = \rho u \mu\left(4\pi R_c^2\right) - \frac{m}{T}\frac{dT}{dt} + \frac{m}{P}\frac{dP}{dt}$$

$$\frac{dm}{dt} = m\frac{S}{V}u\mu - \frac{m}{T}\frac{dT}{dt} + \frac{m}{P}\frac{dP}{dt} \tag{21}$$

Recall that the surface and volume terms in Huebsch's development follow directly from Taylor's, which assumed a spherical cloud. The temperature term of equation (21) can be obtained from equation (1.4D) or (1.4W) of Norment's *Cloud Rise Volume III Revised* and the pressure term can be evaluated using the hydrostatic law $\frac{dP}{dz} = -\rho_e g$ and $\frac{dz}{dt} = u$. (7:13) The final result is Norment's equations (1.7D) and (1.7W) (7:13-14) shown here as equation (22) and (23) respectively. The remaining steps in the derivation of equation (22) and (23) are included in Appendix B.

$$\left.\frac{dm}{dt}\right|_{ent} = \frac{\beta' m}{1 - \frac{\beta'}{T^*\bar{C}_p}\int_{T_e}^{T} C_{pa}(T)dT}\left\{\frac{S}{V}\mu v + \frac{\beta'}{T^*\bar{C}_p}\left[\frac{T^*}{T_e^*}gu - \varepsilon\right] - \frac{gu}{R_a T_e^*}\right\} \tag{22}$$

$$\left.\frac{dm}{dt}\right|_{ent} = \frac{\beta' m \bullet}{1 - \frac{1}{T^*}\left[\frac{\beta'}{1 + \frac{L^2 x\xi}{C_p R_a T^2}}\right]\left[T - T_e + \frac{L(x - x_e)}{C_p}\right]}\left\{\frac{S}{V}\mu v + \frac{\frac{\beta'}{T^*}}{\frac{L^2 x\varepsilon}{C_p R_a T^2}}\left[\frac{guT^*}{T_e^* C_p}\left(1 + \frac{Lx}{R_a T}\right) - \frac{\varepsilon}{C_p}\right] - \frac{gu}{R_a T_e^*}\right\} \tag{23}$$

where

T^* = virtual temperature (K)

T_e^* = virtual ambient temperature (K)

$\bar{C}_p$ = average specific heat $\left(\mathrm{J}/\mathrm{kg\ K}\right)$

L = latent heat of vaporization of water or ice depending on the conditions of the cloud $\left(\mathrm{J}/\mathrm{kg}\right)$

ξ = ratio of molecular weights of water and air $18/29$

$\varepsilon = \dfrac{k_3\left(2E_k\right)^{\frac{3}{2}}}{H_c}$ is turbulent kinetic energy dissipation rate per unit mass $\left(\mathrm{J}/\mathrm{kg\ s}\right)$

k_3 = constant

It is now clear that when the last two terms of equation (21) are neglected we are left with the same form as Huebsch's equation (4).

$$\frac{dm}{dt} = m\frac{S}{V}u\mu \tag{24}$$

A comparison with Huebsch's equation (4) identifies one more difference with equation (24), and that is with the characteristic velocity that Huebsch identified as $\mathrm{v} = \max\left(|u|, \sqrt{2E_k}\right)$. Norment concludes, "the use of turbulent kinetic energy density to control late cloud rise and growth is a major attraction of the Huebsch cloud rise model."(7: 39) He therefore includes the calculation for characteristic velocity in his equation, replacing the cloud rise velocity in equation (21) with Huebsch's definition of characteristic speed.

Given the validity of Norment's entrainment equation and the similarity to Huebsch's equation, what remains is an analysis of the significance of the two additional terms. In his discussion, Norment states that the contribution of the pressure term is

small at all times relative to the other two and therefore neglecting this term should not significantly influence the final results. This statement is supported by Huebsch's analysis of the test runs he did in 1975. (8:12) In contrast, the temperature does have a significant impact. During the early stages of cloud rise the temperature is between 3000 K and 4000 K. This large temperature difference between the cloud and the ambient temperature results in a "gross underestimation of the entrainment rate."(7:38-39) Further, the error produced by the underestimation in the entrainment rate produces an error in the cooling rate as evident by equation (7).

Although Norment's derivation may seem plausible on the surface, Huebsch points out several physical flaws in his 1975 analysis of the revised model. Huebsch returns to Norment's three-term equation for an air burst in a dry air environment at low altitude.

$$\frac{1}{m}\frac{dm}{dt} = \frac{T}{T_e}\left[\overbrace{\frac{S}{V}\mu v}^{1} - \overbrace{\frac{gu}{T_e}\left(\frac{1}{R_a\gamma}\right)}^{2} - \overbrace{\frac{\varepsilon}{TC_p}}^{3}\right] \tag{25}$$

where

$\gamma = \dfrac{C_p}{C_v}$ is the specific heat ratio

$R_a = C_p - C_v \left(\dfrac{\text{J}}{\text{kg K}}\right)$

Although this does not look exactly like Norment's equation 1.7D in his CRM-Revised (7:13) with some manipulation you can see that it is.

$$\frac{1}{m}\frac{dm}{dt} = \frac{\beta' T}{T_e}\left[\overbrace{\frac{S}{V}\mu v}^{1} - \overbrace{\frac{\beta'}{TC_p}\left(\frac{T}{T_e}gu - \varepsilon\right)}^{2} - \overbrace{\frac{gu}{R_a T_e}}^{3}\right]$$

Multiplying out term 2 and combining it with term 3 yields terms 2 and 3 of the equation Huebsch presents.

$$\frac{gu}{C_p T_e} - \frac{\varepsilon}{TC_p} - \frac{gu}{R_a T_e} = \frac{gu}{T_e}\left(\frac{1}{C_p} - \frac{1}{R_a}\right) - \frac{\varepsilon}{TC_p}$$

$$= -\frac{gu}{T_e}\left(\frac{1}{C_p / C_v\left(C_p - C_v\right)}\right) - \frac{\varepsilon}{TC_p} = \frac{gu}{T_e}\left(\frac{1}{R_a \gamma}\right) - \frac{\varepsilon}{TC_p}$$

Let's first consider the $\frac{T}{T_e}$ factor in equation (25). This term affects cloud mass early in the rise when there is a large difference between the cloud temperature and the ambient temperature. Calculation by Huebsch indicate an increase in the cloud mass by a factor of 6 to 8 in the first second of cloud rise for a 1 Kt detonation when the temperature drops from 2600 K to 800 K. (8, 12) This is compensated for by making the entrainment parameter an increasing function of yield.

$$\mu = 0.092W^{0.130} \tag{26}$$

The lower entrainment parameter for low yields also results in a lower entrainment rate later in the cloud history after the cloud has cooled to near ambient conditions and the $\frac{T}{T_e}$ term is close to unity. Therefore, there is an excessive entrainment of low altitude air, while there is an insufficient entrainment of high altitude air (8:12).

Consider a stable atmosphere that requires work to raise a parcel of air in the atmosphere. To raise a parcel adiabatically, that is along the adiabatic lapse rate, requires no work, so the potential temperature at some altitude z_1 and pressure p_1 in a stable atmosphere brought down adiabatically will be at the same potential temperature at altitude z_2 and pressure p_2. It will, however, be at a higher actual temperature. Potential

temperature is the temperature that a parcel of air at temperature T_1 and pressure p_1 would have if it were subject to an adiabatic expansion or compression that is brought

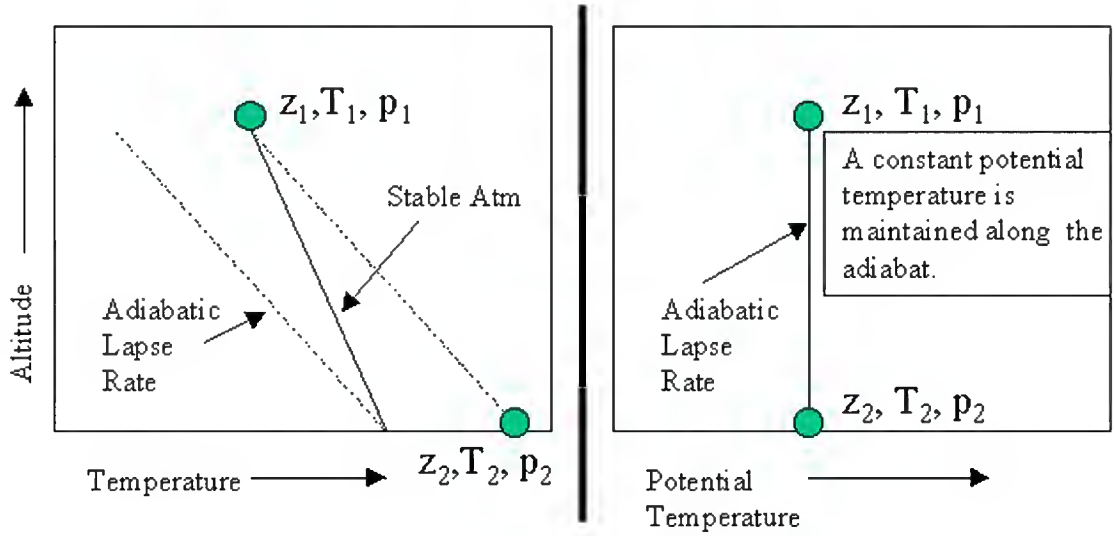

Figure 2. Parcel of air in a stable atmosphere

down along the adiabatic lapse rate line, to a pressure of 100 kPa or 1 atm. Therefore, as shown in Figure 2, a parcel of air rising or falling along the adiabatic lapse rate does not change its potential temperature. In the stable atmosphere, it takes work to raise the parcel and therefore energy is used. This work combined with the fact that the majority of the entrainment takes place at the lower altitudes results in a calculated height lower than that observed.

The second term of equation (25) is negligible for small yield shots, but becomes increasingly significant for higher yield shots. To see this we need only look at the velocity term that is a function of yield, the higher the yield, the higher the velocity and the more significant the contribution to the mass entrainment. Huebsch's calculations indicate that for a 1Mt shot term 2 is 40% of term 1, therefore decreasing term 1 by 40%. At 5Mt it increases to 65%, and between 20 and 25Mt it actually exceeds term 1

indicating a negative entrainment or decrease in mass. (8:12) Norment makes reference to the non-physical behavior of the model for high yield shots, which he claims to be greater than 15 megatons, in his 1977 validation. He attributes the loss in mass due to the significant decrease in the surface to volume ratio in equation (25) for very large clouds, which in turn affects the remainder of the coupled differential equations. (5:43-44) Norment considers this problem a "theoretical shortcoming" with the model but believes the model's validation must be based on matching observed data as well as the physics used to produce the results.

Norment reinforces his stand on the validity of the three-term entrainment equation in his validation report of 1977, and in fact, states that the Euclid Research Group led by Huebsch, substantiated his position by their energy transfer analysis that showed total energy balance when the virtual mass factor and shape factor were removed. (5:50-51) While the theoretical development of his equation was supported, he did acknowledge the problems associated with high yield tests that were also noted by the Euclid Research Group. Norment contributes these problems to the mathematical representation of the cloud volume as a point.

Jodoin points out another potential problem with Norment's derivation in his dissertation. "When Norment derived his version of the equation, he used some rigid empirical fits to the cloud's vertical thickness as a function of rise distance. He basically abandoned these empiricisms in his changes to the CRM's approach to cloud shape in 1977, but chose not to alter his entrainment equation."(9:33) This comment makes reference to Equations (11) and (13) which define the cloud's vertical and horizontal radii. In 1977, Norment abandoned these equations and fixed the cloud shape to be an

oblate spheroid with eccentricity of 0.75 but retained them in the development of his entrainment equation.

C. Wind Shear

Huebsch presented a modification to the entrainment model in 1969 with his work on wind shear. He elected to consider wind shear from an entrainment perspective rather than from the cloud shape perspective due to the irregularities that would be produced in the cloud shape. The "change in cloud shape is far too irregular to be represented by a mathematical model for the cloud form." (10:2-3)

There are two basic affects due to the presence of wind shear that may affect the final height of a cloud. First, the vertical wind shear will influence the vertical path of a rising cloud. Vertical wind shear corresponds to horizontal winds that influence the vertical cross section of the cloud. That is, instead of going straight up the cloud rises at an angle and thus over a longer path between the same vertical displacement points. This longer path causes more ambient, cooler air to be entrained in the rising cloud, and its buoyancy is exhausted sooner. Second, an increase in cloud height could occur in a conditionally unstable atmosphere. "In such an atmosphere an air element, displaced upward so far that it has cooled to the saturation point, is sufficiently warmed, by release of latent heat of condensation, to become lighter than the surrounding atmosphere. Thus entrainment can eventually increase the cloud buoyancy."(10:2-1 - 2-2) The first case is of more practical importance and will therefore drive the development of the changes in the cloud rise model.

Wind shear affects are yield dependent. Since high yield clouds rise faster, they are not exposed to the shear and increased dilution for as long. Also, "air entrainment

into the cloud tends to be proportional to cloud surface area, thus cloud dilution rate is proportional to cloud surface-to-volume ratio. This ratio decreases with increasing yield; thus the dilution, or mixing affect of shear is strongest for low yields."(10:2-2)

$$\text{dilution rate} \propto \frac{S}{V} = \frac{4\pi r^2}{\frac{4}{3}\pi r^3} = \frac{1}{3r}$$

The above expression shows how an increase in yield, which would produce an increase in the horizontal radius of the cloud, will increase the dilution rate to a lesser extent than a low yield detonation.

Huebsch proposes that the increase in entrainment due to wind shear is proportional to the product of "(1) the magnitude of the wind-velocity difference between the top and bottom of the cloud, and (2) the cloud vertical projected surface area, i.e. vertical cross-section."(10:2-3)

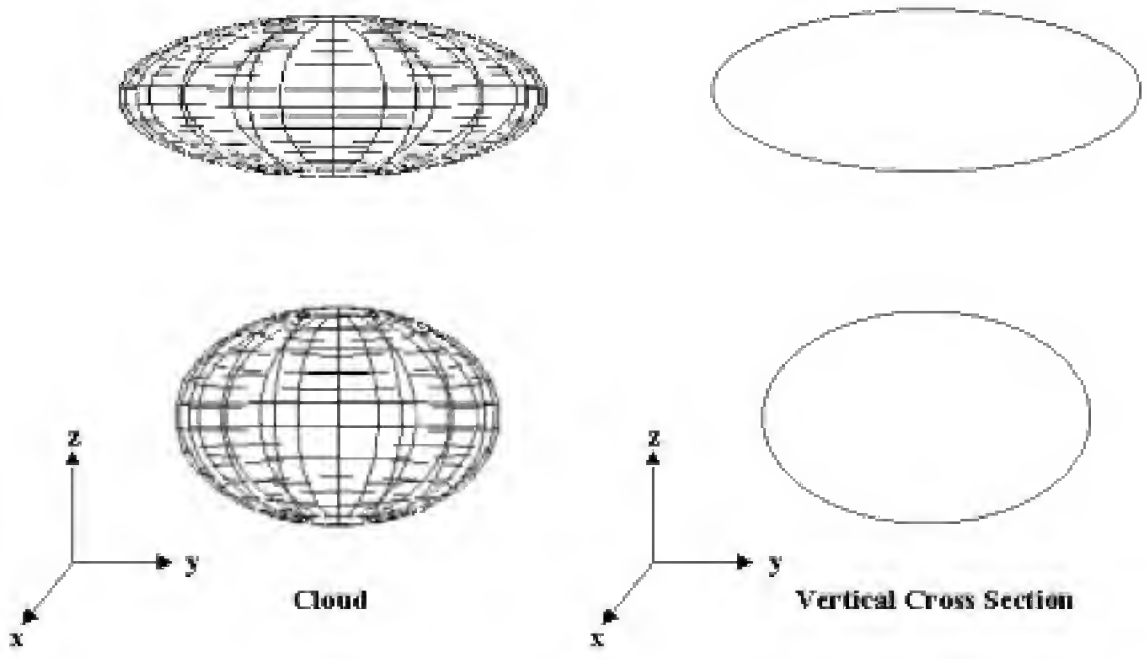

Figure 3. Vertical cross section of the rising cloud with initial eccentricity of 0.75 and a flattening due to lateral expansion later in the cloud rise history

The initial cloud is represented as an oblate spheroid of eccentricity 0.75 until it reaches apogee at which time the cloud expands laterally while maintaining its vertical dimensions. Also, we are using the vertical cross sections because as Figure 4 points out, the horizontal winds can only flow through the vertical projection of the surface to volume ratio, not the horizontal projection.

Therefore the development of the new wind shear term is as follows.

vertical cross-section area of a sphere of radius r is πr^2

vertical cross-section area of a spheroid of semi-axes a and b is πab

volume of a sphere of radius r is $\frac{4}{3}\pi r^3$

volume of a spheroid is $\frac{4}{3}\pi a^2 b$

surface to volume ratios are $\frac{3}{4r}$ and $\frac{3}{4a}$

Both of these terms will be written as $\frac{3}{4r}$, where r is the horizontal radius. Since the vertical cross-section has two faces, $2\times\frac{3}{4r}=\frac{3}{2r}=\frac{1.5}{r}$. The replacement rule then follows from this surface to volume relationship to increase the mass change due to entrainment.

$$\frac{S}{V}\mu v \rightarrow \mu(\frac{S}{V}v + k_6\frac{1.5}{R_c}v_s) \tag{27}$$

where

k_6 = dimensionless empirical constant

Here, v_s is the magnitude of the vector difference between the top and the bottom of the cloud.

$$v_s = \left|\vec{v}\left(z + H_c\right) - \vec{v}\left(z - H_c\right)\right| \tag{28}$$

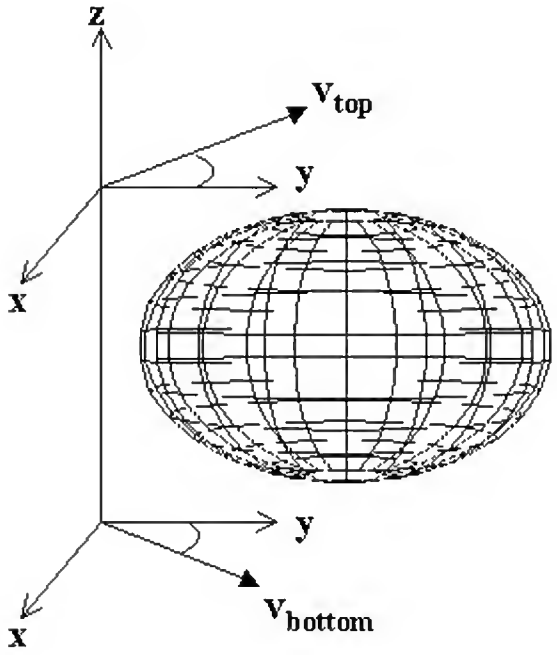

Figure 4. Vector representation of the horizontal winds

Huebsch's study showed that wind shear had a negligible affect on cloud height for the limited number of shots he tested, "within a few hundred meters."(10:2-8 – 2-9) More error can be attributed to round off and approximations in the model than associated with wind shear. There was, however, a substantial increase in the cloud radius when shear was taken into account. This increase will result in a broader fallout pattern from the transport model. Huebsch's study did not include a large number of test cases and he does indicate that a few hundred-meter affect could be significant given the sensitivity to changes in the atmosphere.

D. Parameter Study

As already mentioned in the limitations section, entrainment and eddy viscous drag are only two of many parameters used throughout the model. Validation studies have shown that computed results are largely dependent on these two values. (5:1)

Norment considers these two parameters of interest in his study and identifies the two equations that have been used to determine their value. He clearly indicates that the values of the parameters were chosen because of their ability to accurately predict observed data. Norment states, "extensive calculations have shown that it is not possible to adequately match calculated with observed results if single, yield independent values are used for these parameters."(5:40) He further defines the sensitivity associated with these two parameters. An increase in the k_2 parameter, which represents eddy viscous drag, will result in an overall decrease in the cloud top height due to the increase in conversion of rise energy to turbulent energy and an associated increase in turbulence drag. Similarly an increase in the entrainment parameter results in an overall decrease in cloud top height due to the increase in entrainment of air, which increases entrainment drag, reduces the cloud temperature, and increases turbulent energy density.

Both the sensitivity and best-fit values of the two parameters has been considered in several studies with varying results. Although much of the research suggests a constant value, as stated above, Norment proposed the yield dependent values that are currently modeled in both DELFIC and HPAC.

Taylor first selected a constant value of 0.2 for the entrainment parameter. In Huebsch's development of the *Water-Surface Burst Fallout Model* he states that empirical values of the entrainment parameter for nuclear and other clouds range from

0.07 to 0.34. These empirical results are primarily based on cumulus clouds and turbulent jets of approximately the same density. In 1970, Norment then proposed that the entrainment parameter was a function of yield and supports his claim based on extensive calculations using his parameterized fit to match observed data. In Jodoin's 1994 dissertation *Nuclear Cloud Rise and Growth*, he conducted a parametric study of 54 atmospheric tests that showed a best fit of 0.12 for the entrainment parameter using the single-term mass entrainment equation with wind shear proposed by Huebsch. Most recently, McGahan conducted a parameter study that determined the best-fit value to be between 0.08 and 0.09. (2:2-6) This study, although not documented in the draft, also used the single-term mass entrainment equation, but without wind shear. This value is in agreement with "the best current value of the entrainment constant for a bent over plume of 0.08" as stated in the Atmospheric Science and Power Production. (11:337) Although the cloud from an atomic detonation is considerably different from that of a fossil fuel plant rising from a stack, it is a good place to start. Additionally, the article also concludes that the plume rise from gas turbines, which are much hotter and have higher rise velocities, are consistent with the predictions for buoyant plumes. (11, 360) Interestingly, McGahan states that for high yield shots a value between 0.10 and 0.14 provided the best fit, which seems to indicate some agreement with Norment's proposal of a yield dependent fit. (2:20)

Not as much has been conjectured about the eddy viscous drag parameter. A purely viscous force would convert the loss in kinetic energy of the rise to heat; however, the eddy viscous force converts the loss in kinetic energy of rise to an increase in the turbulent kinetic energy of the cloud. This increase in turbulent kinetic energy will result

in further lateral expansion of the cloud once the rise velocity goes to zero as indicated by the characteristic velocity equation. Huebsch first proposes a value between 0.10 and 0.15. (6:39) Later in his analysis of the revised cloud rise model he suggests a value of 0.10 as providing good agreement but states that further research is required to determine an optimum value. Norment provides a yield dependent best fit for the calculation of the parameter, stating that there is no way to judge a priori what the value should be. (5:11) Jodoin's study supported the value of 0.10, as did the recent study by McGahan. Once again, McGahan further implies the possibility of yield dependence with the high yield shots suggesting a better fit using a value of 0.14.

E. Figures of Merit

The primary cloud dimension that will be used to determine the constant best-fit parameter values for entrainment and eddy viscous drag will be the observed and calculated cloud top height relative to the burst height. This is the same set of values used by Norment in his initial validation as well as Jodoin, Lamarche, and McGahan in their subsequent validations. The primary reason for using the cloud top values is that they are the values that have been consistently recorded for the multitude of tests that were conducted.

Two figures of merit are presented for determining the best-fit constant parameters. The first figure of merit is the fractional root mean square.

$$FRMS = \sqrt{\frac{\sum_{N}\left(\frac{z_{rel}^{obs} - z_{rel}^{calc}}{z_{rel}^{obs}}\right)^2}{N}} \tag{29}$$

The second figure of merit is the fractional mean deviation.

$$FMD = \frac{\sum_{N}\left(\frac{z_{rel}^{obs} - z_{rel}^{calc}}{z_{rel}^{obs}}\right)}{N} \tag{30}$$

where

z_{rel}^{obs} = observed relative cloud top height

z_{rel}^{calc} = calculated relative cloud top height

N = number of shots compared

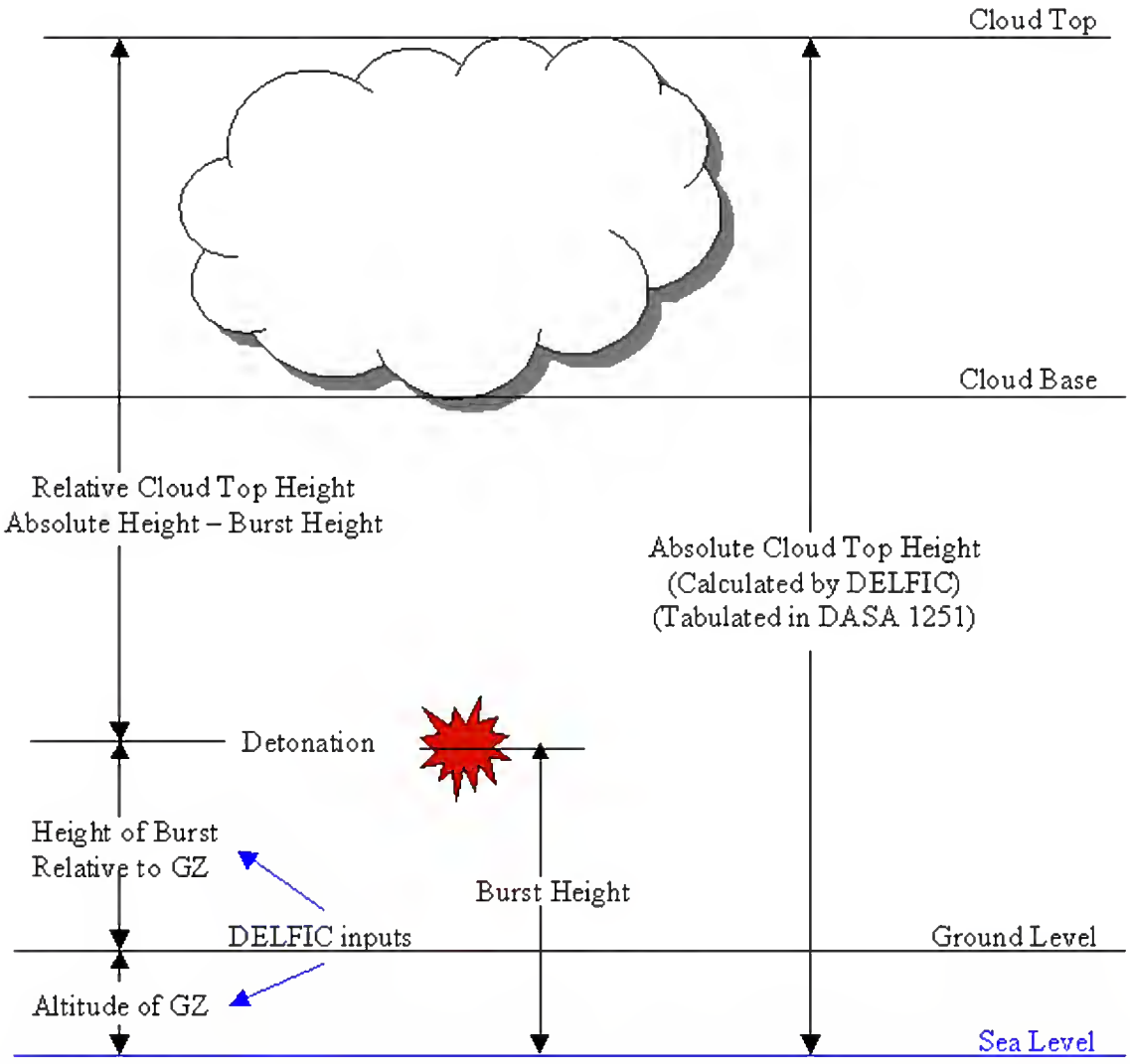

Figure 5. Relative Heights

Both the FRMS and FMD give some indication as to the accuracy of the parameters, however, the FMD will indicate whether the calculated cloud tops tend to under or over predict the observed values depending upon the sign of the result. These are also the figures of merit that were used by Norment during his validation study, (5:22) Jodoin during his subsequent validation (9:38-39), and McGahan. Using these same figures of merit will allow me to make correlations to the studies previously conducted.

III - Data Analysis

The analysis starts with a determination of the best constant values for the entrainment and eddy viscous drag parameters for four separate cases: a three-term entrainment equation with wind shear, a three-term entrainment equation without wind shear, a single-term entrainment equation with wind shear, and a single-term entrainment equation without wind shear. All four cases are based on the corrected version of the 1979 DELFIC Cloud Rise Module with the necessary modifications to the entrainment equation and the wind shear correction factor. Best constant values are based on the figures of merit discussed in Chapter II, Section E. A comparison is made to the yield dependent parameters for each case and in Chapter IV; a recommendation is made based on both the physical representation of the parameters and the ability to predict observed test data.

A closer look is taken at the time dependent significance of each term of the three-term entrainment equation. Several comparisons are made of varying yields. In Chapter IV a recommendation is made based on both the physical representation and ability to predict observed data for the single versus the three-term entrainment equation.

Next, a comparison is made of the effect wind shear has on the cloud top height. This comparison analyzes the differences between the observed and calculated cloud top height for the optimized parameters, and it considers the differences in the optimized parameter values given the single-term entrainment equation with wind shear and single-term entrainment equation without wind shear as well as the three-term entrainment equation with and without wind shear.

The inclusion of a DELFIC Cloud Rise Module option into the HPAC code has resulted in several departures from the 1979 DELFIC code. Many of the departures were in the restructuring of conditional loops and subroutines to take advantage of the new capabilities of FORTRAN and in streamlining the code. Changes of this nature, which do not affect the computations, are not investigated. A detailed listing of changes made can be found in Appendix D. What is investigated is any change that modified the way a variable or set of variables was computed, or conditional statements that deviate from the original DELFIC code. This comparison is made between the 1979 corrected version of DELFIC and the HPAC source code that deals with the cloud rise. These two codes have been modified to produce equivalent results so that individual departures in the code can be analyzed in detail. Table 2 identifies the modifications made to both codes to produce the results.

Each of the modifications is looked at in turn to determine the time dependent impact on cloud rise velocity, top height, temperature, turbulent kinetic energy, total mass, soil ratio, water ratio, and vapor ratio. The atmospheric tables produced by each of the programs are compared to show absolute differences between temperature, pressure, relative humidity, and density as functions of altitude.

A. Parameter Analysis

The following analysis determined the best values for the entrainment and eddy viscous drag parameters based on the empirical data of 64 U.S. atmospheric test shots. Four cases are considered, all with content entrainment and eddy viscous drag parameters. Table 3 identifies the four comparison cases, while Table 4 identifies the U.S. atmospheric test shots.

Table 2. Code Modifications

Modification	DELFIC Modification	HPAC Modification
Particle settling during cloud rise	The ndstr variable, which identifies the number of entries in the particle size class table, is set to zero in the icm subroutine.	The ndstr variable is never read in during the input reading.
Condition to terminate cloud rise at 10 minutes	DELFIC does not terminate the cloud rise based on a time condition so no modification was necessary.	The termination condition that was part of the dcsn subroutine to terminate the cloud rise at 10 minutes was eliminated.
Wind shear corrections	The rs variable, which is the product of the surface to volume ratio and the characteristic velocity, in the deriv subroutine has been modified to eliminate the wind shear correction.	HPAC does not allow for wind shear corrections, so no modifications were necessary.
Cloud oscillation	DELFIC does not allow for cloud oscillation so no modification was necessary.	The cxpn, rkgill, and deriv subroutines were modified to mimic the former structure of DELFIC, which did not permit oscillation.
Expanded atmospheric tables	Although no modifications were made, the calculated atmospheric tables will be compared due to slightly different interpolation routines.	Although no modifications were made, the calculated atmospheric tables will be compared due to slightly different interpolation routines.

Table 3. Comparison Cases

Case	Description
Case 1	1979 Corrected DELFIC with a three-term entrainment equation and wind shear corrections.
Case 2	1979 Corrected DELFIC with a three-term entrainment equation and no wind shear corrections.
Case 3	1979 Corrected DELFIC with a single-term entrainment equation and wind shear corrections.
Case 4	1979 Corrected DELFIC with a single-term entrainment equation and no wind shear corrections.

Based on the best values for each of the cases, the fractional deviation was calculated for each shot and the FRMS and FMD for the complete set of shots. These values were then compared to the values calculated by Norment and Jodoin in their respective analyses.

Table 4. U.S. Atmospheric Test Shots

Reference #	Shot Name	Operation	Yield (kt)	HOB (m)[1]	Type[2]
1	Humboldt	Hardtack II	0.0078	8	T
2	Catron	Hardtack II	0.021	2	T
3	Vesta	Hardtack II	0.024	0	S
4	Dona Ana	Hardtack II	0.037	137	B
5	Hidalgo	Hardtack II	0.077	115	B
6	Quay	Hardtack II	0.079	31	T
7	Eddy	Hardtack II	0.083	152	B
8	Rio Arriba	Hardtack II	0.09	22	T
9	Wrangell	Hardtack II	0.115	457	B
10	Franklin	Plumbbob	0.14	91	T
11	Wheeler	Plumbbob	0.197	152	B
12	Ray	Upshot-Knothole	0.2	31	T
13	Ruth	Upshot-Knothole	0.2	93	T
14	Johnnie Boy	Sunbeam	0.5	-1	C
15	Laplace	Plumbbob	1	229	B
16	Wasp	Teapot	1	232	A
17	Santa Fe	Hardtack II	1.3	457	B
18	Lea	Hardtack II	1.4	457	B
19	John	Plumbbob	2	6096	R
20	Mora	Hardtack II	2	457	B
21	Moth	Teapot	2	91	T
22	Post	Teapot	2	91	T
23	Debaca	Hardtack II	2.2	457	B
24	Ha	Teapot	3	9931	A
25	Wasp Prime	Teapot	3	225	A
26	Hornet	Teapot	4	91	T
27	Franklin Prime	Plumbbob	4.7	229	B
28	Sanford	Hardtack II	4.9	457	B
29	Socorro	Hardtack II	6	442	B
30	Tesla	Teapot	7	91	T
31	Bee	Teapot	8	152	T
32	Morgan	Plumbbob	8	152	B

[1] HOB is the height of the detonation above ground zero.
[2] A - Air drop, B – Balloon, C – Crater, R – Rocket, S - Surface, T - Tower

Reference #	Shot Name	Operation	Yield (kt)	HOB (m)[1]	Type[2]
33	Owens	Plumbbob	9.7	152	B
34	Kepler	Plumbbob	10	152	T
35	Wilson	Plumbbob	10	152	B
36	Fizeau	Plumbbob	11	152	T
37	Galileo	Plumbbob	11	152	T
38	Doppler	Plumbbob	11	457	B
39	Dixie	Upshot-Knothole	11	1836	A
40	Boltzman	Plumbbob	12	152	T
41	Newton	Plumbbob	12	457	B
42	Charleston	Plumbbob	12	457	B
43	Apple1	Teapot	14	152	T
44	Grable	Upshot-Knothole	15	160	A
45	Annie	Upshot-Knothole	16	91	T
46	Shasta	Plumbbob	17	152	T
47	Diablo	Plumbbob	17	152	T
48	Whitney	Plumbbob	19	152	T
49	Stokes	Plumbbob	19	457	B
50	Met	Teapot	22	122	T
51	Badger	Upshot-Knothole	23	91	T
52	Nancy	Upshot-Knothole	24	91	T
53	Encore	Upshot-Knothole	27	739	A
54	Zuchini	Teapot	28	152	T
55	Apple2	Teapot	29	152	T
56	Harry	Upshot-Knothole	32	91	T
57	Priscilla	Plumbbob	37	213	B
58	Lacrosse	Redwing	40	5	S
59	Simon	Upshot-Knothole	43	91	T
60	Turk	Teapot	43	152	T
61	Smokey	Plumbbob	44	213	T
62	Climax	Upshot-Knothole	61	407	A
63	Hood	Plumbbob	74	457	B
64	Koon	Castle	110	4	S

To determine the best parameter values, an iterative routine was set up to run through the 64 U.S. atmospheric test shots in Table 4, varying the entrainment parameter between 0.05 and 0.30 and the eddy viscous drag parameter between 0.08 and 0.20. These ranges encompass all of the proposed values encountered throughout the literature. The FRMS and FMD were calculated for each pair of parameters over the series of shots

and the lowest FRMS value was determined. The FRMS was used as the primary figure of merit in determining the best-fit value since it sums the absolute error between the observed and calculated values for all shots regardless of whether the error was an over or under prediction. The best-fit values are summarized below.

Table 5. Best fit parameter values for entrainment and eddy viscous drag

Case	Entrainment Parameter	Eddy Viscous Drag Parameter
1	0.08	0.13
2	0.11	0.08
3	0.11	0.09
4	0.12	0.08

It is interesting to note that although the parameter values given in Table 5 had the lowest FRMS value over the range of parameter values tested, the two values actually work to compensate for each other making the selection of the values somewhat arbitrary to the degree of accuracy that can be expected. This is most evident by the following plots of the FRMS as a function of the entrainment and eddy viscous drag parameters.

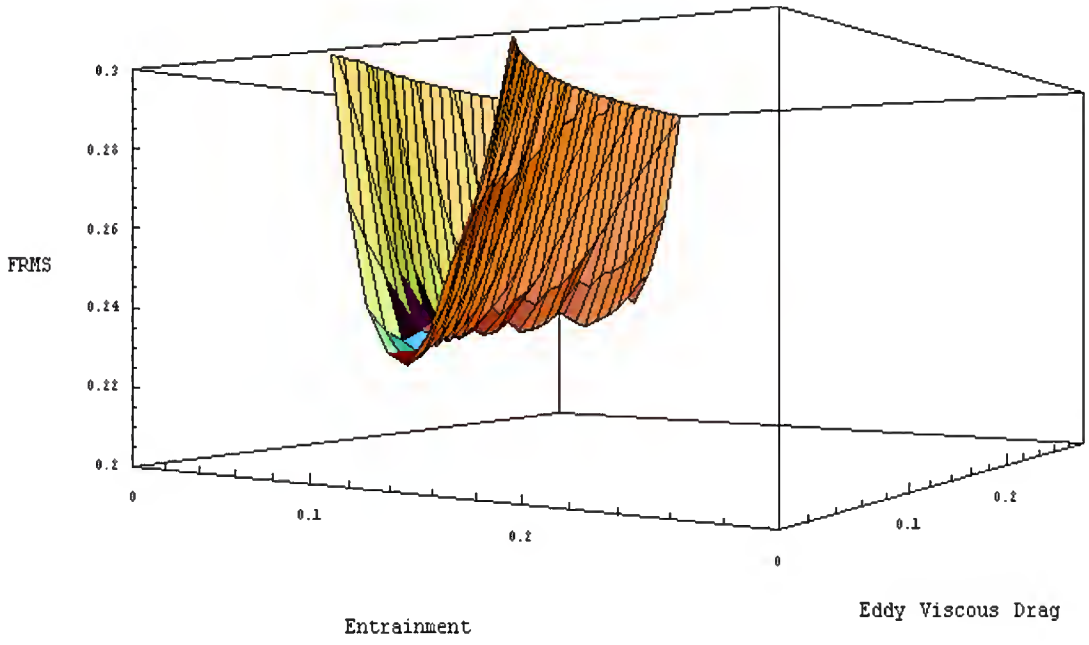

Figure 6. FRMS plot for Case 1: three-term entrainment equation with wind shear

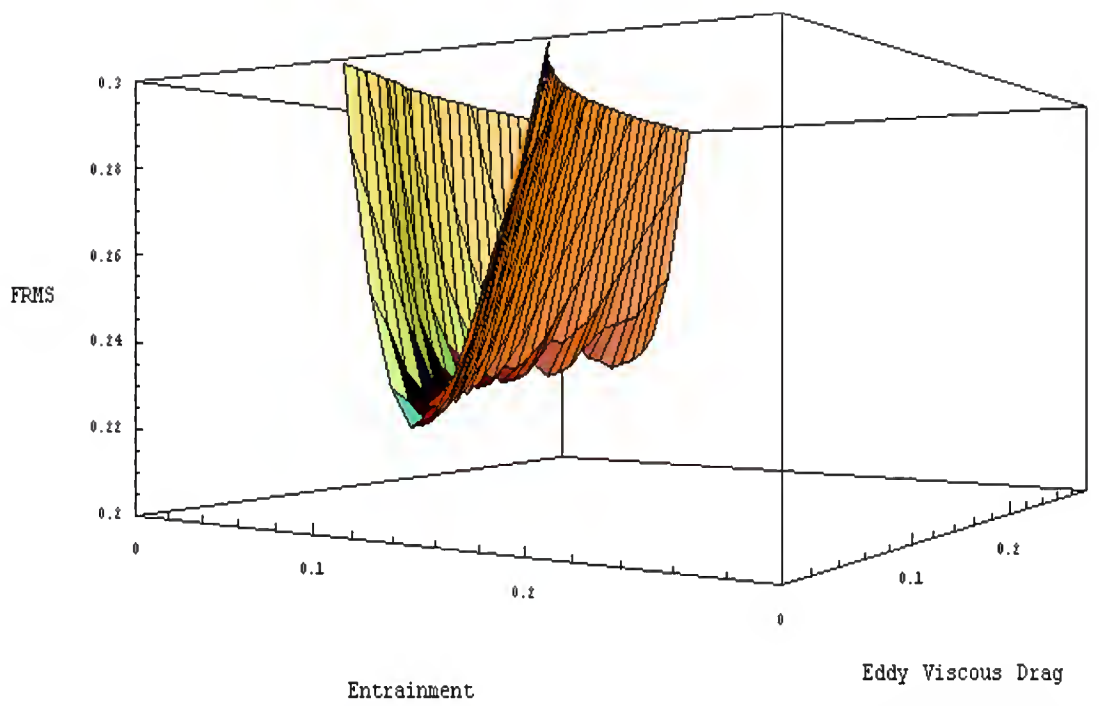

Figure 7. FRMS plot for Case 2: three-term entrainment equation without wind shear

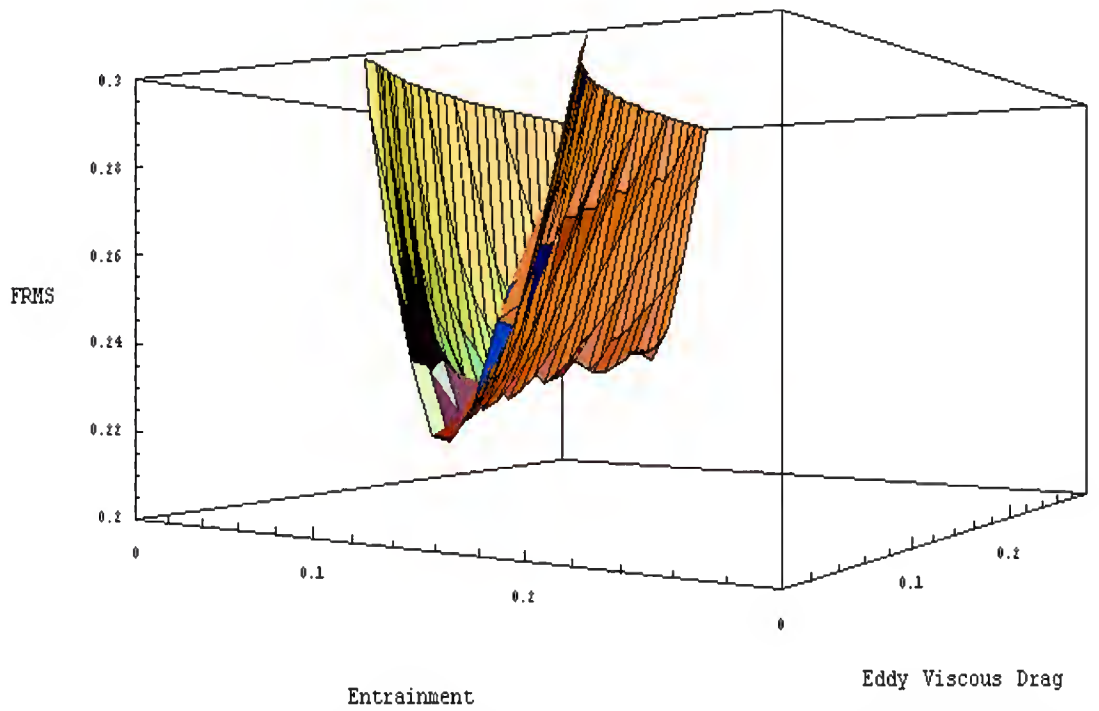

Figure 8. FRMS plot for Case 3: single-term entrainment equation with wind shear

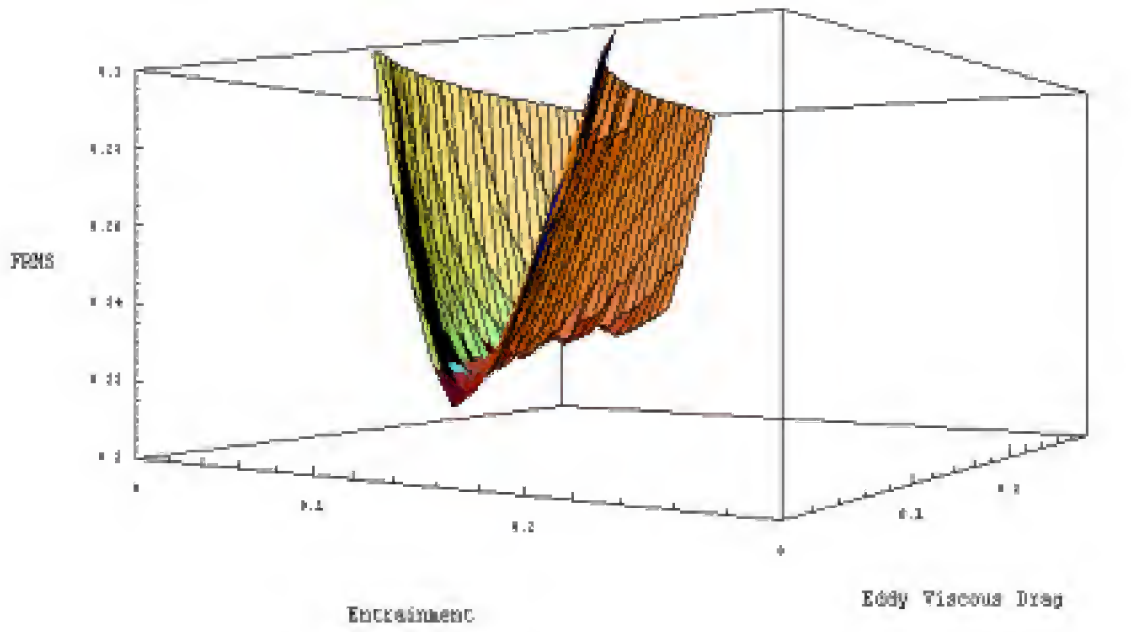

Figure 9. FRMS plot for Case 4: single-term entrainment equation without wind shear

The above figures tend to indicate an optimum value as the eddy viscous drag parameter approaches zero. This would be a non-physical result, however, because it would also result in a much more limited horizontal expansion of the cloud late in the rise as discussed in Chapter II, Section D. Therefore the more restrictive parameter range was used to determine the optimum values.

It should also be noted at this time that no test shot used in the analysis to this point has a yield that exceeds 110 kilotons. Higher yields result in a square root domain error when analyzing the three-term entrainment equation. Norment recognized this limitation and attributed the behavior to the representation of the cloud as a point. His use of yield dependent parameters for entrainment and eddy viscous drag alleviates the error for high yield shots. Depending upon which case is recommended in Chapter IV, Section B, another recommendation will be made concerning the handling of high yield shots.

Table 6 through Table 9 summarize the results of the four cases. Each case was compared to the 1979 corrected version of DELFIC that uses the yield dependent parameter values for entrainment and eddy viscous drag. All of the cloud top values listed are relative to the burst height. Again, these are the same comparisons used by both Norment and Jodoin in their work on cloud rise.

Table 6. Cloud top comparison of the 1979 Corrected DELFIC and Case 1

Shot	Yield (kt)	Observed Cloud Top (m)	Calculated Cloud Top(m)		Fractional Deviation	
			Corrected	Modified	Corrected	Modified
Humboldt	0.0078	1050	827	1081	0.212	-0.030
Catron	0.021	1344	1170	1499	0.130	-0.115
Vesta	0.024	1760	2294	2272	-0.303	-0.291
Dona Ana	0.037	1940	2802	2758	-0.444	-0.422
Hidalgo	0.077	2267	2258	2554	0.004	-0.127
Quay	0.079	1722	1543	1800	0.104	-0.045
Eddy	0.083	1925	2137	2862	-0.110	-0.487
Rio Arriba	0.09	2870	1975	2642	0.312	0.080
Wrangell	0.115	1653	1640	1867	0.008	-0.130
Franklin	0.14	3772	4252	4132	-0.127	-0.095
Wheeler	0.197	3740	3396	3959	0.092	-0.059
Ray	0.2	2644	2141	2629	0.190	0.006
Ruth	0.2	2833	2946	3077	-0.040	-0.086
Johnnie Boy	0.5	3612	2565	3159	0.290	0.125
Laplace	1	4592	4736	4895	-0.031	-0.066
Wasp	1	5042	3740	3987	0.258	0.209
Santa Fe	1.3	3753	3569	4383	0.049	-0.168
Lea	1.4	3449	3925	4696	-0.138	-0.362
John	2	6008	4197	4528	0.301	0.246
Mora	2	3906	4374	4638	-0.120	-0.187
Moth	2	6057	3640	4372	0.399	0.278
Post	2	3341	4148	4745	-0.242	-0.420
Debaca	2.2	3601	3811	4934	-0.058	-0.370
Ha	3	5602	5171	5624	0.077	-0.004
Wasp Prime	3	8250	4781	4899	0.421	0.406
Hornet	4	9965	4985	5569	0.500	0.441
Franklin Prime	4.7	8249	5480	5951	0.336	0.279

Shot	Yield (kt)	Observed Cloud Top (m)	Calculated Cloud Top(m)		Fractional Deviation	
			Corrected	Modified	Corrected	Modified
Sanford	4.9	6530	4986	6090	0.237	0.067
Socorro	6	6207	5792	6242	0.067	-0.006
Tesla	7	7827	5616	5637	0.283	0.280
Bee	8	10655	6114	6147	0.426	0.423
Morgan	8	10755	6379	6867	0.407	0.362
Owens	9.7	9231	7999	8129	0.134	0.119
Kepler	10	7090	7611	8057	-0.074	-0.136
Wilson	10	9226	6389	8067	0.308	0.126
Fizeau	11	10811	7833	7999	0.275	0.260
Galileo	11	9830	7573	8564	0.230	0.129
Doppler	11	9836	7685	8616	0.219	0.124
Dixie	11	10654	8092	8905	0.241	0.164
Boltzman	12	8615	10517	10570	-0.221	-0.227
Newton	12	8021	8008	8156	0.002	-0.017
Charleston	12	8012	6823	6820	0.148	0.149
Apple1	14	8288	5975	6034	0.279	0.272
Grable	15	9570	6147	6421	0.358	0.329
Annie	16	11178	9480	10581	0.152	0.053
Shasta	17	8264	9215	10624	-0.115	-0.286
Diablo	17	8239	8837	9579	-0.073	-0.163
Whitney	19	7624	8474	9249	-0.112	-0.213
Stokes	19	9545	8497	9142	0.110	0.042
Met	22	11223	7760	7748	0.309	0.310
Badger	23	9513	7568	9507	0.204	0.001
Nancy	24	11244	8823	9729	0.215	0.135
Encore	27	11125	8911	9382	0.199	0.157
Zuchini	28	10746	7102	7158	0.339	0.334
Apple2	29	14102	7089	7170	0.497	0.492
Harry	32	11642	11997	13664	-0.031	-0.174
Priscilla	37	11955	10774	12716	0.099	-0.064
Lacrosse	40	11582	9164	10906	0.209	0.058
Simon	43	12028	12183	12739	-0.013	-0.059
Turk	43	12104	7876	8002	0.349	0.339
Smokey	44	10004	11298	11487	-0.129	-0.148
Climax	61	11382	12092	12360	-0.062	-0.086
Hood	74	12884	12724	14334	0.012	-0.113
Koon	110	16150	15713	18772	0.027	-0.162
				FMD	**0.118**	**0.023**
				FRMS	**0.235**	**0.231**

Table 7. Cloud top comparison of the 1979 Corrected DELFIC and Case 2

Shot	Yield (kt)	Observed Cloud Top (m)	Calculated Cloud Top(m)		Fractional Deviation	
			Corrected	Modified	Corrected	Modified
Humboldt	0.0078	1050	827	1038	0.212	0.011
Catron	0.021	1344	1170	1377	0.130	-0.024
Vesta	0.024	1760	2294	2318	-0.303	-0.317
Dona Ana	0.037	1940	2802	2774	-0.444	-0.430
Hidalgo	0.077	2267	2258	2517	0.004	-0.110
Quay	0.079	1722	1543	1752	0.104	-0.018
Eddy	0.083	1925	2137	2542	-0.110	-0.321
Rio Arriba	0.09	2870	1975	2471	0.312	0.139
Wrangell	0.115	1653	1640	1829	0.008	-0.106
Franklin	0.14	3772	4252	4169	-0.127	-0.105
Wheeler	0.197	3740	3396	3753	0.092	-0.003
Ray	0.2	2644	2141	2484	0.190	0.061
Ruth	0.2	2833	2946	3044	-0.040	-0.075
Johnnie Boy	0.5	3612	2565	2943	0.290	0.185
Laplace	1	4592	4736	4900	-0.031	-0.067
Wasp	1	5042	3740	4041	0.258	0.199
Santa Fe	1.3	3753	3569	4089	0.049	-0.090
Lea	1.4	3449	3925	4444	-0.138	-0.289
John	2	6008	4197	4409	0.301	0.266
Mora	2	3906	4374	4545	-0.120	-0.164
Moth	2	6057	3640	4129	0.399	0.318
Post	2	3341	4148	4372	-0.242	-0.309
Debaca	2.2	3601	3811	4525	-0.058	-0.257
Ha	3	5602	5171	5418	0.077	0.033
Wasp Prime	3	8250	4781	4867	0.421	0.410
Hornet	4	9965	4985	5125	0.500	0.486
Franklin Prime	4.7	8249	5480	5649	0.336	0.315
Sanford	4.9	6530	4986	5330	0.237	0.184
Socorro	6	6207	5792	5911	0.067	0.048
Tesla	7	7827	5616	5588	0.283	0.286
Bee	8	10655	6114	6124	0.426	0.425
Morgan	8	10755	6379	6505	0.407	0.395
Owens	9.7	9231	7999	8069	0.134	0.126
Kepler	10	7090	7611	7775	-0.074	-0.097
Wilson	10	9226	6389	6484	0.308	0.297
Fizeau	11	10811	7833	7837	0.275	0.275
Galileo	11	9830	7573	7655	0.230	0.221
Doppler	11	9836	7685	8105	0.219	0.176

Shot	Yield (kt)	Observed Cloud Top (m)	Calculated Cloud Top(m)		Fractional Deviation	
			Corrected	Modified	Corrected	Modified
Dixie	11	10654	8092	8710	0.241	0.183
Boltzman	12	8615	10517	10507	-0.221	-0.220
Newton	12	8021	8008	8049	0.002	-0.004
Charleston	12	8012	6823	6791	0.148	0.153
Apple1	14	8288	5975	5984	0.279	0.278
Grable	15	9570	6147	6317	0.358	0.340
Annie	16	11178	9480	10170	0.152	0.090
Shasta	17	8264	9215	9881	-0.115	-0.196
Diablo	17	8239	8837	8958	-0.073	-0.087
Whitney	19	7624	8474	8716	-0.112	-0.143
Stokes	19	9545	8497	9041	0.110	0.053
Met	22	11223	7760	7763	0.309	0.308
Badger	23	9513	7568	8598	0.204	0.096
Nancy	24	11244	8823	9150	0.215	0.186
Encore	27	11125	8911	9260	0.199	0.168
Zuchini	28	10746	7102	7169	0.339	0.333
Apple2	29	14102	7089	7111	0.497	0.496
Harry	32	11642	11997	13614	-0.031	-0.169
Priscilla	37	11955	10774	11760	0.099	0.016
Lacrosse	40	11582	9164	10443	0.209	0.098
Simon	43	12028	12183	12656	-0.013	-0.052
Turk	43	12104	7876	7936	0.349	0.344
Smokey	44	10004	11298	11435	-0.129	-0.143
Climax	61	11382	12092	12352	-0.062	-0.085
Hood	74	12884	12724	13895	0.012	-0.079
Koon	110	16150	15713	17980	0.027	-0.113
				FMD	**0.118**	**0.061**
				FRMS	**0.235**	**0.228**

A plot of the comparison of the observed cloud top height to the calculated cloud top height is plotted in Figure 10 through Figure 13. Additionally, Table 4 indicates the type of shot.

Ideally, each of the shots would land on the straight line on each of the plots. This line would indicate that the observed height equaled the calculated height. In the

Table 8. Cloud top comparison of the 1979 Corrected DELFIC and Case 3

Shot	Yield (kt)	Observed Cloud Top (m)	Calculated Cloud Top(m)		Fractional Deviation	
			Corrected	Modified	Corrected	Modified
Humboldt	0.0078	1050	827	1052	0.212	-0.002
Catron	0.021	1344	1170	1448	0.130	-0.077
Vesta	0.024	1760	2294	2278	-0.303	-0.294
Dona Ana	0.037	1940	2802	2823	-0.444	-0.455
Hidalgo	0.077	2267	2258	2539	0.004	-0.120
Quay	0.079	1722	1543	1797	0.104	-0.044
Eddy	0.083	1925	2137	2673	-0.110	-0.389
Rio Arriba	0.09	2870	1975	2593	0.312	0.097
Wrangell	0.115	1653	1640	1884	0.008	-0.140
Franklin	0.14	3772	4252	4208	-0.127	-0.116
Wheeler	0.197	3740	3396	3749	0.092	-0.002
Ray	0.2	2644	2141	2563	0.190	0.031
Ruth	0.2	2833	2946	3079	-0.040	-0.087
Johnnie Boy	0.5	3612	2565	2871	0.290	0.205
Laplace	1	4592	4736	4874	-0.031	-0.062
Wasp	1	5042	3740	3968	0.258	0.213
Santa Fe	1.3	3753	3569	4322	0.049	-0.152
Lea	1.4	3449	3925	4620	-0.138	-0.339
John	2	6008	4197	4613	0.301	0.232
Mora	2	3906	4374	4602	-0.120	-0.178
Moth	2	6057	3640	4512	0.399	0.255
Post	2	3341	4148	4653	-0.242	-0.393
Debaca	2.2	3601	3811	5036	-0.058	-0.399
Ha	3	5602	5171	5935	0.077	-0.060
Wasp Prime	3	8250	4781	4983	0.421	0.396
Hornet	4	9965	4985	5596	0.500	0.439
Franklin Prime	4.7	8249	5480	5958	0.336	0.278
Sanford	4.9	6530	4986	6176	0.237	0.054
Socorro	6	6207	5792	6380	0.067	-0.028
Tesla	7	7827	5616	5731	0.283	0.268
Bee	8	10655	6114	6200	0.426	0.418
Morgan	8	10755	6379	6891	0.407	0.359
Owens	9.7	9231	7999	7553	0.134	0.182
Kepler	10	7090	7611	7784	-0.074	-0.098
Wilson	10	9226	6389	8115	0.308	0.121

Shot	Yield (kt)	Observed Cloud Top (m)	Calculated Cloud Top(m)		Fractional Deviation	
			Corrected	Modified	Corrected	Modified
Fizeau	11	10811	7833	8013	0.275	0.259
Galileo	11	9830	7573	8188	0.230	0.167
Doppler	11	9836	7685	7524	0.219	0.235
Dixie	11	10654	8092	8785	0.241	0.176
Boltzman	12	8615	10517	9989	-0.221	-0.160
Newton	12	8021	8008	8141	0.002	-0.015
Charleston	12	8012	6823	6892	0.148	0.140
Apple1	14	8288	5975	6184	0.279	0.254
Grable	15	9570	6147	6558	0.358	0.315
Annie	16	11178	9480	10124	0.152	0.094
Shasta	17	8264	9215	8945	-0.115	-0.082
Diablo	17	8239	8837	9346	-0.073	-0.134
Whitney	19	7624	8474	9195	-0.112	-0.206
Stokes	19	9545	8497	8914	0.110	0.066
Met	22	11223	7760	7775	0.309	0.307
Badger	23	9513	7568	9154	0.204	0.038
Nancy	24	11244	8823	9373	0.215	0.166
Encore	27	11125	8911	9378	0.199	0.157
Zuchini	28	10746	7102	7260	0.339	0.324
Apple2	29	14102	7089	7334	0.497	0.480
Harry	32	11642	11997	12849	-0.031	-0.104
Priscilla	37	11955	10774	11412	0.099	0.045
Lacrosse	40	11582	9164	9278	0.209	0.199
Simon	43	12028	12183	12343	-0.013	-0.026
Turk	43	12104	7876	8180	0.349	0.324
Smokey	44	10004	11298	11314	-0.129	-0.131
Climax	61	11382	12092	12200	-0.062	-0.072
Hood	74	12884	12724	13490	0.012	-0.047
Koon	110	16150	15713	15403	0.027	0.046
				FMD	**0.118**	**0.046**
				FRMS	**0.235**	**0.224**

assumptions and limitations section of Chapter I, several points were made which would cause the shots to vary from this line. The plots, along with the FMD values in Table 6 through Table 9, indicate that the code only slightly under predicts the shots on average.

Table 9. Cloud top comparison of the 1979 Corrected DELFIC and Case 4

Shot	Yield (kt)	Observed Cloud Top (m)	Calculated Cloud Top(m)		Fractional Deviation	
			Corrected	Modified	Corrected	Modified
Humboldt	0.0078	1050	827	1078	0.212	-0.027
Catron	0.021	1344	1170	1436	0.130	-0.069
Vesta	0.024	1760	2294	2296	-0.303	-0.305
Dona Ana	0.037	1940	2802	2795	-0.444	-0.441
Hidalgo	0.077	2267	2258	2542	0.004	-0.122
Quay	0.079	1722	1543	1817	0.104	-0.055
Eddy	0.083	1925	2137	2537	-0.110	-0.318
Rio Arriba	0.09	2870	1975	2593	0.312	0.097
Wrangell	0.115	1653	1640	1892	0.008	-0.145
Franklin	0.14	3772	4252	4195	-0.127	-0.112
Wheeler	0.197	3740	3396	3735	0.092	0.001
Ray	0.2	2644	2141	2586	0.190	0.022
Ruth	0.2	2833	2946	3080	-0.040	-0.087
Johnnie Boy	0.5	3612	2565	2893	0.290	0.199
Laplace	1	4592	4736	4892	-0.031	-0.065
Wasp	1	5042	3740	4040	0.258	0.199
Santa Fe	1.3	3753	3569	4271	0.049	-0.138
Lea	1.4	3449	3925	4570	-0.138	-0.325
John	2	6008	4197	4575	0.301	0.239
Mora	2	3906	4374	4601	-0.120	-0.178
Moth	2	6057	3640	4492	0.399	0.258
Post	2	3341	4148	4509	-0.242	-0.350
Debaca	2.2	3601	3811	5001	-0.058	-0.389
Ha	3	5602	5171	5905	0.077	-0.054
Wasp Prime	3	8250	4781	4976	0.421	0.397
Hornet	4	9965	4985	5468	0.500	0.451
Franklin Prime	4.7	8249	5480	5915	0.336	0.283
Sanford	4.9	6530	4986	6171	0.237	0.055
Socorro	6	6207	5792	6352	0.067	-0.023
Tesla	7	7827	5616	5718	0.283	0.269
Bee	8	10655	6114	6207	0.426	0.418
Morgan	8	10755	6379	6877	0.407	0.361
Owens	9.7	9231	7999	7601	0.134	0.177
Kepler	10	7090	7611	7796	-0.074	-0.100
Wilson	10	9226	6389	7905	0.308	0.143

Shot	Yield (kt)	Observed Cloud Top (m)	Calculated Cloud Top(m)		Fractional Deviation	
			Corrected	Modified	Corrected	Modified
Fizeau	11	10811	7833	7967	0.275	0.263
Galileo	11	9830	7573	8024	0.230	0.184
Doppler	11	9836	7685	7450	0.219	0.243
Dixie	11	10654	8092	8920	0.241	0.163
Boltzman	12	8615	10517	9962	-0.221	-0.156
Newton	12	8021	8008	8129	0.002	-0.014
Charleston	12	8012	6823	6876	0.148	0.142
Apple1	14	8288	5975	6175	0.279	0.255
Grable	15	9570	6147	6671	0.358	0.303
Annie	16	11178	9480	10083	0.152	0.098
Shasta	17	8264	9215	8881	-0.115	-0.075
Diablo	17	8239	8837	9180	-0.073	-0.114
Whitney	19	7624	8474	9040	-0.112	-0.186
Stokes	19	9545	8497	8922	0.110	0.065
Met	22	11223	7760	7778	0.309	0.307
Badger	23	9513	7568	9138	0.204	0.039
Nancy	24	11244	8823	9275	0.215	0.175
Encore	27	11125	8911	9396	0.199	0.155
Zuchini	28	10746	7102	7278	0.339	0.323
Apple2	29	14102	7089	7287	0.497	0.483
Harry	32	11642	11997	13033	-0.031	-0.119
Priscilla	37	11955	10774	11098	0.099	0.072
Lacrosse	40	11582	9164	9345	0.209	0.193
Simon	43	12028	12183	12260	-0.013	-0.019
Turk	43	12104	7876	8134	0.349	0.328
Smokey	44	10004	11298	11282	-0.129	-0.128
Climax	61	11382	12092	12191	-0.062	-0.071
Hood	74	12884	12724	13342	0.012	-0.036
Koon	110	16150	15713	15233	0.027	0.057
				FMD	**0.118**	**0.050**
				FRMS	**0.235**	**0.221**

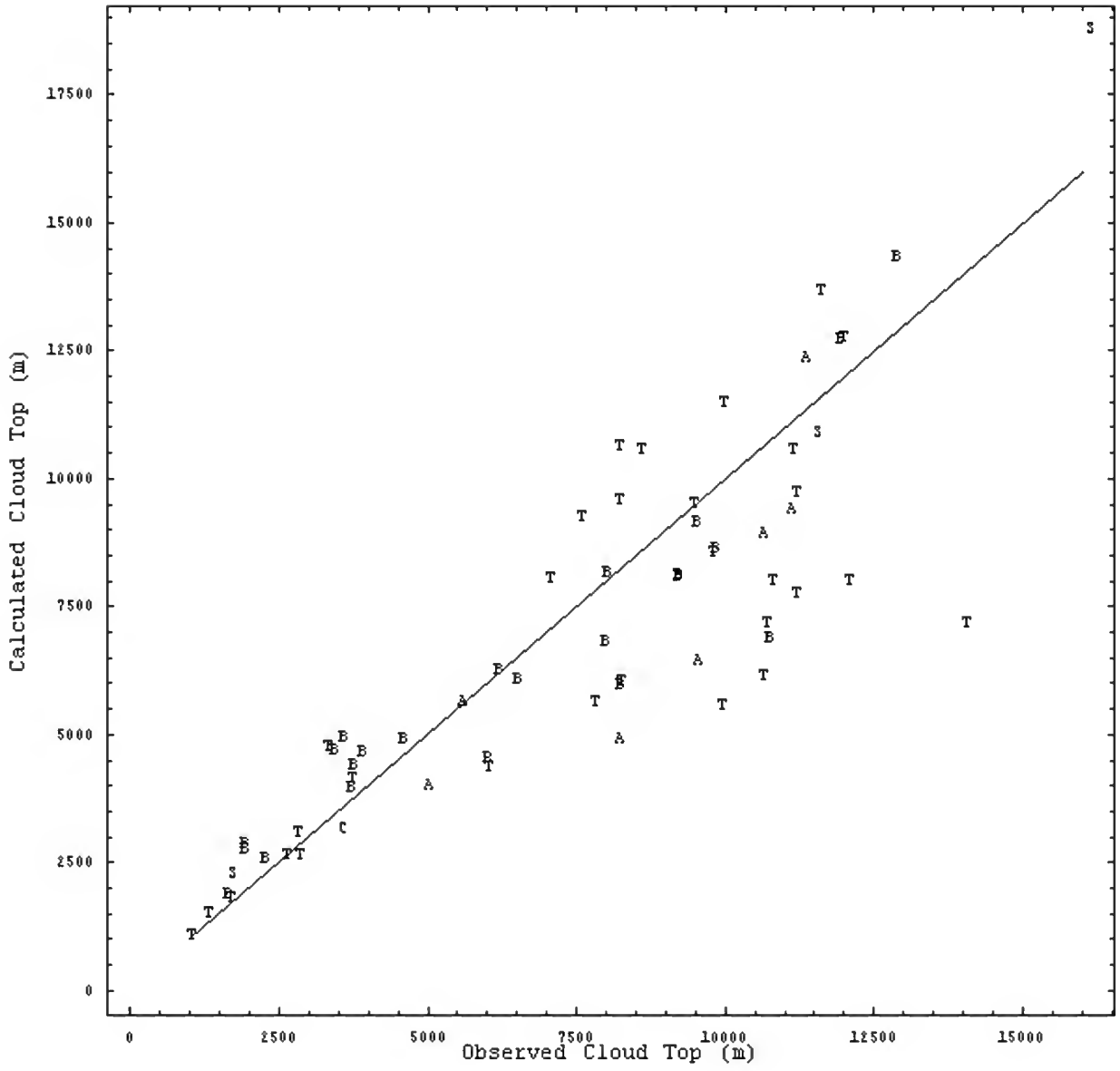

Figure 10. Calculated versus observed cloud top height comparison for Case 1

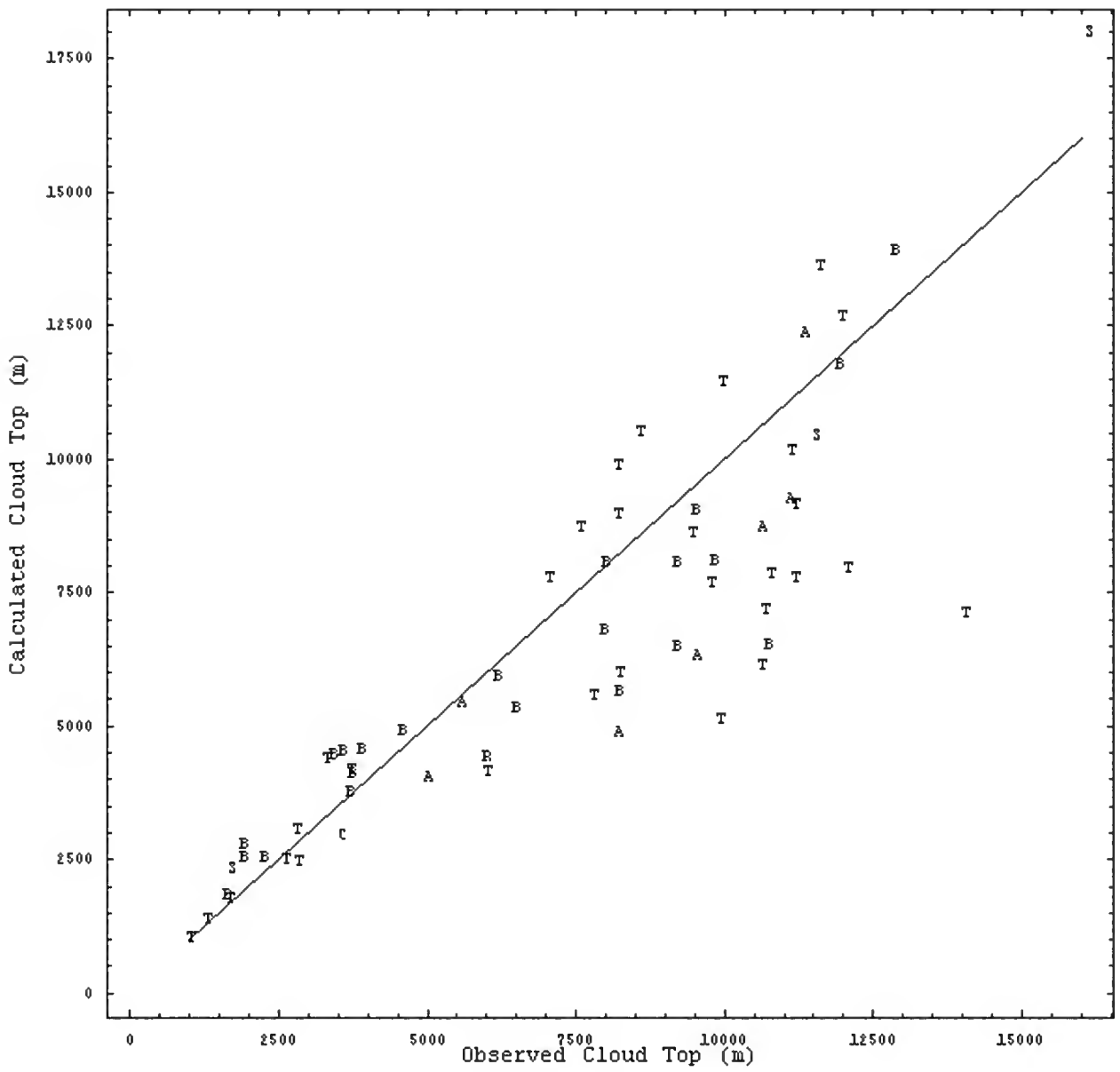

Figure 11. Calculated versus observed cloud top height comparison for Case 2

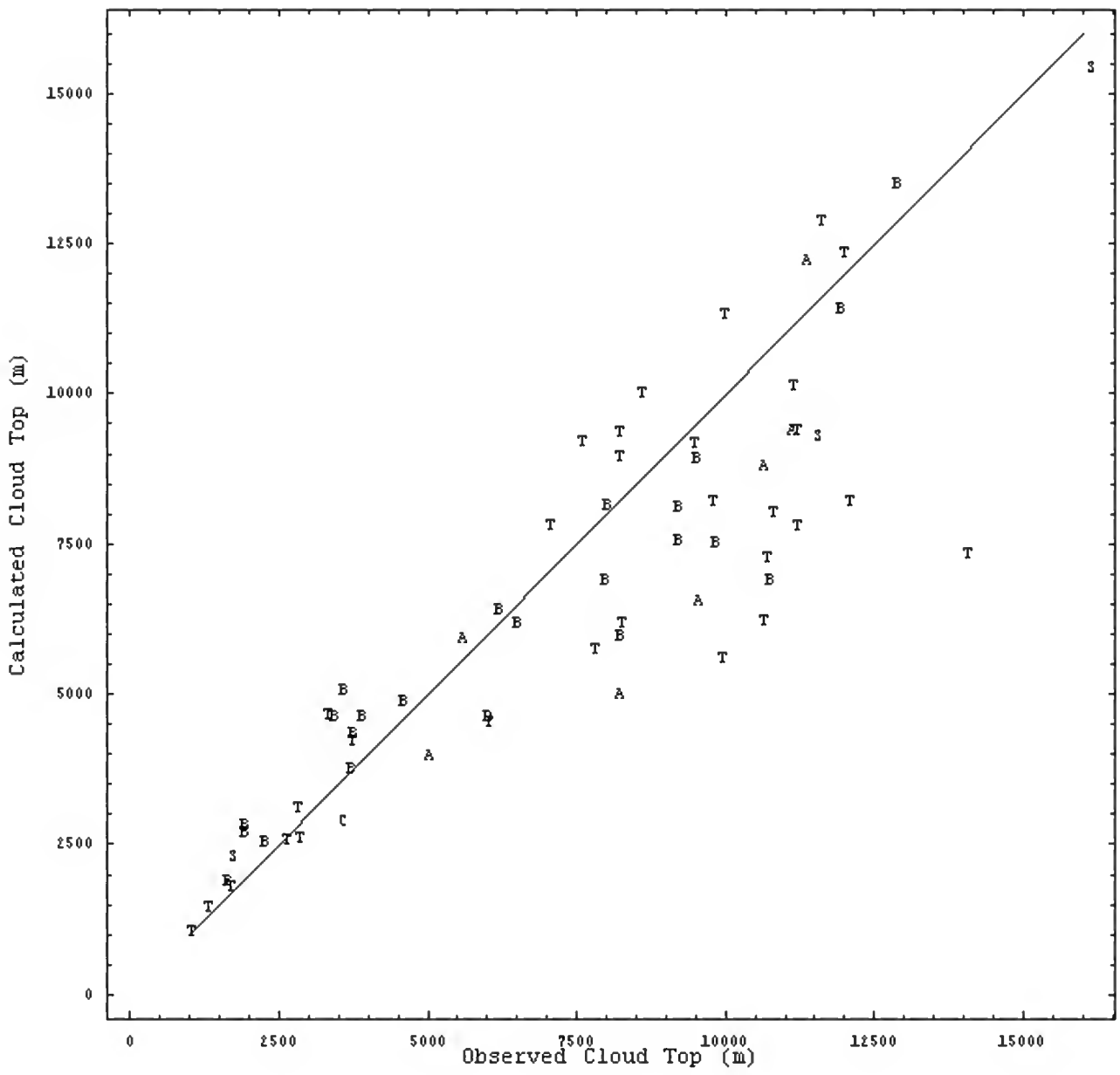

Figure 12. Calculated versus observed cloud top height comparison for Case 3

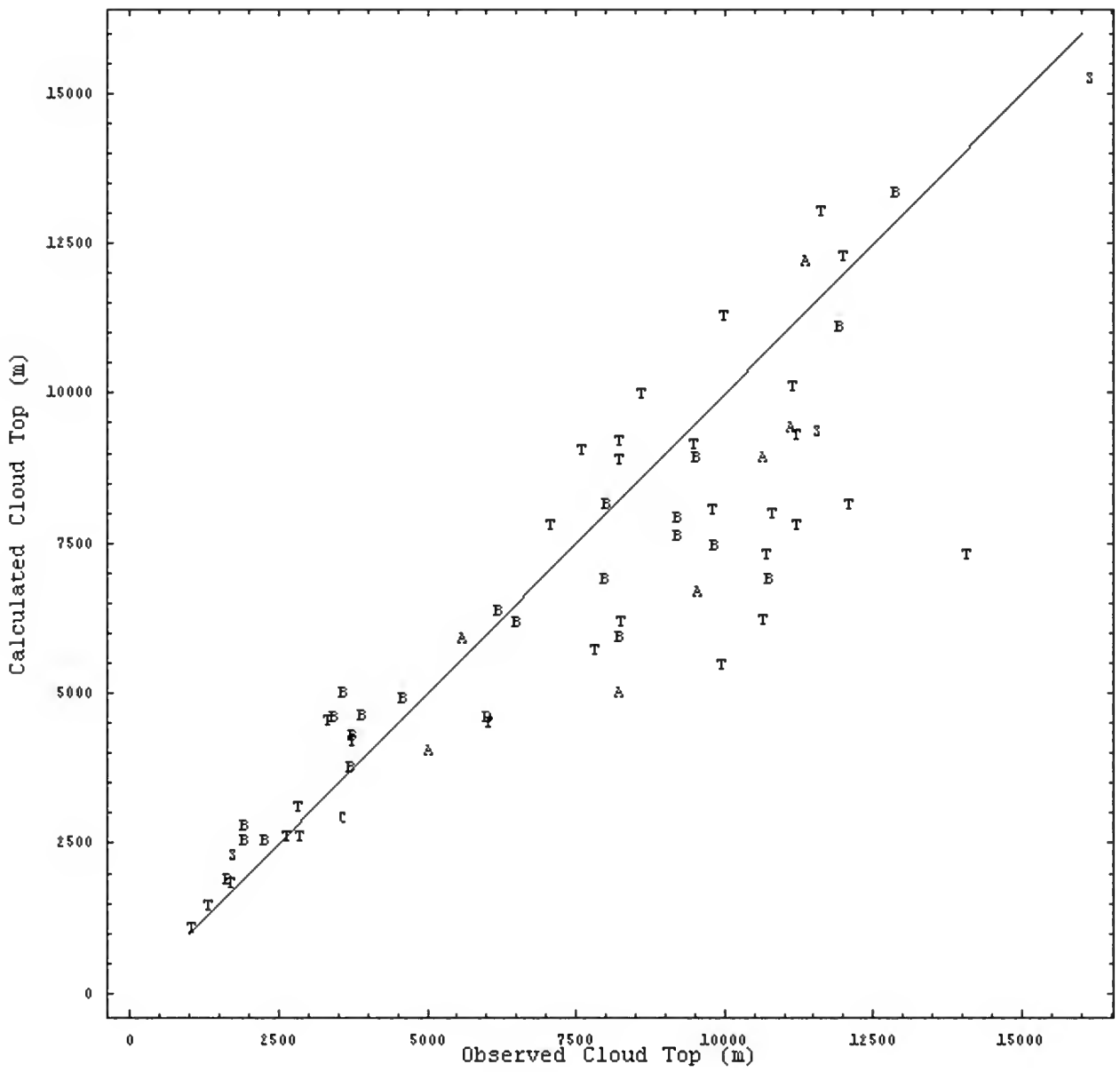

Figure 13. Calculated versus observed cloud top height comparison for Case 4

It is noted that several shots vary from the line considerably and perhaps a closer look at some of those shots in particular may give some indication as to why the code resulted in such an error. Figure 14 is a plot of Case 1, where each point on the plot corresponds to the reference number in Table 4. Also of interest are the dashed lines,

which represent the accuracy limitation proposed by Eisenbud that was introduced in Chapter I, Section E.

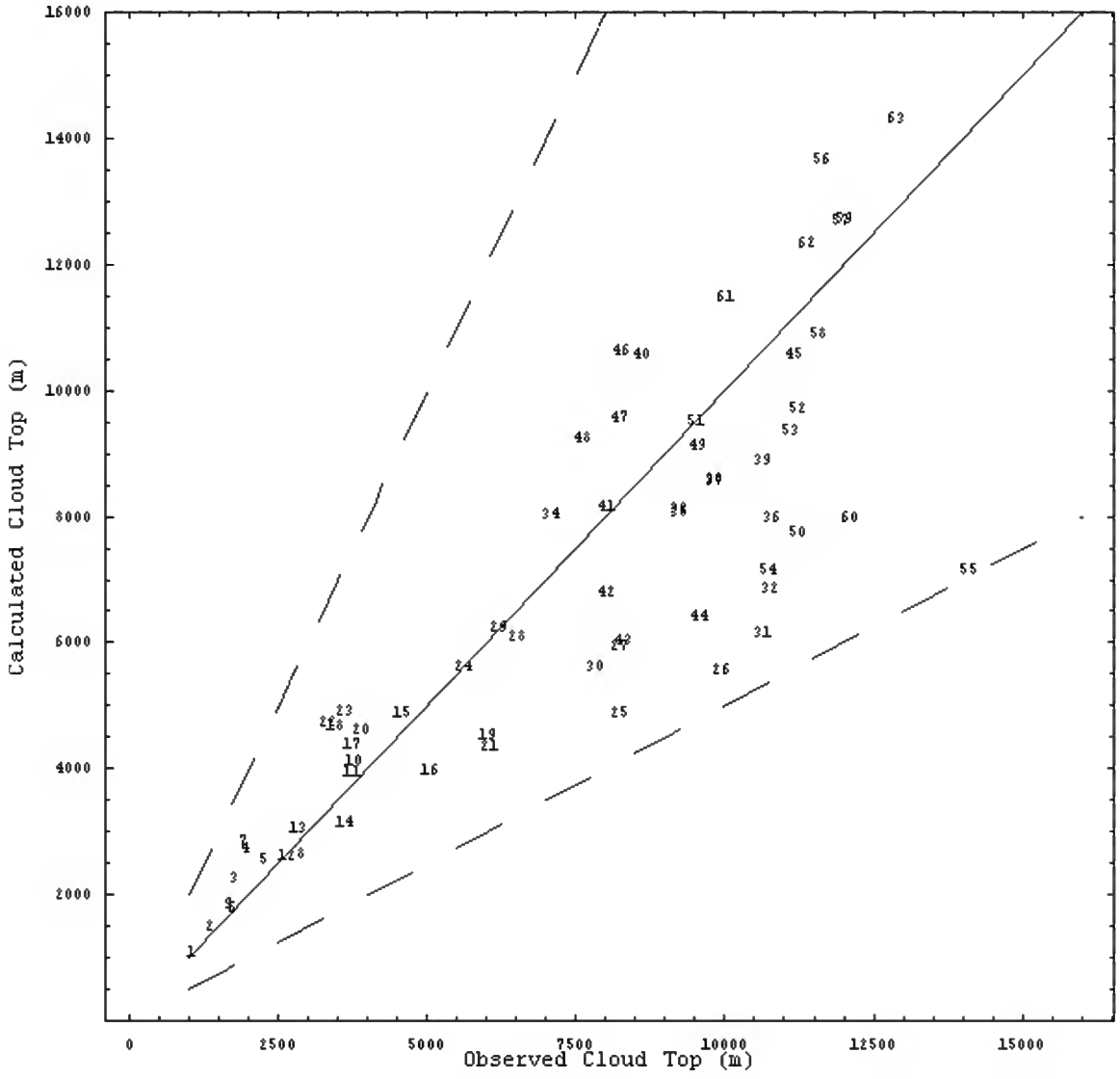

Figure 14. Shot identification plot for Case 1

Table 10 identifies the particular shots on Figure 14 where the absolute value of the fractional deviation is greater than the FRMS value of Case 1. This is obviously a more restrictive criterion than that proposed by Eisenbud, which incorporates all of the test data. A sampling from operations Hardtack II, Teapot, and Plumbbob are represented

using the more restrictive criterion. Of particular note is that 11 of the 13 Teapot shots are outside the defined tolerance. Only operation Upshot-Knothole is not well

Table 10. Shots outside the FRMS of Case 1

Ref #	Shot	Operation	Frac Dev	Yield (kt)	HOB (m)	Type*	Date of shot (mm/yr)
55	Apple2	Teapot	0.492	29	152	T	05/55
26	Hornet	Teapot	0.441	4	91	T	03/55
31	Bee	Teapot	0.423	8	152	T	03/55
25	Wasp Prime	Teapot	0.406	3	225	A	03/55
32	Morgan	Plumbbob	0.361	8	152	B	10/57
60	Turk	Teapot	0.339	43	152	T	03/55
54	Zuchini	Teapot	0.334	28	152	T	05/55
44	Grable	Upshot-Knothole	0.329	15	160	A	05/53
50	Met	Teapot	0.310	22	122	T	04/55
30	Tesla	Teapot	0.28	7	91	T	03/55
27	Franklin Prime	Plumbbob	0.279	4.7	229	B	08/57
21	Moth	Teapot	0.278	2	91	T	02/55
43	Apple1	Teapot	0.272	14	152	T	03/55
36	Fizeau	Plumbbob	0.260	11	152	T	09/57
19	John	Plumbbob	0.246	2	6096	R	07/57
46	Shasta	Plumbbob	-0.286	17	152	T	08/57
3	Vesta	Hardtack II	-0.291	0.024	0	S	10/58
18	Lea	Hardtack II	-0.362	1.4	457	B	10/58
23	Debaca	Hardtack II	-0.370	2.2	457	B	10/58
22	Post	Teapot	-0.42	2	91	T	04/55
4	Dona Ana	Hardtack II	-0.422	0.037	137	B	10/58
7	Eddy	Hardtack II	-0.487	0.083	152	B	09/58

represented. Also, the error does not seem to be associated with the yield, since a wide range of yields is represented. It is also interesting to note that cloud top heights were typically over-predicted for operations Hardtack II, while they were under-predicted for operations Teapot and Plumbbob. Given that a correlation can be made between operations and the propensity to over or under predict the stabilized cloud top height, a

* A-Airdrop, B-Balloon, S-Surface, T-Tower

correlation can also be made between the date of the shot and the propensity to over or under predict. Hardtack II were the latest U.S. atmospheric test shots in the test set, occurring in 1958, while the other series were all detonated in 1957 or earlier. Additionally, if you consider that the cloud top heights for Hardtack II were calculated using aircraft measurements and Teapot were calculated using photographic analysis this may provide some indication on the tendency to over or under predict the stabilized cloud top height. There is uncertainty in the aircraft measurements because they were not always made at the time of cloud stabilization (12:1). Typically, the measurements were taken after stabilization when the cloud had a chance to diffusively expand. The uncertainties associated with photographic analysis stem from the fact that the cloud top is not always visible from the photographic stations on the ground. No information could be found on the type of measurements taken for operations Plumbbob and Upshot-Knothole, which provided the smallest fractional deviations of the operations considered. Although not presented here, the same analysis was conducted on the other three cases and reinforced the findings. There was a consistent over prediction in the values for the Hardtack II operation and a consistent under prediction in the values for the Teapot operation.

B. Three Term Analysis

Chapter II presented the derivation of the three-term entrainment equation and presented Norment's justification for the use and development of each term. Also, Huebsch's validation and arguments in regards to the development were presented, where he makes his argument for returning to the single-term entrainment equation. Both Norment and Huebsch discuss the relative importance of each term in the cloud rise

history, and on this point there is agreement. Both indicate that the third term is of little importance during the cloud rise calculation. The second term, however, becomes increasingly important with increasing yield. A situation that Huebsch claims results in non-physical behavior for yields greater than 15 megatons, that is, a behavior of negative entrainment or decrease in mass. In order to better quantify the impact of each of the terms, an analysis of the relative importance of each of the terms during the cloud rise was conducted for various yields. The analysis makes a direct comparison of the three terms presented by Norment. Unlike Huebsch's comparison in his *Analysis and Revision of the Cloud Rise Module of the Department of Defense Land Fallout Prediction System (DELFIC)*, this analysis maintains the integrity of each of the terms. Readers are referred to reference (8) page 12 for more information on Huebsch's analysis.

Each term of the mass entrainment equation was computed after all derivative functions were calculated in both the dry and wet conditions. Then the three terms of the equation were calculated based on the following equation.

$$\left.\frac{dm}{dt}\right|_{ent} = \beta' m \frac{S}{V} \mu v - \frac{\beta' m}{T^*}\frac{dT}{dt} - \frac{\beta' mgu}{R_a T_e^*}$$

This is Equation (6) with the pressure term solved for. Each of the terms was then divided by the mass entrainment rate to get a relative importance to the whole and plotted as a function of time. The following graph is the result for the DELFIC test case. The 1979, corrected version of DELFIC with wind shear corrections and yield dependent parameters was used for this analysis.

It was predicted that the second term would have a large impact on the equation during initial rise times, which it does. The second term's influence during the early rise time is due to the initial heat of the cloud. It was also predicted that the third term would

have a negligible impact for all yields, which it does at stabilization. The third term does not, however, have a negligible impact for all times. During the early time of the rise, since it is also a function of cloud rise velocity, the third term has an inverse impact to

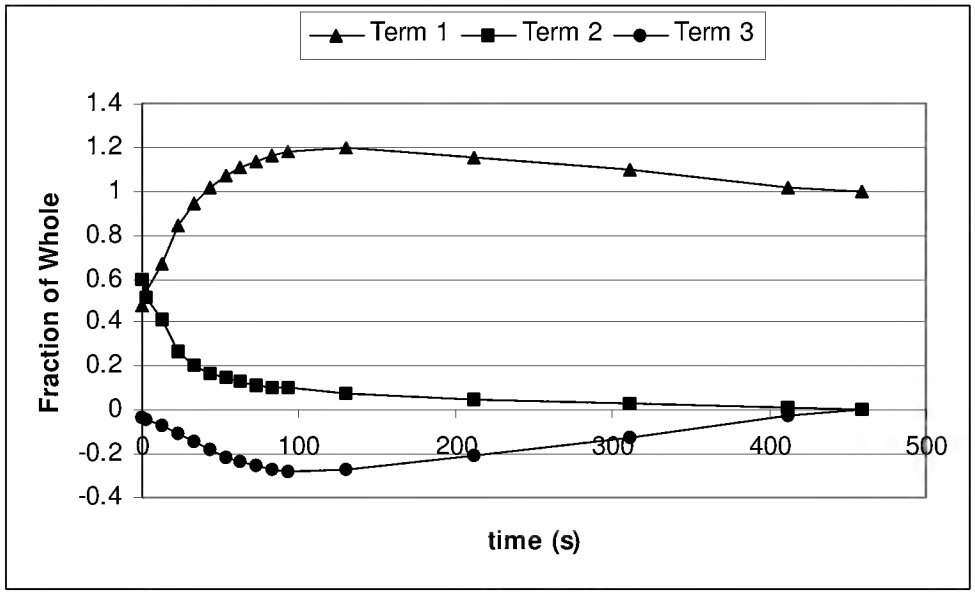

Figure 15. Relative importance of the first, second, and third terms of the mass entrainment equation for the 1979 DELFIC test case

that of the first term. At later times, when the cloud rise velocity goes to zero, so does the impact of the third term. Since the first term is proportional to the characteristic speed as defined by Equation (5), its relative importance is maintained even after the cloud rise velocity goes to zero.

To determine the effect yield had on this relative importance, the yield of the test case was changed to 1 kiloton and 1 megaton resulting in Figure 16 and Figure 17. As predicted, the relative importance of the second and third term has dropped off for the one-kiloton test case, while it has increased significantly for the one-megaton case. The above analysis suggests that at the time of stabilization the additional two terms have little impact.

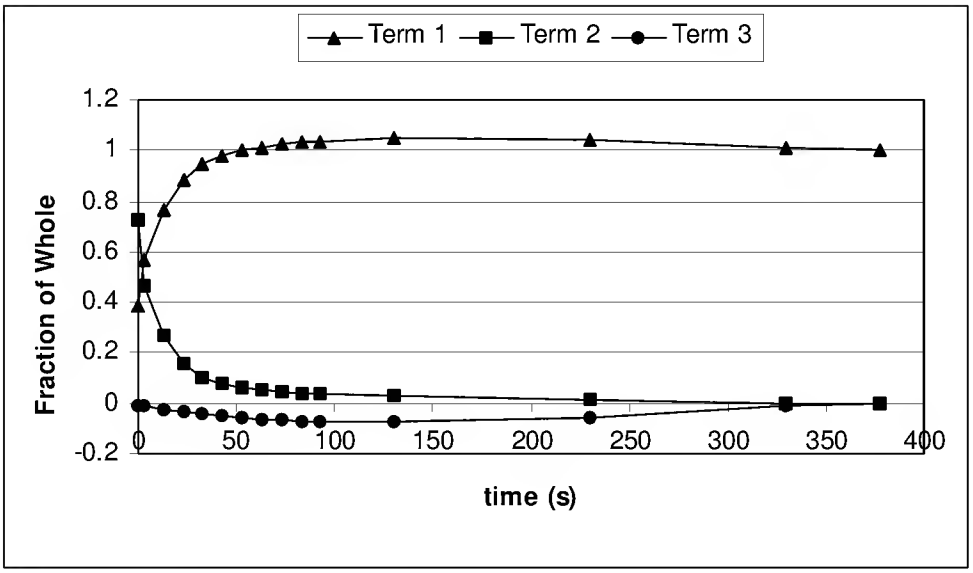

Figure 16. Relative importance of the first, second, and third terms of the mass entrainment equation for the 1979 DELFIC test case modified to a 1-kiloton yield

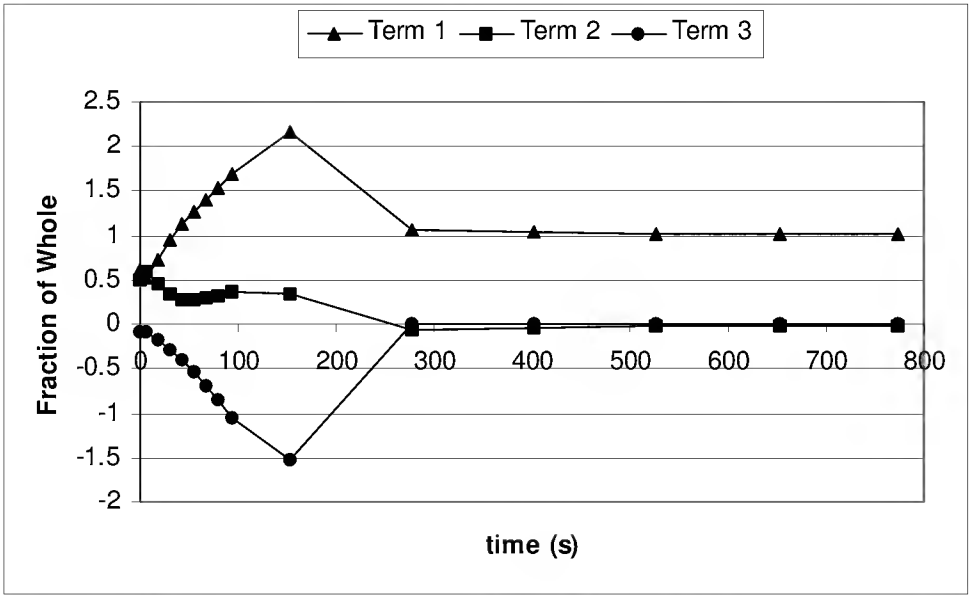

Figure 17. Relative importance of the first, second, and third terms of the mass entrainment equation for the 1979 DELFIC test case modified to a 1-megaton yield

C. Wind Shear Analysis

The effect of eliminating wind shear from the entrainment equation results in a slight decrease in the eddy viscous drag parameter, and a slight increase in the entrainment parameter.

Table 11. Wind shear comparison of the entrainment and eddy viscous drag parameters

Entrainment Equation	Entrainment Parameter		Eddy Viscous Drag	
	With Wind Shear	Without Wind Shear	With Wind Shear	Without Wind Shear
Three-Term	0.08	0.11	0.13	0.08
Single-Term	0.11	0.12	0.09	0.08

Wind shear has the effect of increasing the entrainment during cloud rise and decreasing the cloud top height, as was discussed in Chapter II, Section C. Therefore, in order to predict the same approximate height with wind shear, a lower entrainment parameter is needed. In Chapter II, Section D it is stated that an increase in the eddy viscous drag parameter will result in a decrease in cloud height. Since the presence of wind shear also results in a decrease in cloud height, the decrease in the eddy viscous drag parameter will result in an increase in cloud height in the absence of wind shear. Another way of considering the change in parameter values in the absence of wind shear is to consider Figure 6 through Figure 9, where the compensating effect of the parameters was pointed out. The increase in the entrainment parameter is offset by the decrease in the eddy viscous drag parameter. Figure 6 through Figure 9 also gives some indication as to just how similar the cases are with and without wind shear. Superimposing the plots for the three-term equation with and without wind shear and the single-term equation with and without wind shear makes them nearly indistinguishable.

Given the small change in parameter values, the next analysis considered the effect eliminating wind shear from the model had on cloud top height and radius. The mean deviation (MD) and root mean square (RMS) was calculated using the with shear values as the base. The MD then indicates the tendency for wind shear to increase the height or radius with a positive value or the tendency to decrease the height or radius

Table 12. Cloud top comparison with and without wind shear corrections

Shot	Yield (kt)	Single-Term Entrainment Equation Top Height (m)			Three-Term Entrainment Equation Top Height (m)		
		With Shear	Without Shear	Difference	With Shear	Without Shear	Difference
Humboldt	0.008	2196	2253	-58	2169	2200	-31
Catron	0.021	2545	2591	-46	2528	2523	5
Vesta	0.024	3564	3570	-7	3583	3602	-19
Dona Ana	0.037	4221	4194	27	4199	4180	18
Hidalgo	0.077	3835	3875	-40	3828	3838	-10
Quay	0.079	2991	3066	-74	2963	2997	-34
Eddy	0.083	3627	3685	-58	3730	3708	23
Rio Arriba	0.09	3381	3658	-277	3343	3395	-52
Wrangell	0.115	3176	3218	-42	3140	3156	-16
Franklin	0.14	5575	5512	63	5518	5497	21
Wheeler	0.197	5005	5057	-52	5054	5046	8
Ray	0.2	3575	3672	-97	3551	3584	-32
Ruth	0.2	4322	4338	-16	4299	4294	5
Johnnie Boy	0.5	4220	4296	-75	4297	4318	-21
Laplace	1	6299	6329	-31	6318	6342	-24
Wasp	1	5352	5466	-114	5345	5473	-128
Santa Fe	1.3	5732	5851	-119	5568	5559	9
Lea	1.4	6080	6183	-103	5922	5888	34
John	2	11918	11986	-68	11660	11654	7
Mora	2	6274	6340	-66	6149	6160	-11
Moth	2	5683	5818	-135	5122	5182	-60
Post	2	5890	5899	-10	5631	5527	103
Debaca	2.2	6753	6752	1	5745	5678	68
Ha	3	17127	17245	-118	16314	16318	-4
Wasp Prime	3	6507	6541	-33	6275	6283	-8
Hornet	4	7012	7092	-81	6201	6153	48
Franklin Prime	4.7	7671	7934	-263	6830	6826	4
Sanford	4.9	8137	8461	-324	6131	6180	-49
Socorro	6	8369	8536	-167	7284	7278	5
Tesla	7	7206	7259	-54	6800	6784	15
Bee	8	7802	7865	-63	7431	7456	-25
Morgan	8	8736	8953	-216	7571	7570	1
Owens	9.7	9253	9452	-198	9126	9244	-118
Kepler	10	9555	9804	-248	8770	8847	-76
Wilson	10	9964	10245	-281	7554	7483	72
Fizeau	11	9581	9644	-63	9042	8987	55
Galileo	11	9960	10096	-136	8701	8510	191

Shot	Yield (kt)	Single-Term Entrainment Equation Top Height (m)			Three-Term Entrainment Equation Top Height (m)		
		With Shear	Without Shear	Difference	With Shear	Without Shear	Difference
Doppler	11	9651	9931	-279	9102	9186	-83
Dixie	11	12178	12445	-267	10944	11248	-303
Boltzman	12	11627	11756	-130	11720	11737	-17
Newton	12	10058	10185	-127	9580	9550	30
Charleston	12	8822	8871	-49	8449	8448	1
Apple1	14	7876	7959	-83	7282	7297	-15
Grable	15	8017	8587	-571	7052	7136	-85
Annie	16	11611	11792	-181	10439	10650	-212
Shasta	17	10738	11103	-365	10307	10490	-183
Diablo	17	11146	11261	-115	10163	10041	122
Whitney	19	10988	11077	-90	9753	9637	116
Stokes	19	10912	11073	-160	10018	10226	-208
Met	22	9008	9090	-82	8671	8692	-21
Badger	23	10875	11219	-344	8876	9027	-151
Nancy	24	11007	11247	-240	10054	10016	38
Encore	27	11246	11480	-235	10475	10590	-115
Zuchini	28	8904	9049	-145	8392	8446	-54
Apple2	29	9005	9073	-68	8362	8361	1
Harry	32	13916	14916	-1000	13840	14327	-487
Priscilla	37	12591	12799	-207	12043	11685	359
Lacrosse	40	9301	9774	-474	9138	9302	-164
Simon	43	13688	13954	-266	13683	13682	2
Turk	43	9907	9978	-72	9256	9238	18
Smokey	44	13038	13096	-58	12790	12782	8
Climax	61	13938	14052	-113	13723	13741	-18
Hood	74	14989	15280	-291	14943	14908	35
Koon	110	14045	14551	-507	16927	16873	54
Mean Dev				**-159**			**-21**
Root Mean Square				**229**			**113**

with a negative value. The RMS is a measure of the absolute deviation between the top heights or radii associated with wind shear. This analysis used the yield dependent parameters for the four cases listed in Table 3 in order to more closely match the method currently used to predict cloud dimensions at stabilization. As Huebsch predicted and

confirmed by Table 12, the wind shear effect on cloud top height is insignificant in most cases, within a few hundred meters, but tends to decrease cloud top height. More error can be attributed to round off and approximations to the model than associated with wind shear.

Table 13. Cloud radius comparisons with and without wind shear corrections

Shot	Yield (kt)	Single-Term Entrainment Equation Radius (m)			Three-Term Entrainment Equation Radius (m)		
		With Shear	Without Shear	Difference	With Shear	Without Shear	Difference
Humboldt	0.008	296	260	36	283	246	37
Catron	0.021	367	344	23	354	332	21
Vesta	0.024	546	515	31	487	487	0
Dona Ana	0.037	827	625	202	744	630	114
Hidalgo	0.077	708	606	102	667	590	77
Quay	0.079	456	427	29	444	430	13
Eddy	0.083	582	553	29	609	557	52
Rio Arriba	0.09	565	673	-108	534	529	5
Wrangell	0.115	486	449	38	470	451	19
Franklin	0.14	1122	943	179	983	898	85
Wheeler	0.197	987	897	91	946	847	98
Ray	0.2	649	602	46	626	584	42
Ruth	0.2	826	710	116	786	722	64
Johnnie Boy	0.5	729	676	54	694	679	15
Laplace	1	1228	1176	52	1163	1093	70
Wasp	1	1320	979	340	1237	976	261
Santa Fe	1.3	1098	1045	53	1056	994	62
Lea	1.4	1245	1134	111	1117	1078	39
John	2	1381	1294	87	1324	1304	21
Mora	2	1144	1083	61	1143	1124	19
Moth	2	1221	1109	111	1088	1059	30
Post	2	1180	1083	96	1062	1082	-20
Debaca	2.2	1391	1210	181	1200	1098	102
Ha	3	1977	2031	-54	1843	1815	28
Wasp Prime	3	1427	1343	83	1237	1236	1
Hornet	4	1416	1312	104	1298	1289	9
Franklin Prime	4.7	1548	1526	22	1395	1390	5
Sanford	4.9	1961	1709	252	1386	1351	35
Socorro	6	1648	1696	-48	1536	1443	94

Shot	Yield (kt)	Single-Term Entrainment Equation Radius (m)			Three-Term Entrainment Equation Radius (m)		
		With Shear	Without Shear	Difference	With Shear	Without Shear	Difference
Tesla	7	1737	1640	97	1644	1597	48
Bee	8	1839	1824	15	1701	1733	-31
Morgan	8	1924	1849	75	1712	1669	43
Owens	9.7	2257	2192	65	2219	2139	80
Kepler	10	2272	2164	108	2096	2086	10
Wilson	10	2271	2177	94	1810	1791	18
Fizeau	11	2474	2292	181	2114	2048	66
Galileo	11	2213	2173	40	1863	1889	-26
Doppler	11	2286	2201	85	2258	2150	109
Dixie	11	2624	2721	-97	2186	2282	-96
Boltzman	12	2991	2839	152	2909	2704	205
Newton	12	2549	2415	134	2277	2205	72
Charleston	12	2204	2178	26	2101	2157	-56
Apple1	14	2077	1998	79	1958	1943	15
Grable	15	2295	2162	133	2279	2007	272
Annie	16	2829	2833	-4	2459	2541	-82
Shasta	17	2779	2698	81	2567	2261	306
Diablo	17	2799	2717	81	2405	2408	-3
Whitney	19	2967	2813	155	2338	2379	-40
Stokes	19	3014	2919	95	2710	2609	102
Met	22	2862	2714	148	2729	2540	190
Badger	23	2806	2895	-89	2402	2346	56
Nancy	24	3062	3013	49	2688	2736	-48
Encore	27	3803	3348	454	3418	2953	465
Zuchini	28	2893	2695	198	2814	2561	253
Apple2	29	2841	2660	181	2536	2529	7
Harry	32	3944	3708	236	3311	3235	75
Priscilla	37	3977	3799	178	3370	3271	99
Lacrosse	40	3582	3278	304	3166	2948	217
Simon	43	4394	4421	-28	3878	3857	20
Turk	43	3457	3263	194	2972	2966	6
Smokey	44	4509	4571	-62	3896	3917	-20
Climax	61	5588	5463	125	4692	4607	85
Hood	74	5528	5352	176	4249	4315	-67
Koon	110	5860	5133	727	5180	4835	346
MD				**105**			**64**
RMS				**164**			**121**

Huebsch's claim was that wind shear had a more significant impact on the cloud radius at stabilization. Using the same conditions from above, Table 13 identifies the

difference associated with the cloud radius at stabilization with and without shear for both the single and three-term entrainment equation.

As indicated by the RMS in Table 13, wind shear also has a negligible affect on the cloud radius at stabilization. This is not to say that one more closely predicts the observed radius, because a comparison to observation was not done, only that the wind shear has a stronger impact on the stabilized radius when the additional two terms of the entrainment equation are omitted. Also, while wind shear had the net effect of decreasing cloud top height, it has the net effect of increasing the cloud radius.

D. Code Modification Analysis

In analyzing the modifications to the code, unless otherwise specified, the 1979 DELFIC test case was consistently used as the analysis shot. Additionally, only the given modification was varied. For example, in the case of particle settling during cloud rise, the corrected version of DELFIC without wind shear corrections will be compared to the corrected version of DELFIC without wind shear corrections and the modification of setting the ndstr variable, which controls particle fallout during cloud rise, to zero. Also, in all cases the yield dependent values of the entrainment and eddy viscous drag parameters will be used. The first set of plots in Figure 18 was used to validate the variables that are to be plotted by comparing them to the plots presented by Jodoin in his *Critique of DELFIC's Cloud Rise Module* (15:8). These variables from the uncorrected DELFIC would then be compared against the corrected DELFIC code without wind shear corrections and the corrected DELFIC code with wind shear corrections. The

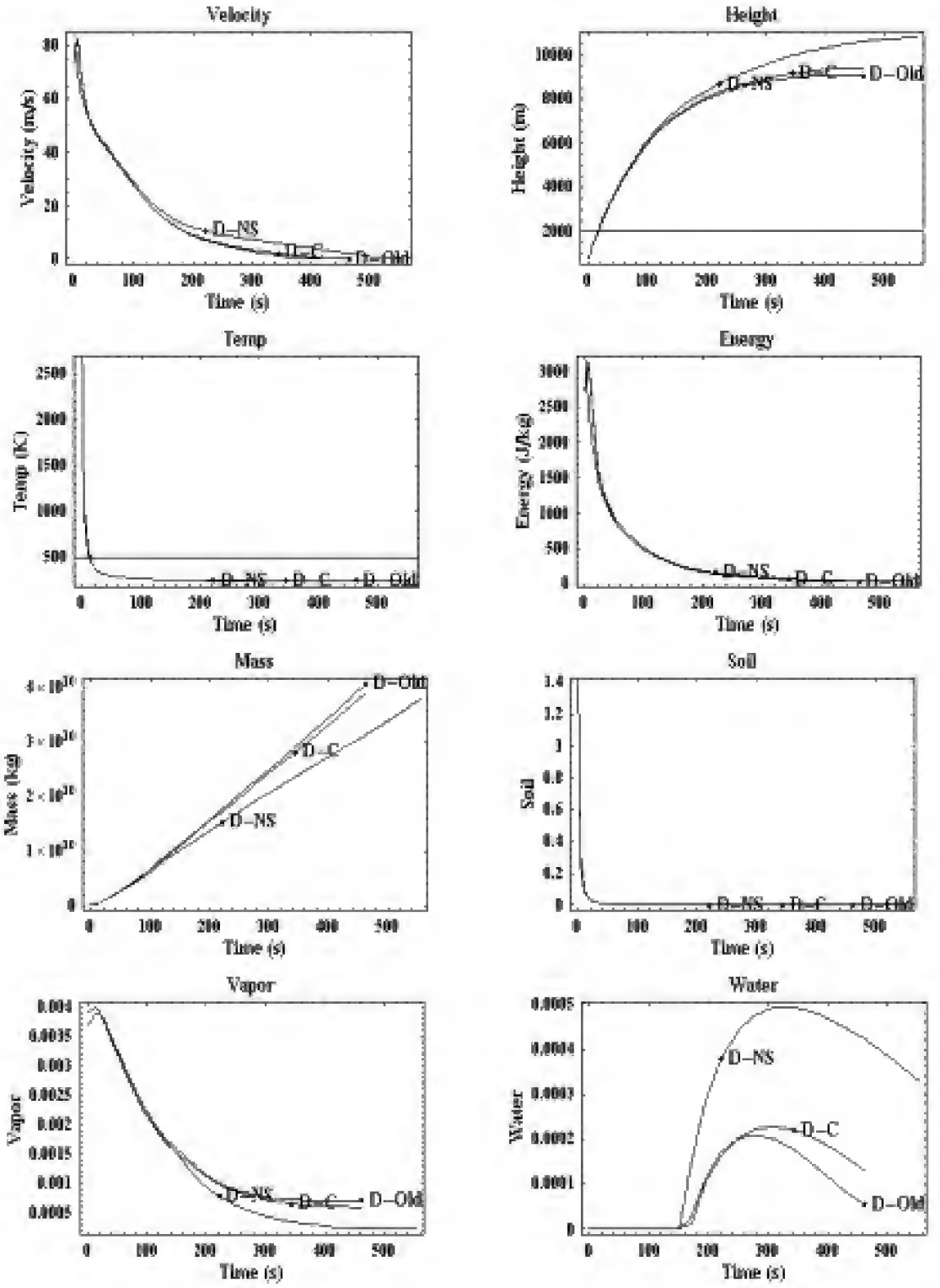

Figure 18. Comparison of the CRM variables for DELFIC uncorrected ("D-Old"), corrected ("D-C"), and corrected without wind shear ("D-NS")

uncorrected DELFIC graphs were in agreement with Jodoin's graphs. It is clear, by the plots in Figure 18, that the corrections listed in Appendix C do not have a large impact on cloud rise variables for this test case. The most noticeable difference is between the corrected case with wind shear and the corrected case without wind shear. This will be examined in more detail later.

The modified DELFIC code without wind shear was then compared to the modified stand-alone HPAC source code provided by the Defense Threat Reduction Agency to ensure good agreement. Since both codes were modified to produce nearly the same behavior in the cloud rise history both graphs should be nearly on top of each other. As expected, and shown in Figure 19, the graphs are very close with only minor variations. It is likely that the variations are due to the changes in the atmospheric table that does have some minor fluctuations.

The next comparisons were done to see what changes would occur when we returned the modifications to their original state in the DELFIC or HPAC codes. This would provide some indication as to what modifications, in going from DELFIC to HPAC, result in significant changes in the predicted cloud dimensions at stabilization.

The first modification considered is that of the particle fallout during cloud rise. The fallout of particles during the cloud rise will increase the buoyancy of the cloud and thus increase the stabilized height. The variations were negligible which verifies what Jodoin states in his *Critique of DELFIC's Cloud Rise Model.* "In the test case as currently modeled in the CRM, fallout's contribution to the buoyancy in the cloud is negligible." (15:14)

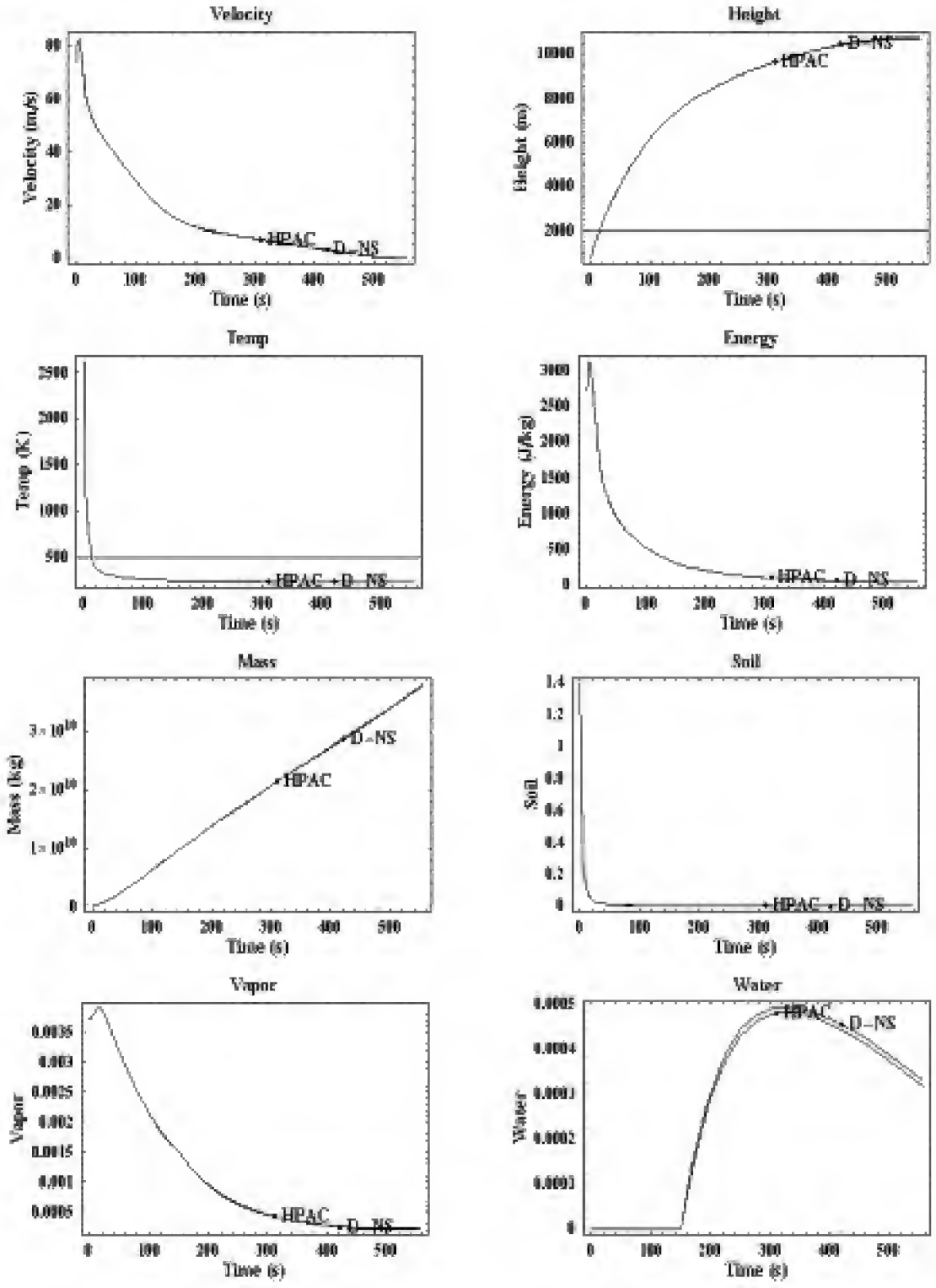

Figure 19. Comparison of the CRM variables for the DELFIC corrected, without wind shear ("D-NS") to the corrected, HPAC code without wind shear ("HPAC")

The next modification considered was the 600-second termination criteria added to HPAC. This condition will terminate the cloud rise after 10 minutes regardless of whether or not the R-Rate switch or turbulent kinetic energy condition are met. It is likely that the condition will have more of an impact on mid range and high yield shots than low yield shots. Since it is apparent that the DELFIC test case does not exceed a 600 second stabilization time another shot will be used. The Climax shot of operation Upshot-Knothole was used for this analysis. The only difference between the two calculations was the early termination at 600 seconds when the condition was active. Making the termination of the cloud time dependent does not make physical sense. The stabilized cloud should be a cloud that is passed to the dispersion model when the conditions are right for diffusive transport, or as stated in the *DELFIC Fundamentals*, when "ambient transport and dispersion of the cloud becomes dominant over internally generated rise and expansion." (13:15)

It was shown in Chapter II that wind shear adds to the mass entrainment equation, therefore, when analyzing the effect wind shear has on the CRM variables we expect to see an increase in the cloud mass and a decrease in the cloud height. In addition to the increase in mass and decrease in cloud height, Figure 20 indicates an early termination when the effect of wind shear is included. Since there is no apparent change in the turbulent kinetic energy, it must be that the radial expansion rate terminated the rise earlier for the case without wind shear. This is in keeping with the earlier statement in Chapter II that the R-Rate switch terminates the majority of high yield shots.

HPAC now provides oscillations in the cloud before stabilization. Oscillations are a physical phenomena observed during some atmospheric tests that stabilize the cloud

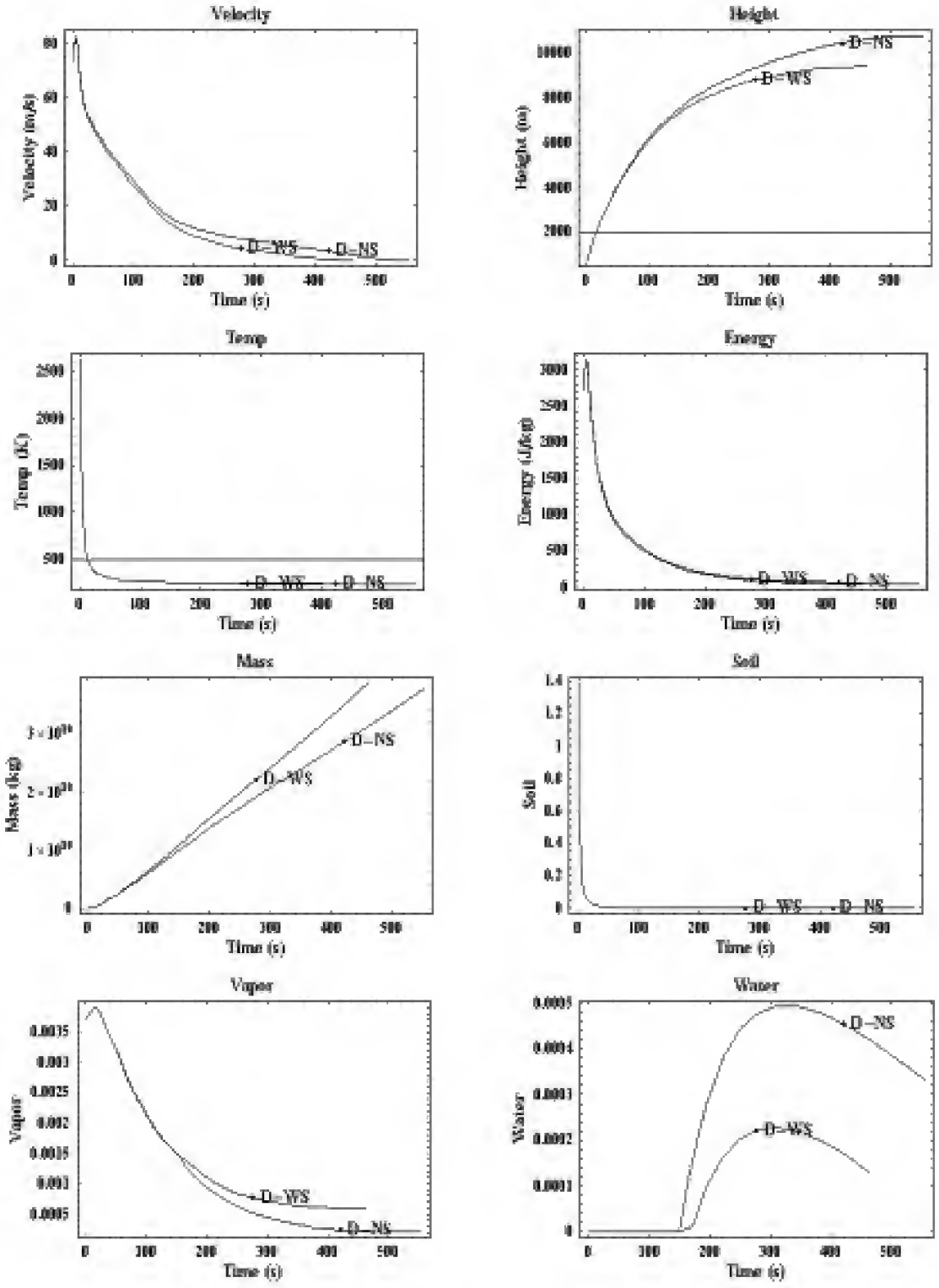

Figure 20. Comparison of the CRM variables for DELFIC corrected with wind shear ("D-WS") and DELFIC corrected, without wind shear ("D-NS")

at a lower altitude than the maximum height obtained.

As it turns out, the DELFIC test case was not an ideal case for showing the effects of cloud oscillation. While a close examination of the cloud history table does show a decrease in cloud top height late in the cloud rise, it is not evident in a plot of the CRM variables. Two cases that do show oscillations are Zuchini from operation Teapot, and Climax from operation Upshot-Knothole. Their plots are depicted in Figure 21 and Figure 22. From these two cases, it can be seen that representing the oscillations of the cloud before stabilization, results in the increase in cloud mass and the decrease in cloud height. This added capability of HPAC does represent a physical phenomenon that happens during some cloud rise calculations. What remains is a determination of whether or not the phenomenon is accurately modeled.

The final analysis was with the expanded atmospheric tables produced by DELFIC and HPAC. Although both codes use an interpolation technique, the exact method of calculations are not the same and lead to minor fluctuations in the tables. A comparison between the two tables showed the magnitude of the difference between the HPAC and DELFIC tables were 0.01 Pa for the pressure, 5×10^{-5} K for the temperature, 2×10^{-5} for the relative humidity, and 5×10^{-6} $\frac{kg}{m^3}$ for the density. The differences in the pressure, temperature, relative humidity, and density were calculated at each altitude level, which had no variation between the HPAC and DELFIC outputs. While there are some definite differences between the two tables, the magnitude of the differences is negligible.

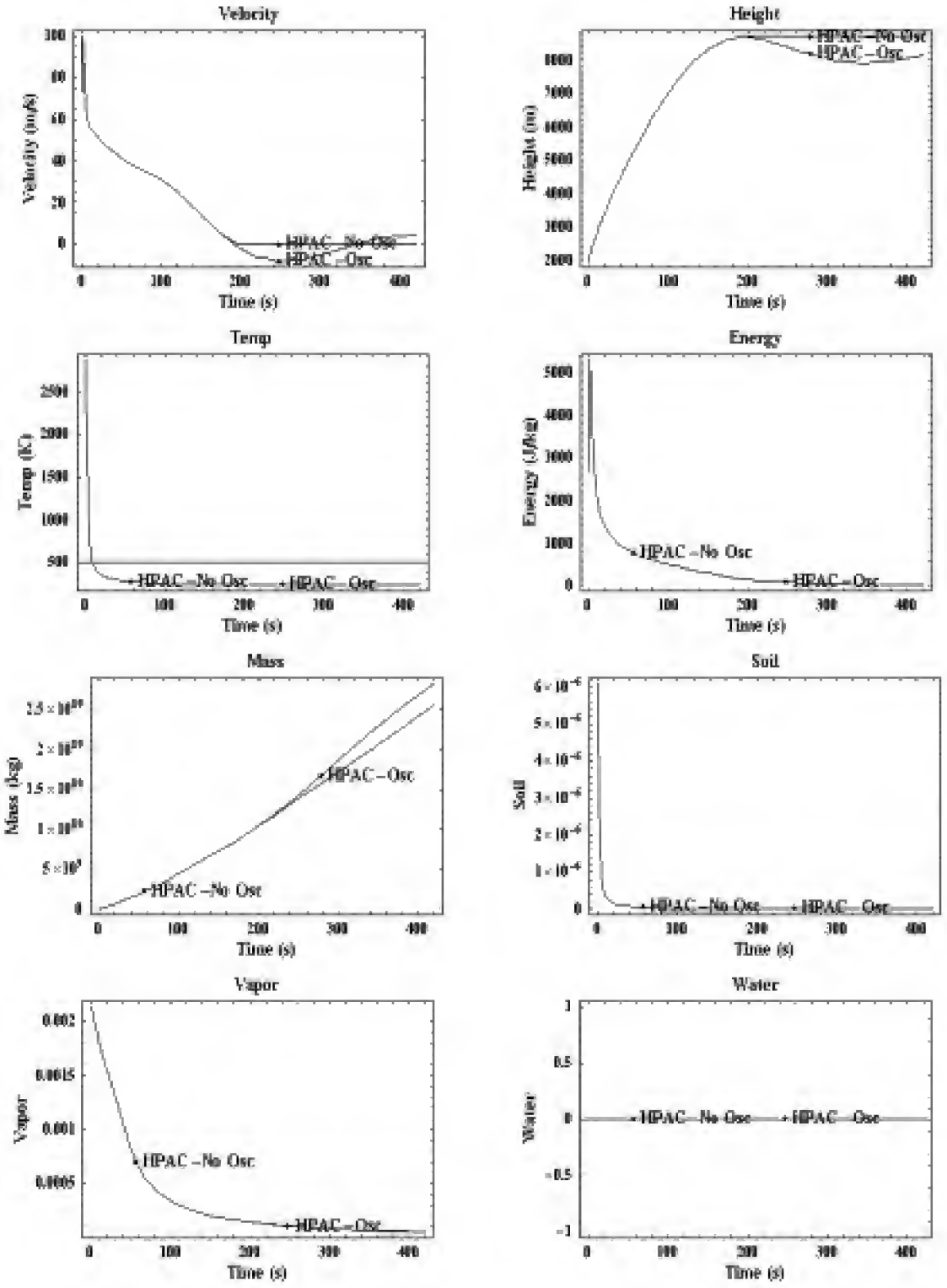

Figure 21. Comparison of the CRM variables for the HPAC code with cloud oscillations ("HPAC-Osc") and the HPAC code without oscillations ("HPAC-No Osc") for shot Zuchini of operation Teapot

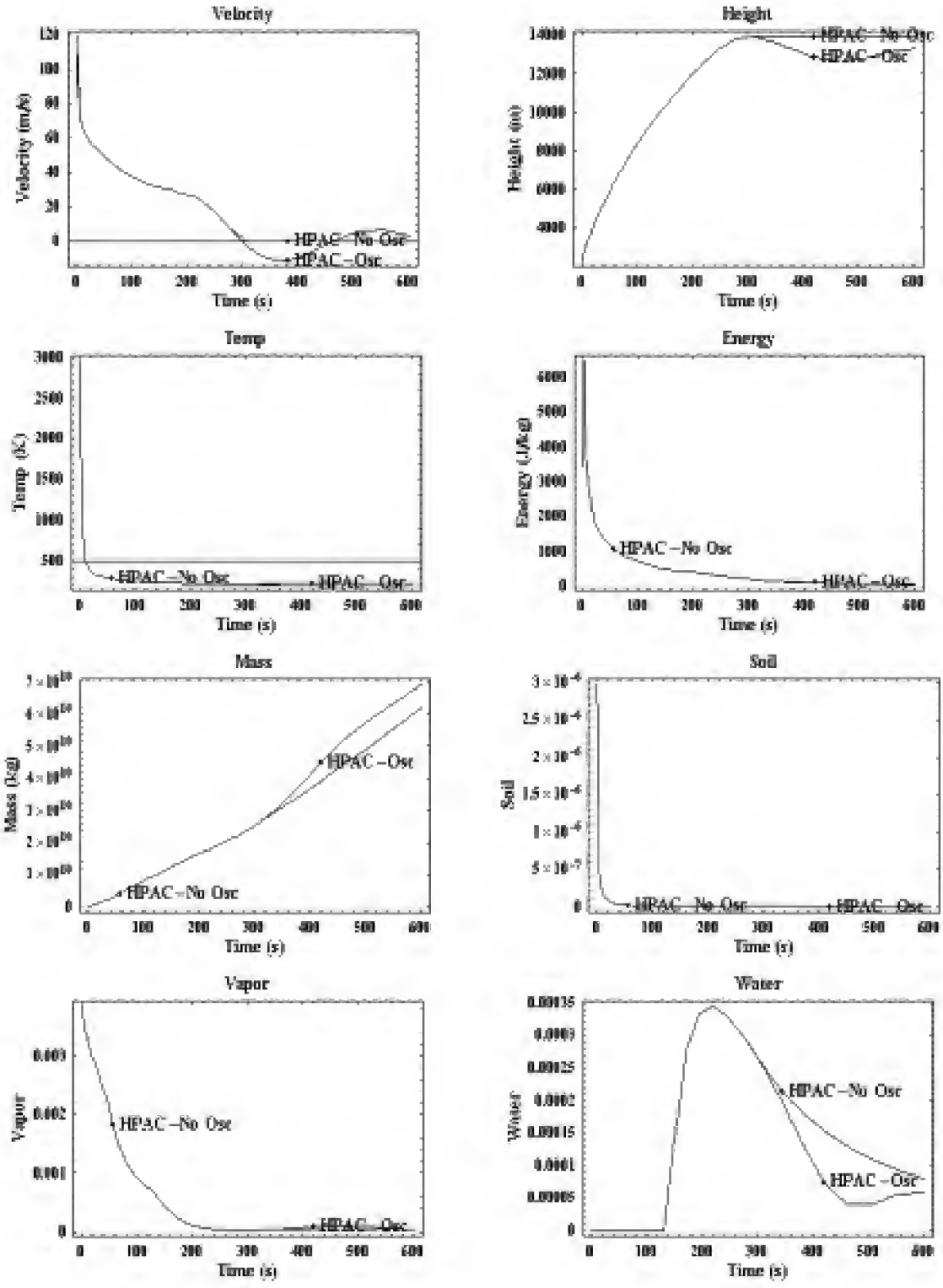

Figure 22. Comparison of the CRM variables for the HPAC code with cloud oscillations ("HPAC-Osc") and the HPAC code without oscillations ("HPAC-No Osc") for shot Climax of operation Upshot-Knothole

E. HPAC Weather Files

The differences in the atmospheric tables between the HPAC stand-alone source code and the 1979 corrected version of DELFIC are minor. The differences between the weather input files and the weather files used in the DELFIC model are more significant. The cloud rise for the HPAC software uses a weather file, newtrans.met, that is created based on the user input atmospheric file. HPAC's weather input file is limited to 25 atmospheric levels, while the HPAC stand-alone code and DELFIC are not. An analysis of several input files showed that HPAC takes the weather input from the user and calculates the pressure using U.S. standard atmosphere for each altitude level in the input file to create the newtrans.met file, regardless of what pressures are input. The method used to calculate the temperature and relative humidity at each level could not be determined. However, these conditions are dependent on the user input pressures. Modifications to the pressures in the input file, while holding temperature and relative humidity constant, do result in changes to the temperatures and relative humidity in the newtrans.met file.

To verify the modifications to the weather file, the user input file for atmospheric shot Annie, operation Upshot-Knothole was compared to the newtrans.met output file as shown in Table 14. The output file ends at 12192.0 meters because 12000.0 meters was used as the maximum height for the cloud rise. Altitudes were not affected between the input and the output files.

Figure 23 provides some indication to the significance of the file modification. Clearly, the most significant changes occur in the relative humidity values. Lamarche

discusses the impact of relative humidity on cloud top height and cloud base in his thesis (14:55-57).

Table 14. Input/Output weather file comparison for HPAC software

Input Values				Output Values		
Altitude (m)	Pressure (mb)	Temp (°C)	Relative Humidity (%)	Pressure (mb)	Temp (°C)	Relative Humidity (%)
1290.8	866	7.9	38	867.4	8.0	38.1
1828.8	816	6.8	32	811.9	6.4	33.1
2438.4	757	3.0	33	752.5	2.5	34.3
3048.0	700	-1.2	34	696.7	-1.6	34.7
3657.6	648	-6.2	29	644.3	-6.6	28.3
4267.2	599	-11.5	31	595.1	-12.0	28.9
4876.8	554	-16.0	32	549.1	-16.7	29.0
5486.4	509	-19.7	31	505.9	-20.2	26.8
6096.0	470	-24.1	0	465.5	-24.8	0.1
6705.6	432	-29.5	0	427.8	-30.2	0.0
7315.2	398	-34.0	0	392.6	-34.9	0.0
7924.8	365	-40.0	0	359.8	-41.0	0.0
8534.4	332	-45.5	0	329.3	-46.1	0.0
9144.0	304	-51.5	0	300.8	-52.2	0.0
9753.6	278	-55.8	0	274.4	-56.6	0.0
10363.2	250	-60.5	0	249.9	-60.5	0.0
10972.8	228	-64.5	0	227.3	-64.7	0.0
11582.4	205	-56.5	0	206.4	-56.1	0.0
12192.0	188	-53.0	0	187.5	-53.2	0.0
12801.6	171	-53.0	0			
13411.2	155	-55.2	0			
14020.8	142	-57.3	0			
14630.4	129	-60.2	0			
15240.0	118	-62.9	0			

As a further test, the resulting weather file, newtrans.met, was used as the input file for a subsequent run. The new resulting weather file, newtrans.met, matched the input file with the exception of the relative humidity values. The final non-zero relative humidity remained fixed, while the other values were perturbed. Table 15 illustrates the subsequent changes for three sequential runs of shot Annie, operation Upshot-Knothole. The altitude, pressure, and temperature remained constant, however the relative humidity has changed for each run.

Subsequent runs of the same shot, using the output weather file as an input weather file results in a perturbation of the relative humidity. Figure 24 shows the level

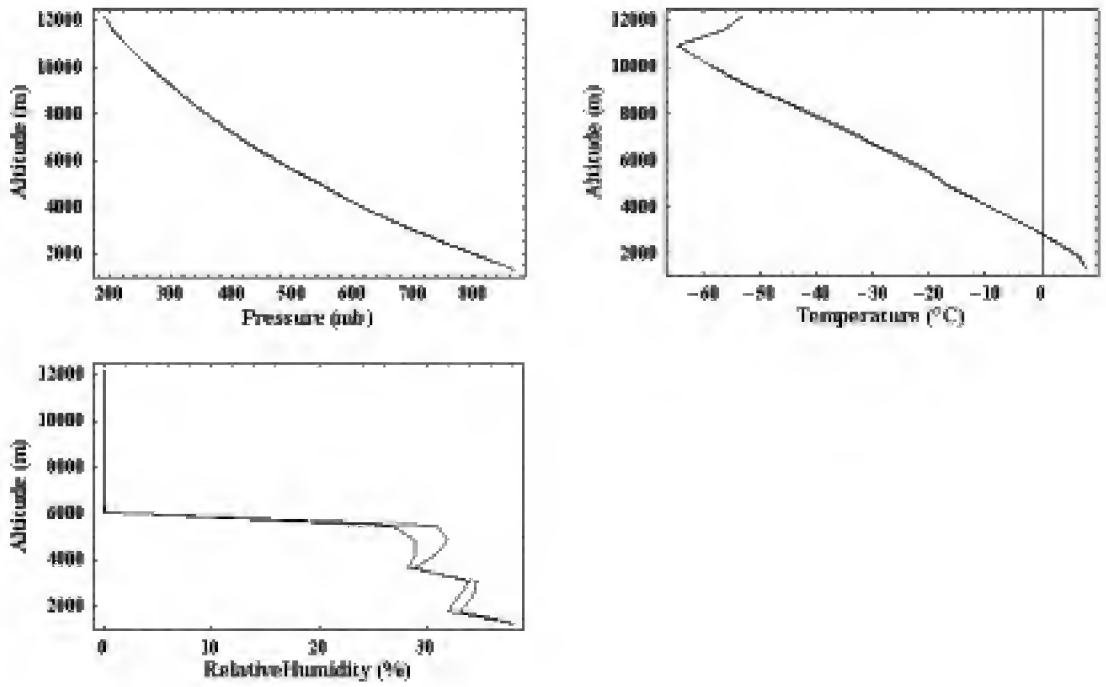

Figure 23. Comparison plots for input/output HPAC weather files

Table 15. Relative humidity comparison for shot Annie, operation Upshot-Knothole

Altitude	Pressure	Temp	Rel Hum Init	Rel Hum 1	Rel Hum 2	Rel Hum 3
1290.8	867.4	8.0	38	38.1	38.5	38.9
1828.8	811.9	6.4	32	33.1	33.5	33.9
2438.4	752.5	2.5	33	34.3	34.6	34.9
3048.0	696.7	-1.6	34	34.7	34.5	34.3
3657.6	644.3	-6.6	29	28.3	26.8	25.4
4267.2	595.1	-12.0	31	28.9	26.0	23.4
4876.8	549.1	-16.7	32	29.0	24.9	21.4
5486.4	505.9	-20.2	31	26.8	22.3	18.5
6096.0	465.5	-24.8	0	0.1	0.1	0.1
6705.6	427.8	-30.2	0	0.0	0.0	0.0
7315.2	392.6	-34.9	0	0.0	0.0	0.0
7924.8	359.8	-41.0	0	0.0	0.0	0.0
8534.4	329.3	-46.1	0	0.0	0.0	0.0
9144.0	300.8	-52.2	0	0.0	0.0	0.0
9753.6	274.4	-56.6	0	0.0	0.0	0.0
10363.2	249.9	-60.5	0	0.0	0.0	0.0
10972.8	227.3	-64.7	0	0.0	0.0	0.0
11582.4	206.4	-56.1	0	0.0	0.0	0.0
12192.0	187.5	-53.2	0	0.0	0.0	0.0

to which the relative humidity is changed, given no change in input altitudes, pressures, or temperatures. This behavior could not be studied further since the method of calculating the temperature, and relative humidity could not be determined.

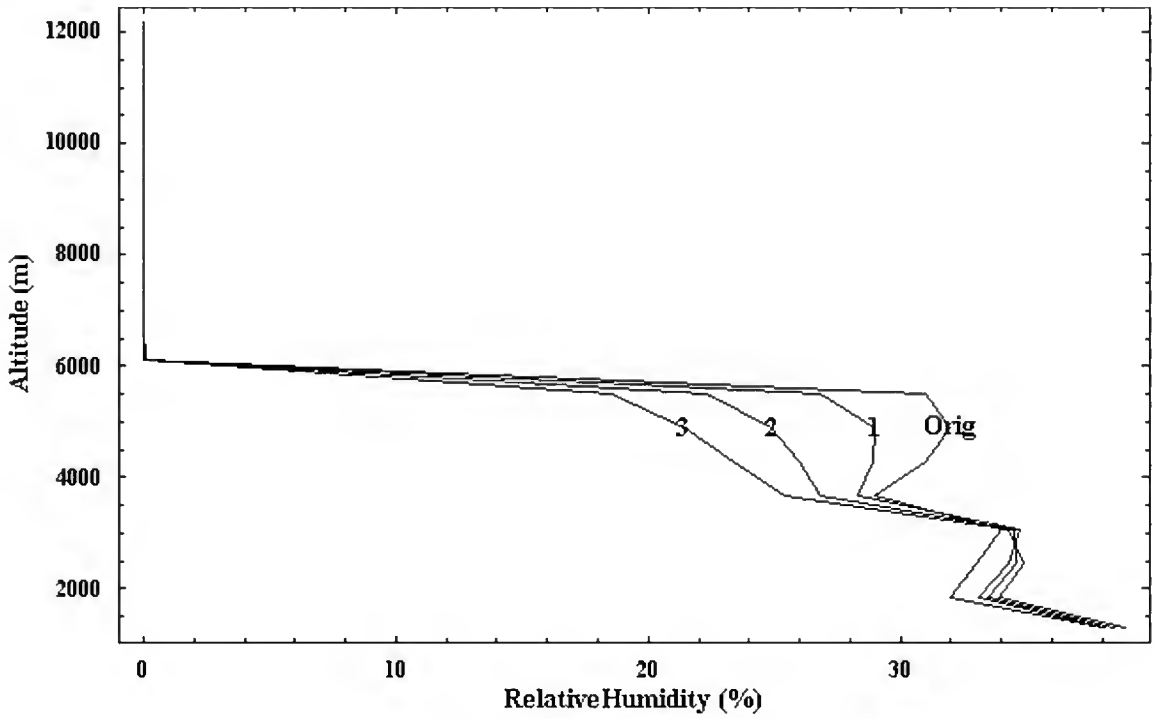

Figure 24. Perturbation of the relative humidity for subsequent runs in HPAC, original input "Orig", subsequent outputs "1", "2", "3"

These changes in the input files will make comparisons between DELFIC codes or the HPAC stand-alone source code, where atmospheric input files are comparable, and the HPAC packaged software somewhat questionable. They were, however, useful in determining which code better represents observed values given the level of detail in atmospheric information that was available for previous test shots.

IV - Summary and Conclusions

This chapter will summarize the analysis and present conclusions to the problems identified in Chapter I, based on both the analysis and theory. A final recommendation is then made concerning the form of the mass entrainment equation used to model the cloud rise from an atomic detonation. Specifically, recommendations relating to the cloud rise model are made on the use of constant versus yield dependent entrainment and eddy viscous drag parameters, the use of a single versus a three-term entrainment equation, and finally, the inclusion of wind shear versus the omission of wind shear. Finally, a summary of the changes made and the effect of the changes are presented for the inclusion of the DELFIC cloud rise model into HPAC.

A. Constant Versus Yield Dependent Parameters

From a strictly empirical stand point, the question of constant or yield dependent parameters goes back to the FRMS and FMD values calculated during the analysis. Do the FRMS values for the yield dependent parameters better represent the observed values than the optimized constant values for the parameters?

Table 16. Figure of merit comparison for tested cases

Figure of Merit	Corrected	Case 1	Case 2	Case 3	Case 4
FMD	0.118	0.023	0.061	0.046	0.050
FRMS	0.235	0.231	0.228	0.224	0.221

Using the figures of merit in Table 16 a constant value for the entrainment and eddy viscous drag parameters better represents the observed in all cases. The next question is whether the yield dependent fits proposed by Norment can be improved to produce better results than shown. Figure 25 through Figure 28 presents the optimized

parameter values for entrainment and eddy viscous drag for each of the 64 atmospheric test shots and the yield dependent fit equations proposed by Norment for each of the four cases.

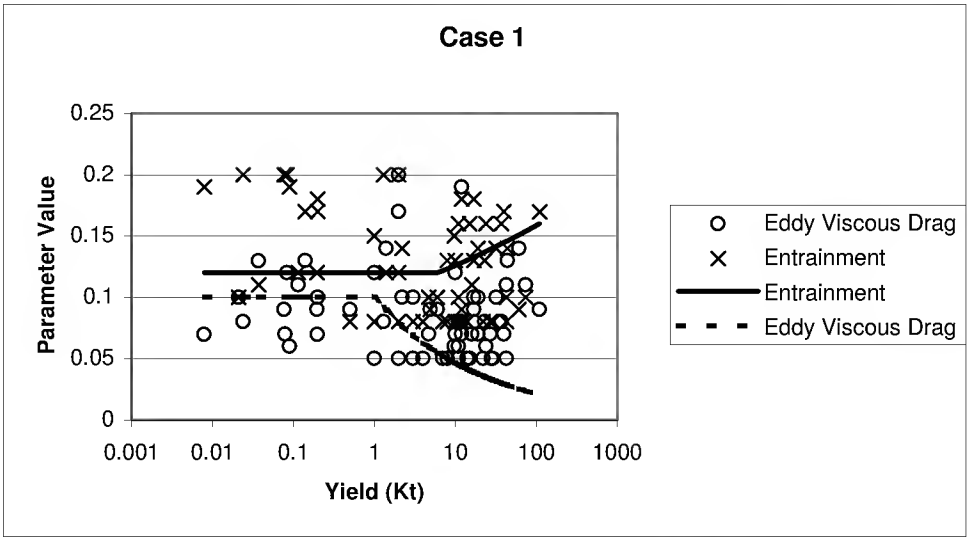

Figure 25. Yield dependent parameter comparison for Case 1

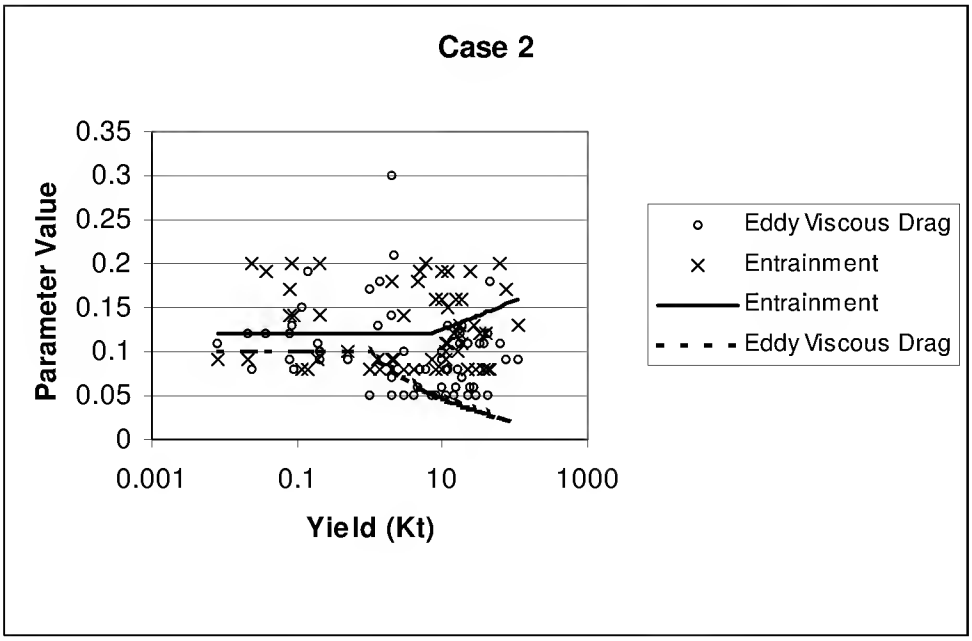

Figure 26. Yield dependent parameter comparison for Case 2

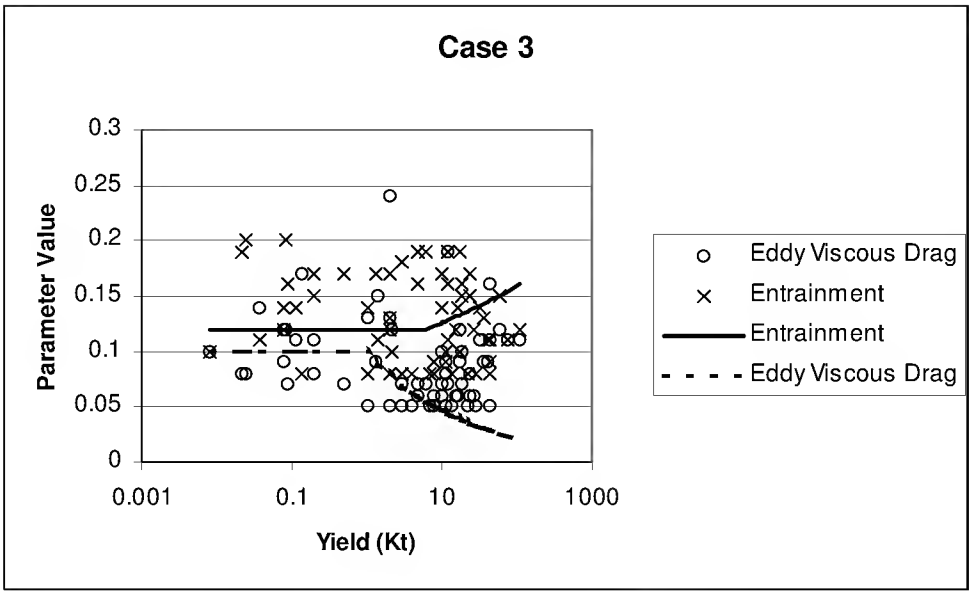

Figure 27. Yield dependent parameter comparison for Case 3

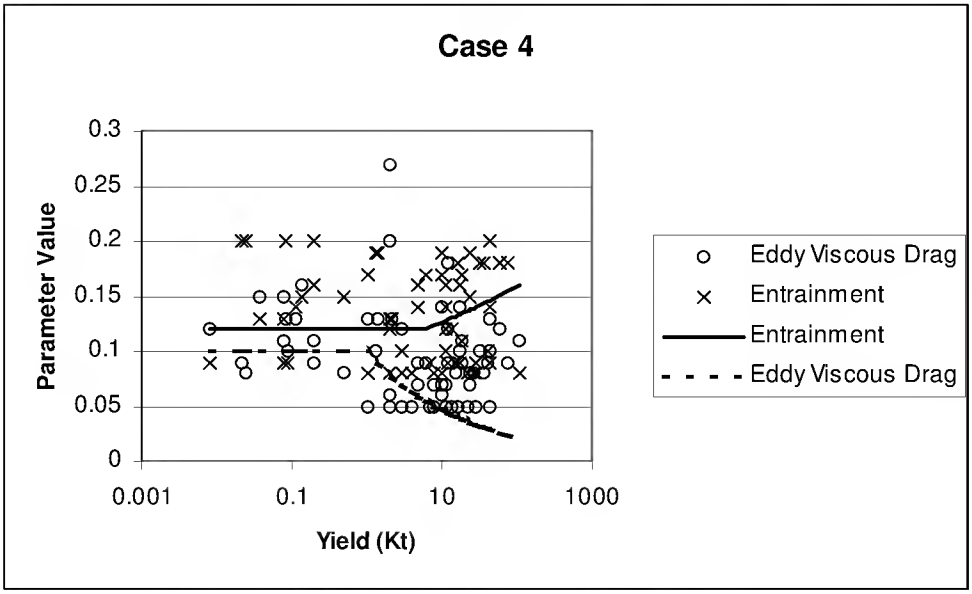

Figure 28. Yield dependent parameter comparison for Case 4.

It cannot be concluded that any of the four cases are well represented by the yield dependent fits proposed by Norment. The erratic behaviors of the points on the graphs do not suggest any yield dependence for the two values. The best constant values identified in Table 5 would be a line approximately through the middle of the scattering for each of

the cases. From a physical perspective any dependence associated with the entrainment or eddy viscous drag, such as, rise velocity, surface to volume ration, and atmospheric densities are accounted for in the coupled differential equations of Appendix A. Therefore, it is recommended that constant values for the entrainment and eddy viscous drag parameters should be adopted in lieu of the yield dependent fits currently used. The values for the parameters should be the suggested values in Table 5.

Before we can determine what set of values to use from Table 5, we must first determine which case best models the cloud rise, not only from an empirical (gives the best value) approach, but from a physical (best represents the physics) approach.

B. Three-term Versus Single-term Entrainment Equation

When determining whether the mass entrainment equation is best represented by the single-term equation, as presented by Huebsch, or the three-term equation, as presented by Norment, we consider both the results of the figures of merit for each case and the legitimacy of Norment's development.

It is clear after examination of the figures of merit in Table 16, that the single-term mass entrainment equation provides a lower absolute error between observed and calculated cloud top heights than the three-term mass entrainment equation. From a more physical perspective, several problems exist with the use of the three-term entrainment equation.

Huebsch pointed out several physical flaws in the development of the equation as mentioned in Chapter II, Section B. Jodoin also points out a problem in Norment's use of empirical fits to represent cloud dimensions in his derivation, which Norment later abandons when defining the cloud as an oblate spheroid of eccentricity 0.75 during the

early rise of the cloud. A final problem with the development is the adoption of constant values for the entrainment and eddy viscous drag parameters. As indicated by Huebsch, Norment used an entrainment parameter that was an increasing function of yield in his development to offset the significant increase in mass for low yields during the early rise times. (8:12) By adopting a constant entrainment parameter, the non-physical properties identified by Huebsch are introduced during early rise times for low yield shots. Specifically, "physically implausible increases in cloud mass." (8:12)

We recall from Chapter II, Section B that Norment's development of the three-term equation was to better represent the cloud rise, particularly at early times. Appendix E provides a closer looks at the cloud rise history of several shots. These plots illustrate that the three-term entrainment equation, with or without a wind shear correction, does not provide any increase in fidelity of the model, and in fact, in many cases actually provides a less accurate representation. In the case of the cloud rise history plots in Appendix E, error bars given by Table 1 are included in the observed points, but are insignificant in comparison to the scale.

Based on the empirical evidence and physical argument, the single-term entrainment equation is recommended for the modeling of cloud rise. Since the single-term equation is recommended, high yield shots do not present the square root domain problem that was introduced in Chapter III, Section A. Therefore, the three high yield shots identified by Table 17 were introduced into the analysis.

Table 17. High Yield Shots

Shot Name	Operation	Yield (kt)	HOB (m)
Zuni	Redwing	3500	2.7
Tewa	Redwing	5000	4.6
Bravo	Castle	15000	2.1

The analyses for the three additional shots in Table 17 are given in Table 18 and Table 19. The addition of the high yield shots had a slight effect on the FMD and FRMS for the corrected case, as well as Case 3 and Case 4. In all cases the figures of merit were decreased, however, not to such a degree as to change the order of precedence. The analysis showed no change in the recommended entrainment and eddy viscous drag parameters of Table 5.

Table 18. Cloud Top Comparison of Additional High Yield Shots for Case 3

Shot	Yield (kt)	Observed Cloud Top (m)	Calculated Cloud Top(m)		Fractional Deviation	
			Corrected	Modified	Corrected	Modified
Zuni	3500	24076	27341	27961	-0.136	-0.161
Tewa	5000	30171	29398	30537	0.026	-0.012
Bravo	15000	34745	37085	37427	-0.067	-0.077
				FMD	**0.110**	**0.040**
				FRMS	**0.231**	**0.220**

Table 19. Cloud Top Comparison of Additional High Yield Shots for Case 4

Shot	Yield (kt)	Observed Cloud Top (m)	Calculated Cloud Top(m)		Fractional Deviation	
			Corrected	Modified	Corrected	Modified
Zuni	3500	24076	27341	27933	-0.136	-0.160
Tewa	5000	30171	29398	30449	0.026	-0.009
Bravo	15000	34745	37085	37374	-0.067	-0.076
				FMD	**0.110**	**0.044**
				FRMS	**0.231**	**0.217**

C. Wind Shear Requirement

Based on the recommendation of constant parameter values and the single-term entrainment equation, all that remains is the question of whether a wind shear correction should be used in the cloud rise model. Once again, this is considered from both the empirical and the physical perspective.

Empirically, there is little difference in the FRMS of Case 3, with wind shear, and Case 4, without wind shear. The FRMS value without wind shear was; however, slightly better as indicated by Table 18 and Table 19. Conversely, the calculations with wind shear resulted in less under prediction than the calculations without wind shear. Keep in mind, that while the figures of merit do indicate one method with a lower absolute error and one with a lower potential for over predicting, the analysis indicates that the differences associated with and without wind shear calculations are negligible when compared to the approximations used in the development of the model. Next, consider a comparison between the observed and calculated cloud radius using the recommended single-term entrainment equation with the optimized parameters for the cases of with and without wind shear corrections. That is, an examination of Case 3 and Case 4. Only a limited number of shots have the cloud radius tabulated. Table 20 shows that when wind shear is accounted for, there is slightly less under prediction and error in the stabilized cloud radius.

Before concluding, since it has been determined a single term equation is more representative of cloud rise dynamics and the FRMS between a single-term equation with and without wind shear is so close, a perturbing of the wind shear constant in Equation (27) was considered. The constant was varied between 0.0 and 1.0 in steps of 0.05. It was determined that the cloud top height at stabilization was optimized for a k_6 value of 0.85. The optimum value, however, resulted in no change to the FRMS of the test cases, but did improve the FMD from 0.04 to 0.037.

Table 20. Cloud Radius Comparison with and without Wind Shear for a 1-Term Entrainment Equation with Constant Parameter Values

Shot	Yield (kt)	Observed Cloud Radius (m)	Calculated Cloud Radius (m)		Fractional Deviation	
			With Shear	Without Shear	With Shear	Without Shear
Wasp	1	2286	1206	919	0.473	0.598
Moth	2	1250	1164	1077	0.069	0.139
Post	2	1844	1121	1084	0.392	0.412
Ha	3	1235	1975	1921	-0.600	-0.556
Hornet	4	3201	1442	1315	0.550	0.589
Tesla	7	1661	1613	1610	0.029	0.031
Bee	8	2286	1699	1682	0.257	0.264
Apple1	14	3810	1966	1880	0.484	0.507
Zuchini	28	2286	2593	2431	-0.135	-0.063
Apple2	29	5639	2537	2392	0.550	0.576
Lacrosse	40	4847	3132	2901	0.354	0.402
Turk	43	4755	2995	2851	0.370	0.400
Zuni	3500	12802	19116	16286	-0.493	-0.272
Bravo	15000	26124	22571	22674	0.136	0.132
				FMD	**0.174**	**0.226**
				FRMS	**0.395**	**0.403**

From a physical perspective, wind shear does have an effect on the cloud rise, but there is no evidence to conclude that the method used provides an accurate representation of the effects during an atomic cloud rise. In fact, a look at the optimum wind shear parameter values in Table 23, Appendix F, indicate that about half the cloud top heights from our test shots are improved using a wind shear correction, while approximately half are improved without a wind shear correction. Based on this, there is no reason to believe that incorporating wind shear corrections results in an improvement to the fidelity or physical representation of observed cloud dimensions.

Now, a revised recommendation can be made concerning the form of the parameters, the number of terms of the entrainment equation and the inclusion of wind shear calculation. Based on the analysis, a single-term entrainment equation without

wind shear calculations and constant entrainment and eddy viscous drag parameters should be used in the cloud rise model. The constant parameter values should be the values identified by Table 5, Case 4.

D. Code Modifications and the Impact on Parameter Values

The analysis of modifications to the HPAC code consisted of a comparison between the 1979 version of DELFIC with the corrections, identified by Appendix C, to a stand-alone HPAC code that was constructed from the HPAC source code for the cloud rise, provided by the Defense Threat Reduction Agency for the purposes of this thesis. The HPAC source code is the DELFIC cloud rise model with some modifications to enhance performance, fix identified problems, and take advantage of new programming capabilities in FORTRAN. A detailed listing of the modifications can be found in Appendix D. It is recognized that while this analysis is useful in identifying the impact the modifications had on incorporating the DELFIC code into HPAC, it is limited only to changes within the cloud rise source code. Any data manipulation that takes place between the user interface and the cloud rise code that impacts the cloud rise calculations was not studied and therefore, cannot be addressed directly.

Of all the modifications, only two had a noticeable impact on final cloud top height, wind shear and the oscillation capability. In the previous section of this chapter the recommendation was made not to include the wind shear correction in the calculation. Since the cloud oscillation is a physical phenomenon of atomic cloud rise, and it is now part of the cloud rise model, it must be determined what effect, if any, it has on the parameters we have defined, and whether or not the phenomenon is accurately modeled. A final constant value parameter comparison was made between Case 4, which was the

recommended case, and a modified Case 4 that includes the oscillation capability. This comparison indicated much different optimized constant values for the entrainment and eddy viscous drag parameters that are identified for Case 4 in Table 5. The new parameter value comparison is given in Table 21. The range used for the eddy viscous drag parameter had to be changed since the optimum value during the first test was the maximum of the original range. The new range for the eddy viscous drag parameter was 0.15 through 0.27.

Table 21. Parameter comparison of Case 4 with and without cloud oscillations

Case 4	Entrainment Parameter	Eddy Viscous Drag Parameter
Without Oscillations	0.12	0.08
With Oscillations	0.06	0.26

The cloud top height comparison is in Table 24, Appendix G. Oscillations, while physically meaningful not only detracts slightly from the fidelity of the model, but physical problems exist with the oscillation modeling. Since the oscillations occur only in the final stages of the cloud rise, it would be expected that any change in the entrainment of the atmosphere and drag on the cloud would be minimum, while the changes indicated by Table 21 are drastic. Additionally, during an actual cloud oscillation, the cloud shrinks and heats as it falls as depicted in Figure 1, yet the modeling fixes the vertical thickness of the cloud when the rise velocity reaches apogee and the horizontal dimension continues to expand. Since it cannot be shown that the current method of modeling the cloud oscillation accurately models the phenomenon, it is recommended that this capability be eliminated from the code and further study be done.

The final comparison considers the packaged HPAC software, the recommended DELFIC case, and the HPAC stand-alone software. As before, all heights are relative.

The HPAC software was run using the terrain option with the latitude and longitude locations specified by DASA 1251. The 25 atmospheric levels consisted of a sampling of the atmospheric tables used as input to the HPAC stand-alone case and Case 4. Results of the comparison are in Appendix H along with more specific information on the atmospheric levels used.

Several reasons may contribute to the differences between the packaged HPAC software and the stand-alone version. First, the particle distribution information has not been included in the stand-alone version, which means that particle fallout during rise is not considered. The analysis of Chapter III, Section D indicates that the effect of particle fallout during cloud rise for the test case is negligible, however, the effect may vary for any given shot. The more likely cause is the differences between the weather input file and the weather output file that was discussed in Chapter III, Section E.

As a final recommendation, the DELFIC cloud rise model that has been included as an option in the packaged HPAC software should be modified to run using a single term entrainment equation without wind shear, without cloud oscillations, and with constant parameter values as indicated by Table 5. The cloud rise model should read in the weather input file that is created by the user, and not a modified file created by the program. Additionally, the number of levels should not be limited to 25.

This analysis has shown that by making the necessary corrections in Appendix C, and making the recommended modifications identified in the above paragraph, a rise model can be achieved that more accurately predicts the observed behavior of atomic cloud rise. A model based on better representation of historical clouds should then provide a model that more accurately predicts future detonations.

E. Final Recommendation

The final recommendation is a single-term entrainment equation without wind shear corrections, without cloud oscillations, and with constant entrainment and eddy viscous drag parameters as given by Case 4 in Table 5. As a minimum, the corrections identified by Jodoin (15) and restated in Appendix C should be incorporated into the HPAC code, the single-term entrainment equation should replace the three-term entrainment equation, and the current method of calculating the cloud oscillations should be removed. The corrections and single-term entrainment equation simply provide a more accurate representation of the model as it was developed. The oscillations clearly influence the parameter values for the entrainment and eddy viscous drag. The current yield dependent method of calculating the values, while somewhat close for the DELFIC model, is not close for the HPAC model that allows for cloud oscillations.

In addition to the final recommendation, additional work is needed to develop a wind shear model that accurately predicts the influence of wind during cloud rise. This becomes more critical when you consider actual fallout predictions will likely have to be done under far more adverse wind conditions than those experienced during U.S. atmospheric test shots. The method of calculating the oscillatory behavior of the cloud should also be researched further to correctly model this phenomenon.

Appendix A. Cloud Equations

A. Dry Equations

$$\frac{du}{dt}=\left(\frac{T^*}{T_e^*}\beta'-1\right)g-\left(\frac{2k_2\mathrm{v}}{H_c}\frac{T^*}{T_e^*}\beta'+\frac{1}{m}\frac{dm}{dt}\right)u \tag{31}$$

$$\frac{dT}{dt}=-\frac{\beta'}{\bar{C}_p(T)}\left[\frac{T^*}{T_e^*}gu+\left(\int_{T_e}^{T}C_{pa}(T)dT\right)\frac{1}{\beta' m}\frac{dm}{dt}\bigg|_{ent}-\varepsilon\right] \tag{32}$$

$$\frac{dE}{dt}=2k_2\frac{T^*}{T_e^*}\beta'\frac{u^2\mathrm{v}}{H_c}+\frac{u^2}{2}\frac{1}{m}\frac{dm}{dt}\bigg|_{ent}-E\frac{1}{m}\frac{dm}{dt}\bigg|_{ent}-\varepsilon \tag{33}$$

$$\frac{dm}{dt}\bigg|_{ent}=\frac{\beta' m}{1-\frac{\beta'}{T^*\bar{C}_p}\int_{T_e}^{T}C_{pa}(T)dT}\left\{\frac{S}{V}\mu\mathrm{v}+\frac{\beta'}{T^*\bar{C}_p}\left[\frac{T^*}{T_e^*}gu-\varepsilon\right]-\frac{gu}{R_aT_e^*}\right\} \tag{34}$$

$$\frac{ds}{dt}=-\frac{1}{\beta'}\frac{1+x}{1+x_e}s\frac{1}{m}\frac{dm}{dt}\bigg|_{ent}-\frac{1+x+s+w}{m}\left(\frac{s}{s+w}\right)F \tag{35}$$

$$\frac{dx}{dt}=-\frac{1+x+s}{1+x_e}(x-x_e)\frac{1}{m}\frac{dm}{dt}\bigg|_{ent} \tag{36}$$

$$\frac{dw}{dt}=-\frac{1}{\beta'}\left(\frac{1+x}{1+x_e}\right)(w+x-x_e)\frac{1}{m}\frac{dm}{dt}\bigg|_{ent}-\frac{dx}{dt} \tag{37}$$

$$\varepsilon=\frac{k_3(2E)^{\frac{3}{2}}}{H_c} \tag{38}$$

$$\mathrm{v}=Max\left(u,\sqrt{2E}\right) \tag{39}$$

B. Wet Equations

$$\left.\frac{dm}{dt}\right|_{ent} = \frac{\beta' m}{1-\frac{1}{T^*}\left[\frac{\beta'}{1+\frac{L^2 x\varepsilon}{C_p R_a T^2}}\right]\left[T-T_e+\frac{L(x-x_e)}{C_p}\right]}\left\{\frac{S}{V}\mu v+\frac{\frac{\beta'}{T^*}}{\frac{L^2 x\varepsilon}{C_p R_a T^2}}\left[\frac{guT^*}{T_e^* C_p}\left(1+\frac{Lx}{R_a T}\right)-\frac{\varepsilon}{C_p}\right]-\frac{gu}{R_a T_e^*}\right\} \quad (40)$$

$$\frac{dT}{dt} = -\frac{\beta'}{1+\frac{L^2 x\xi}{C_p R_a T^2}}\left\{\left[(T-T_e)+\frac{L(x-x_e)}{C_p}\right]\frac{1}{m\beta'}\left.\frac{dm}{dt}\right|_{ent}+\frac{T^*}{T_e^*}\frac{g}{C_p}u\left(1+\frac{Lx}{R_a T}\right)-\frac{\varepsilon}{C_p}\right\} \quad (41)$$

$$\frac{1}{x}\frac{dx}{dt} = \left(1+\frac{x}{\xi}\right)\frac{L\xi}{R_a T^2}\frac{dT}{dt}+\left(1+\frac{x}{\xi}\right)\frac{g}{R_a T_e^*}u \quad (42)$$

Appendix B. Entrainment Equations

This derivation will start with equation (21) with the ratio of cloud gas density to total cloud density included.

$$\left.\frac{dm}{dt}\right|_{ent} = \beta' m \frac{S}{V}\mu u - \frac{\beta' m}{T}\frac{dT}{dt} + \frac{\beta' m}{P}\frac{dP}{dt}$$

Given the universal gas law in the form

$$V = m\beta' \frac{R_a T^*}{P} \rightarrow P = \frac{m\beta'}{V} R_a T^*$$

the relationship

$$\frac{\rho_e}{\rho} = \frac{T^*}{T_e^*}\beta' \rightarrow \rho_e = \frac{\rho T^* \beta'}{T_e^*} = \frac{mT^*\beta'}{VT_e^*}$$

Norment's equation 1.4D (7:8)

$$\frac{dT}{dt} = -\frac{\beta'}{\overline{C_p(T)}}\left[\frac{T^*}{T_e^*}gu + \left(\int_{T_e}^{T} C_{pa}(T)dT\right)\frac{1}{\beta' m}\left.\frac{dm}{dt}\right|_{ent} - \varepsilon\right]$$

Norment's equation 1.2 (7:4) and the hydrostatic law

$$\frac{dz}{dt} = u \qquad \frac{dP}{dz} = -\rho_e g$$

Consider first, the third term of the entrainment equation.

$$\frac{\beta' m}{P}\frac{dP}{dt} = \frac{\beta' m}{P}\left(\frac{dP}{dz}\frac{dz}{dt}\right) = \frac{\beta' m}{P}\left(-\rho_e g u\right) = \frac{\beta' m}{P}\left(-\frac{mT^*\beta'}{VT_e^*}gu\right)$$

$$\frac{\beta' m}{P}\left(-\frac{mT^*\beta'}{VT_e^*}gu\right) = \frac{\beta' m}{\frac{m\beta'}{V}R_a T^*}\left(-\frac{mT^*\beta'}{VT_e^*}gu\right) = -\frac{\beta' m g u}{R_a T_e^*}$$

This we recognize at the third term of Norment's equation1.7D (7:13) Substituting this back into the entrainment equation we started with and substituting the equation for $\frac{dT}{dt}$

we can solve for $\left.\frac{dm}{dt}\right|_{ent}$ Also note that we have made the substitution of the characteristic velocity for the cloud rise velocity.

$$\left.\frac{dm}{dt}\right|_{ent} = \beta' m \frac{S}{V}\mu v - \frac{\beta' m}{T}\frac{dT}{dt} + \frac{\beta' m}{P}\frac{dP}{dt}$$

$$\left.\frac{dm}{dt}\right|_{ent} = \beta' m \frac{S}{V}\mu v - \frac{\beta' m}{T}\left\{-\frac{\beta'}{\overline{C_p(T)}}\left[\frac{T^*}{T_e^*}gu + \left(\int_{T_e}^{T} C_{pa}(T)dT\right)\frac{1}{\beta' m}\left.\frac{dm}{dt}\right|_{ent} - \varepsilon\right]\right\} - \frac{\beta' mgu}{R_a T_e^*}$$

$$\left.\frac{dm}{dt}\right|_{ent} = \beta' m \frac{S}{V}\mu v - \frac{\beta' m}{T}\left[-\frac{\beta'}{\overline{C_p(T)}}\frac{T^*}{T_e^*}gu - \frac{\cancel{\beta'}}{\overline{C_p(T)}}\left(\int_{T_e}^{T} C_{pa}(T)dT\right)\frac{1}{\cancel{\beta' m}}\left.\frac{dm}{dt}\right|_{ent} + \frac{\beta'\varepsilon}{\overline{C_p(T)}}\right] - \frac{\beta' mgu}{R_a T_e^*}$$

$$\left.\frac{dm}{dt}\right|_{ent} = \beta' m \frac{S}{V}\mu v + \frac{\beta' m}{T}\frac{\beta'}{\overline{C_p(T)}}\frac{T^*}{T_e^*}gu + \frac{\beta'\cancel{m}}{\overline{C_p(T)}T}\left(\int_{T_e}^{T} C_{pa}(T)dT\right)\frac{1}{\cancel{m}}\left.\frac{dm}{dt}\right|_{ent} - \frac{\beta' m}{T}\frac{\beta'\varepsilon}{\overline{C_p(T)}} - \frac{\beta' mgu}{R_a T_e^*}$$

$$\left.\frac{dm}{dt}\right|_{ent} - \frac{\beta'}{\overline{C_p(T)}T}\left(\int_{T_e}^{T} C_{pa}(T)dT\right)\left.\frac{dm}{dt}\right|_{ent} = \beta' m \frac{S}{V}\mu v + \frac{\beta' m}{T}\frac{\beta'}{\overline{C_p(T)}}\frac{T^*}{T_e^*}gu - \frac{\beta' m}{T}\frac{\beta'\varepsilon}{\overline{C_p(T)}} - \frac{\beta' mgu}{R_a T_e^*}$$

$$\left.\frac{dm}{dt}\right|_{ent}\left[1 - \frac{\beta'}{\overline{C_p(T)}T}\left(\int_{T_e}^{T} C_{pa}(T)dT\right)\right] = \beta' m\left(\frac{S}{V}\mu v + \frac{\beta'}{\overline{C_p(T)}T}\frac{T^*}{T_e^*}gu - \frac{\beta'\varepsilon}{\overline{C_p(T)}T} - \frac{gu}{R_a T_e^*}\right)$$

$$\left.\frac{dm}{dt}\right|_{ent} = \frac{\beta' m}{1 - \frac{\beta'}{\overline{C_p(T)}T}\left(\int_{T_e}^{T} C_{pa}(T)dT\right)}\left[\frac{S}{V}\mu v + \frac{\beta'}{\overline{C_p(T)}T}\left(\frac{T^*}{T_e^*}gu - \varepsilon\right) - \frac{gu}{R_a T_e^*}\right]$$

The derivation for the wet entrainment equation follows the same steps as above. Once again we start with equation (21) with the ratio of cloud gas density to total cloud density included. The development of the third term follows the exact same argument

above, however, this time we use Norment's equation 1.4W (7:8) for the temperature differential term.

$$\frac{dT}{dt} = -\frac{\beta'}{1+\dfrac{L^2 x\xi}{C_p R_a T^2}}\left\{\left[\left(T-T_e\right)+\frac{L\left(x-x_e\right)}{C_p}\right]\frac{1}{m\beta'}\frac{dm}{dt}\bigg|_{ent}+\frac{T^*}{T_e^*}\frac{g}{C_p}u\left(1+\frac{Lx}{R_a T}\right)-\frac{\varepsilon}{C_p}\right\}$$

Making all of the above substitutions and solving for $\left.\dfrac{dm}{dt}\right|_{ent}$ yield the following.

$$\left.\frac{dm}{dt}\right|_{ent} = \beta' m\frac{S}{V}\mu\mathrm{v}-\frac{\beta' m}{T}\frac{dT}{dt}+\frac{\beta' m}{P}\frac{dP}{dt}$$

$$\left.\frac{dm}{dt}\right|_{ent} = \beta' m\frac{S}{V}\mu\mathrm{v}$$

$$-\frac{\beta' m}{T}\left\{-\frac{\beta'}{1+\dfrac{L^2 x\xi}{C_p R_a T^2}}\left\{\left[\left(T-T_e\right)+\frac{L\left(x-x_e\right)}{C_p}\right]\frac{1}{m\beta'}\frac{dm}{dt}\bigg|_{ent}+\frac{T^*}{T_e^*}\frac{g}{C_p}u\left(1+\frac{Lx}{R_a T}\right)-\frac{\varepsilon}{C_p}\right\}\right\}$$

$$-\frac{\beta' mgu}{R_a T_e^*}$$

$$\left.\frac{dm}{dt}\right|_{ent} = \beta' m\frac{S}{V}\mu\mathrm{v}$$

$$-\frac{\beta' m}{T}\left\{-\frac{\beta'}{1+\dfrac{L^2 x\xi}{C_p R_a T^2}}\left[\left(T-T_e\right)+\frac{L\left(x-x_e\right)}{C_p}\right]\frac{1}{m\beta'}\frac{dm}{dt}\bigg|_{ent}-\frac{\beta'}{1+\dfrac{L^2 x\xi}{C_p R_a T^2}}\frac{T^*}{T_e^*}\frac{g}{C_p}u\left(1+\frac{Lx}{R_a T}\right)+\frac{\beta'}{1+\dfrac{L^2 x\xi}{C_p R_a T^2}}\frac{\varepsilon}{C_p}\right\}$$

$$-\frac{\beta' mgu}{R_a T_e^*}$$

$$\left.\frac{dm}{dt}\right|_{ent} = \beta' m \frac{S}{V} \mu \mathrm{v}$$

$$\frac{\frac{\beta'^{\not 2}\, \not m}{T}}{1+\frac{L^2 x\xi}{C_p R_a T^2}}\left[(T-T_e)+\frac{L(x-x_e)}{C_p}\right]\frac{1}{\not m\, \not\beta'}\left.\frac{dm}{dt}\right|_{ent} + \frac{\frac{\beta'^2 m}{T}}{1+\frac{L^2 x\xi}{C_p R_a T^2}}\frac{T^*}{T_e^*}\frac{g}{C_p}u\left(1+\frac{Lx}{R_a T}\right) - \frac{\frac{\beta'^2 m}{T}}{1+\frac{L^2 x\xi}{C_p R_a T^2}}\frac{\varepsilon}{C_p}$$

$$-\frac{\beta' mgu}{R_a T_e^*}$$

$$\left.\frac{dm}{dt}\right|_{ent} - \frac{\frac{\beta'}{T}}{1+\frac{L^2 x\xi}{C_p R_a T^2}}\left[(T-T_e)+\frac{L(x-x_e)}{C_p}\right]\left.\frac{dm}{dt}\right|_{ent} = \beta' m \frac{S}{V}\mu \mathrm{v} + \frac{\frac{\beta'^2 m}{T}}{1+\frac{L^2 x\xi}{C_p R_a T^2}}\left[\frac{T^*}{T_e^*}\frac{g}{C_p}u\left(1+\frac{Lx}{R_a T}\right)-\frac{\varepsilon}{C_p}\right]$$

$$-\frac{\beta' mgu}{R_a T_e^*}$$

$$\left.\frac{dm}{dt}\right|_{ent}\left\{1-\frac{\frac{\beta'}{T}}{1+\frac{L^2 x\xi}{C_p R_a T^2}}\left[(T-T_e)+\frac{L(x-x_e)}{C_p}\right]\right\} =$$

$$\beta' m\left\{\frac{S}{V}\mu \mathrm{v} + \frac{\frac{\beta'}{T}}{1+\frac{L^2 x\xi}{C_p R_a T^2}}\left[\frac{T^*}{T_e^*}\frac{g}{C_p}u\left(1+\frac{Lx}{R_a T}\right)-\frac{\varepsilon}{C_p}\right]-\frac{gu}{R_a T_e^*}\right\}$$

$$\left.\frac{dm}{dt}\right|_{ent} = \frac{\beta' m}{1-\frac{1}{T}\left[\frac{\beta'}{1+\frac{L^2 x\xi}{C_p R_a T^2}}\right]\left[(T-T_e)+\frac{L(x-x_e)}{C_p}\right]}\left\{\frac{S}{V}\mu \mathrm{v} + \frac{\frac{\beta'}{T}}{1+\frac{L^2 x\xi}{C_p R_a T^2}}\left[\frac{T^*}{T_e^*}\frac{g}{C_p}u\left(1+\frac{Lx}{R_a T}\right)-\frac{\varepsilon}{C_p}\right]-\frac{gu}{R_a T_e^*}\right\}$$

Appendix C. Corrections to HPAC

This appendix will outline the changes that were or were not made between the 1979 version of DELFIC and the current version of HPAC. I will focus on those corrections that were identified by Jodoin in his *Critique of DELFIC's Cloud Rise Module*. (15) Each of the errors will be referenced to Jodoin's original document with a brief description of the action needed. The particular reference is provided for additional information.

CRMIN 66 page 78 (15:7)

current equation:

```
soilht=ssam*(tad+781.6*(tpr-te)+0.2856*(tpr**2-te**2)+
```

required equation:

```
soilht=ssam*(tad+781.6*(tpr-te)+0.2806*(tpr**2-te**2)+
```

DERIV 91 page 85 (15:7)

current equation:

```
qq=qt*qx*qxe*(1.+x+wt)/(1.+w+s+wt)
```

required equation:

```
qq=qt*qx*qxe*(1.+x)/(1.+w+s+wt)
```

DERIV 113, page 86 (15:9)

current equation:

```
100 drm=(rm/(1.-cpai/(cp*t*qx)))*rmix*(rs*rl+(qt*qx*qxe*9.8*u-eps)*
```

required equation:

```
100 drm=(rm/(1.-rmix*cpai/(cr*t*qx)))*rmix*(rs*rl+(qt*qx*qxe*9.8*u-eps)*
```

ATMR 187 thru ATMR 203 page 72 (15:9)

This was a correction to the expansion of the atmospheric table. HPAC has a new method of expanding the table that incorporates the changes recommended by Jodoin.

HPAC source code, subroutine ATMR

Corrections were made to the maximum atmospheric values in subroutine atmr

Previously, 50000., 270.65, 79.779, .16269e-2, 4.0, .17637e-4
Currently, 50000., 270.65, 79.779, .10269e-2, 0.0, .17037e-4

Appendix D. HPAC Modifications from 1979 DELFIC

This appendix will outline the modifications that were made when the 1979 version of DELFIC was incorporated as an option in HPAC. Although this analysis is primarily concerned with those subroutines that impact the calculations of the cloud rise model, some reference will be made to subroutines that are used for cloud transport. Also note that this analysis is concerned with corrections or modifications that affect the calculations in the program. Modifications that merely change the programming structure, such as the restructuring of an if/then loop, are not addressed.

Table 22. 1979 DELFIC to HPAC Modifications

DELFIC Subroutine	HPAC Subroutine	Remarks
Program Main		The programming that acquires the input required to run the program is now contained in a C++ front end that was not evaluated in this analysis.
trpl	trpl	No changes
error	format_error	Eliminated the call to this subroutine within subroutines. It is now done more globally in the format_error subroutine
icrmex	delrise	This subroutine mimics the icrmex subroutine in DELFIC. It is used to make the calls to icm, atmr, crmint, crm and rsxp subroutines. It should be noted that the subroutine does not make a call to a shwind subroutine which is used to read in the wind profile data for use in the wind shear correction to the cloud rise.
settle	falrat	This subroutine has a negligible affect on cloud rise calculations. The subroutine falrat uses a different set of equations/different approach to solving for a modified cg(i) value which is then passed back to cpfr to calculate a new y(i) value. Cg(i) are the falling speeds of particles in the cloud, while y(i) are the number of particles per unit volume. Subroutine settle used the equations of Beard and Davies, while the falrat subroutine uses the VORDUM equations.
shwind		Eliminated from HPAC.
cpfr	cpfr	HPAC eliminated the test for a particle of negative

		density. Instead of calling subroutine settle, the falrat subroutine is called.
icm	icm	There are only minor changes made to the functioning of this routine, but there are some major restructuring changes. This subroutine now encompasses all of icm, airbrs, timee, temp, mass, and vapor subroutines. HPAC makes a variable change. The variable idistr has taken the place of the ic( ) array, which identifies the type of particle distribution in the dstrb subroutine. Two calculation changes that were made are in the assignment value for the sldtmp variable. That is, the temperature at which the particular type of soil solidifies. DELFIC has two temperature options, 2200 for siliceous soil and 2800 for calcareous soil. The 2800 value was determined to be more representative of the coral type shots in the pacific. The vapor temperature no longer branches according to the type of soil. Once again, calculations are based on the conditions of siliceous soil.
airbrs	icm	No changes in the calculations.
dstbn	dstbn	Idistr replaces ic(j): idistr = 1 (Lognormal distribution) idistr = 2 (Power function distribution) idistr = 3 (Tabular distribution) In the Lognormal distribution, the diam is never multiplied by 1E-6. In the Power function distribution, ssam is added to the dmin function. In the Tabular distribution the equation for calculating ps(i) is different: DELFIC – ps(i)=sqrt(daim(i)*diam(I+1))*1.0e-6 HPAC – ps(i)=0.5*(diam(i) + daim(I+1))*1.0e-6
mass	icm	No changes in the calculations.
vapor	icm	The vapor temperature no longer branches according to the type of soil. Calculations are based on the conditions of siliceous soil.
temp	icm	No changes in the calculations.
timee	icm	No changes in the calculations.
atmr	atmr	This subroutine has been totally reworked and a new interpolation technique has been developed for the spacing of the altitudes. The subroutine now works like the corrected version presented by Jodoin in his critique. There are however a couple of changes. 1. In the data assignments of atmsub, atmzro, and

		atmmax the fourth and fifth positions have been switched. Upon further investigation, the assignments all made correctly. Within the HPAC program, alt(i), prs(i), atp(i), and rlh(i) are read in from the C:\HPAC\DATA\Temp\NWPNTEMP\Newtrans .met file. 2. In the data assignment of atmmax, the parameters have been changed as follows. There is a comment annotating the fix to this data. Previously, 50000., 270.65, 79.779, .16269e-2, 4.0, .17637e-4 Currently, 50000., 270.65, 79.779, .10269e-2, 0.0, .17037e-4 3. The pressure calculation based on other parameters has been eliminated. Pressure at each level must be inputted. The pressure is now simply converted from mb to Pa. Previously, prs(i)=286.79 + rho(i)*alt(i)*es*rlh(i)*watcor Currently, prs(i)=prs(i)*100. The pressure term is then used in the calculation of the density term, rho(i).
crm	crm	No changes in the calculations.
crmint	crmint	HPAC added the statement: jtmflag = 0 This statement was added to fix the cloud thickness after apogee. The value is changed in the subroutine rkgill to jtmflag = 1 as soon as the velocity is less than zero. This then fixes the vertical radius while the cloud continues to oscillate.
crmw	crmw	HPAC has commented out the write statements for the cloud history table.
cxpn	cxpn	The lines that calculate "al" and "al10" have been deleted. These variables were passed to subroutine rsxp in the DELFIC 79 code that is not used in the cloud rise calculations. In the HPAC code the reference to "al" has been eliminated. Neither of the codes used the "al10" variable. The code that permitted cloud oscillations has been commented out. The termination condition of cloud velocity being less than or equal to zero has been commented out. This allows the cloud to drop, thus allowing for oscillations.
dbg		Called by crm, commented out in HPAC
dcsn	dcsn	Added the following anomaly check but runs the same. elseif (smallt .GT. 600.) then This stops the crm calculation if the time exceeds 10 minutes.

deriv	deriv	A change was made in subroutine to remove test of cloud height so that velocity could go negative. This affected the initialization of several variables and will affect the branching due to variables ks and nnn. ks variable is used in rkgill subroutine for looping control. nnn variable is no longer variable in HPAC, it was assigned in a test for cloud height to prevent velocity from going negative. Velocity is now allowed to go negative to allow for oscillations.
rkgill	rkgill	Introduction of the variable "jtmflag" which fixes the cloud's vertical radius once the cloud velocity is less than zero.
rstr	rstr	No changes in the calculations.
rsxp	rsxp	Not used for this analysis
wndsft		This subroutine deals with the shifting of particles due to wind after the particle distribution has been passed to the transport model and is therefore not part of this analysis
advec		Not used for this analysis
cntr		Not used for this analysis
datin		Called by dtmex, which is commented out for this analysis
dtmex		Called by main, but commented out for this analysis
function cmult		Not used for this analysis
function cdiv		Not used for this analysis
	newmain format_error *ntransctl* *cldhgt_agl* *wrtcloud* *bin_up* *out_mcd* readmet	Italicized routines are not actually needed in cloud rise computations when using the DELFIC option. This subroutine reads in the atmospheric data saved in the Newtrans.met file. The file contains the number of atmospheric layers, followed by the alt(i)(*m*) prs(i)(*mb*) atp(i)(*C*) rlh(i)(%) data for each of the layers. The HPAC comments state it sets the number of wind levels, but it is really the number of atmospheric levels. Wind is not part of the Newtrans.met file.
	newtrans	Multiple subroutines are part of the newtrans file, all of which are used in the transport model and not required

	newset *newadd* *newout* *bin* *siginv* *init_error* *report_error* *WarningMessage*	for this analysis.
	recog_cldinit	Forces Fortran to read a DLL file
	function nblank	These functions are used to retrieve file names and variables from external files.
	function len_trim1	
	cstrcpy	
	fstrcpy	
	finit_buff	
	inparm	This subroutine is used to input the particle size data for use in the transport of the particles in the newtrans subroutine.
	cloud	This subroutine is used to define the cloud dimensions at stabilization. In this research the subroutine is only important in defining several variables and calling the delrise subroutine to run the cloud rise dynamics. It is noted that none of the variables calculated in the subroutine are actually passed to the rise subroutines.

Appendix E. Cloud Rise History Plots

The cloud rise history plots present the observed cloud top height and cloud base, as well as the calculated values for the single and three term entrainment equations. The programs used for the calculated values were the four cases described in Table 3 using the best-fit parameter values given in Table 5. The observed plots were produced from extracting cloud top height and base height values off the plots in DASA 1251 at each minute until stabilization was reached. (16) The observed cloud top and cloud base heights are represented by the points in Figure 29 through Figure 46. The calculated cloud top and base heights for the single and three-term equations are labeled "1" and "3" respectively.

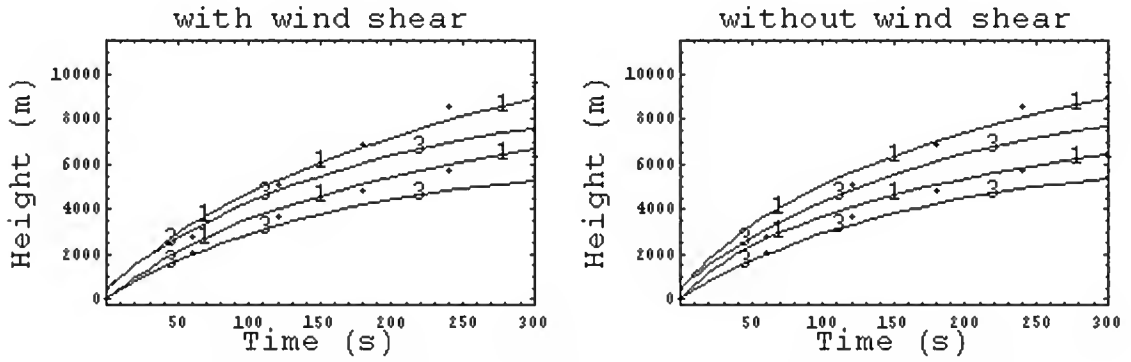

Figure 29. Cloud rise history plot for shot Annie, operation Upshot-Knothole

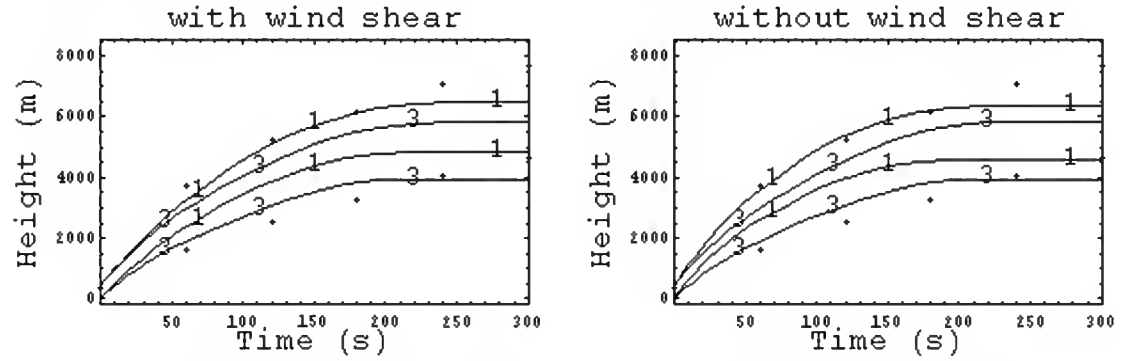

Figure 30. Cloud rise history plot for shot Apple 1, operation Teapot

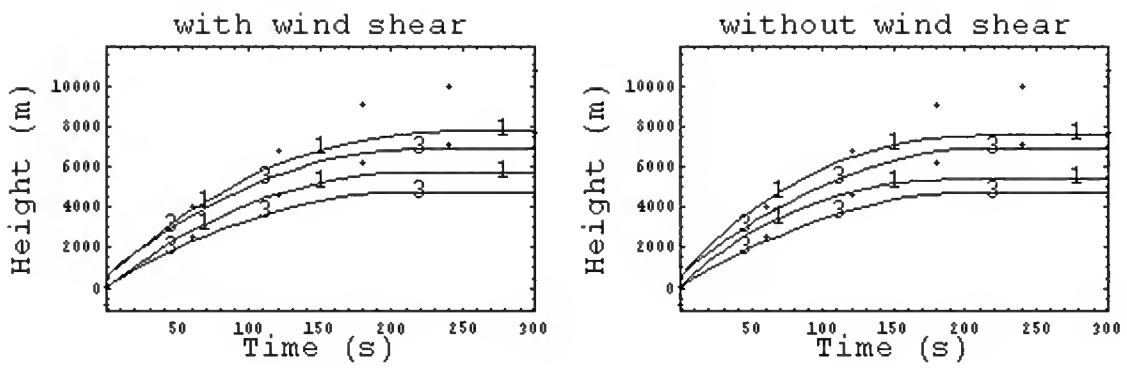

Figure 31. Cloud rise history plot for shot Apple 2, operation Teapot

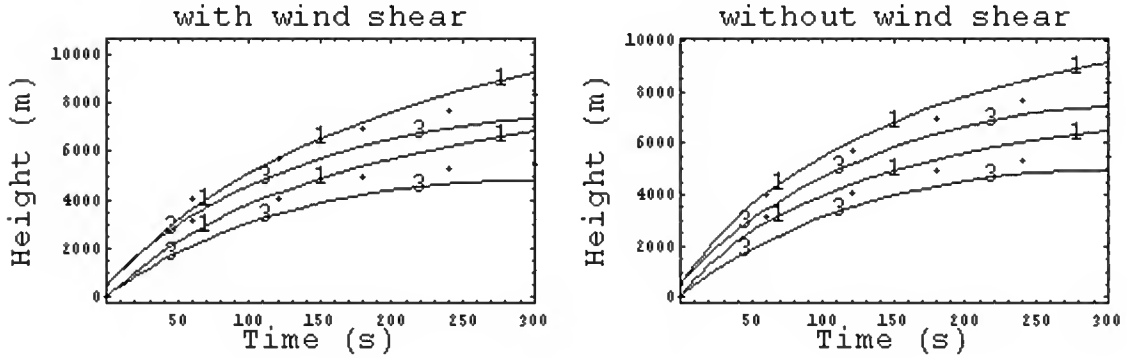

Figure 32. Cloud rise history plot for shot Badger, operation Upshot-Knothole

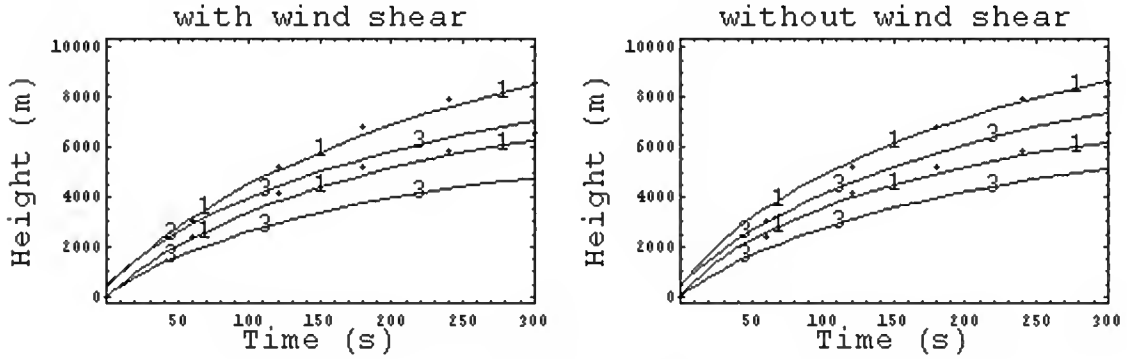

Figure 33. Cloud rise history plot for shot Dixie, operation Upshot-Knothole

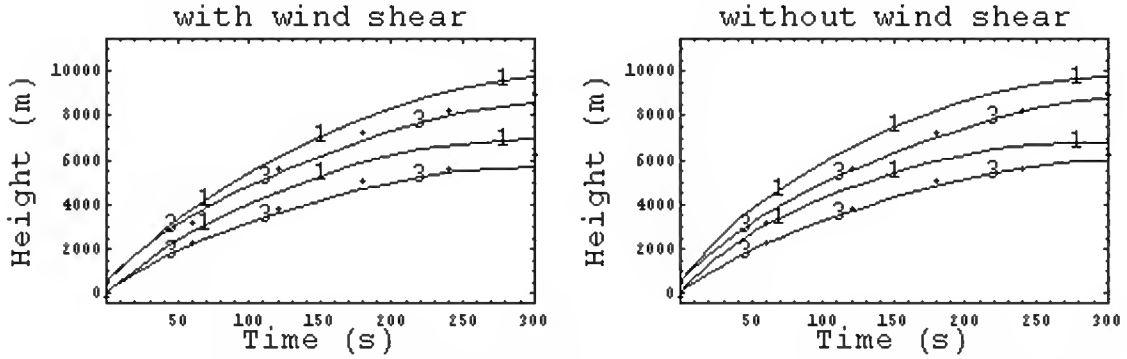

Figure 34. Cloud rise history plot for shot Encore, operation Upshot-Knothole

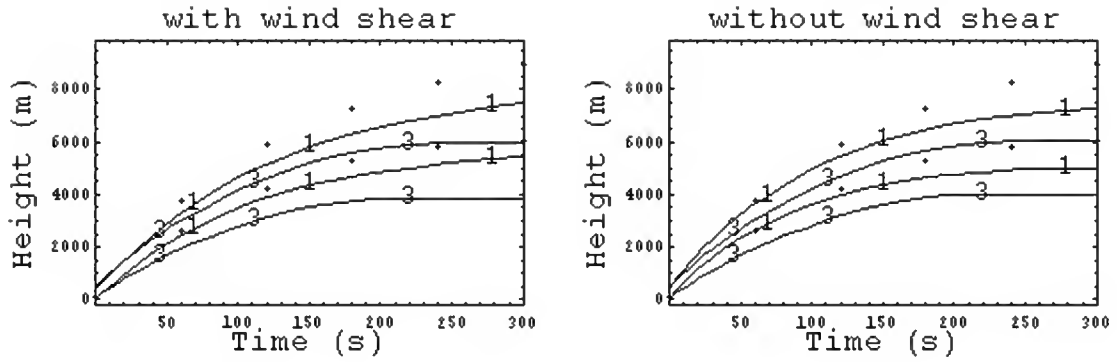

Figure 35. Cloud rise history plot for shot Grable, operation Upshot-Knothole

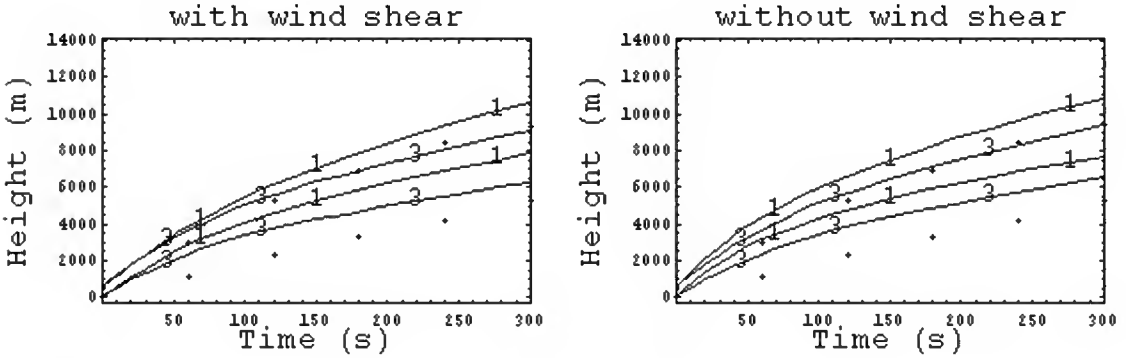

Figure 36. Cloud rise history plot for shot Harry, operation Upshot-Knothole

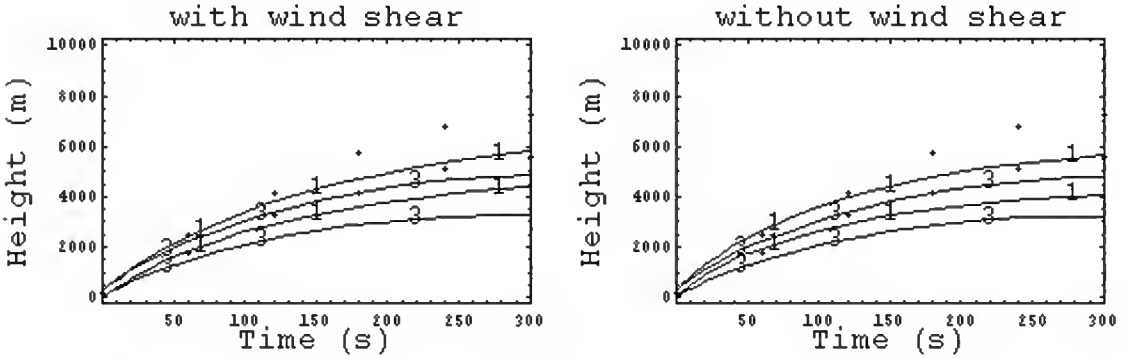

Figure 37. Cloud rise history plot for shot Hornet, operation Teapot

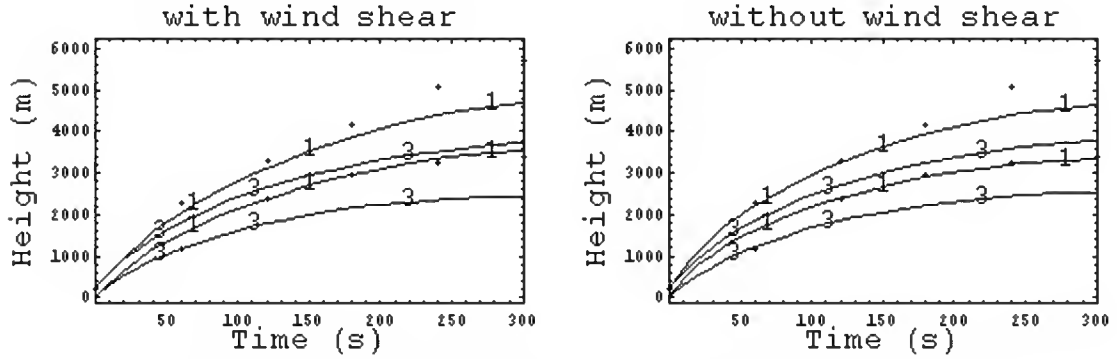

Figure 38. Cloud rise history plot for shot Moth, operation Teapot

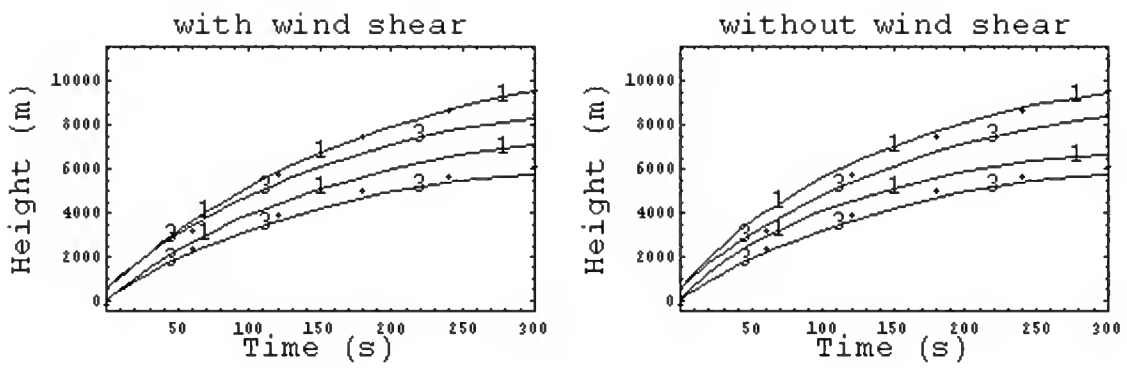

Figure 39. Cloud rise history plot for shot Nancy, operation Upshot-Knothole

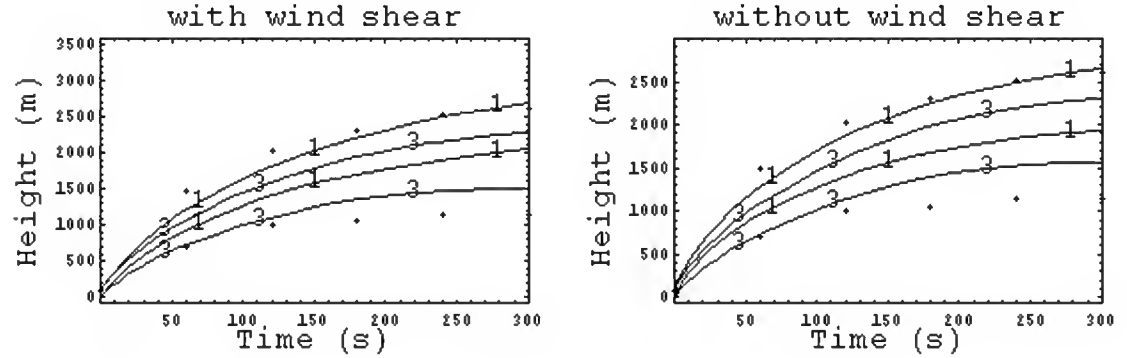

Figure 40. Cloud rise history plot for shot Ray, operation Upshot-Knothole

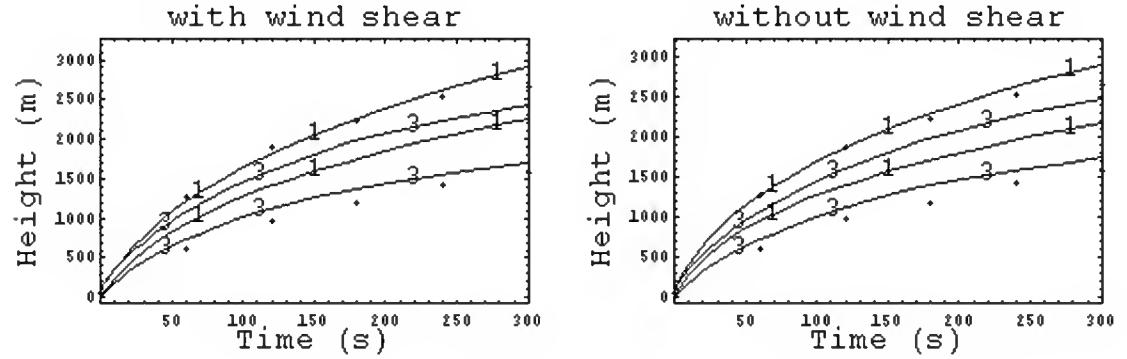

Figure 41. Cloud rise history plot for shot Ruth, operation Upshot-Knothole

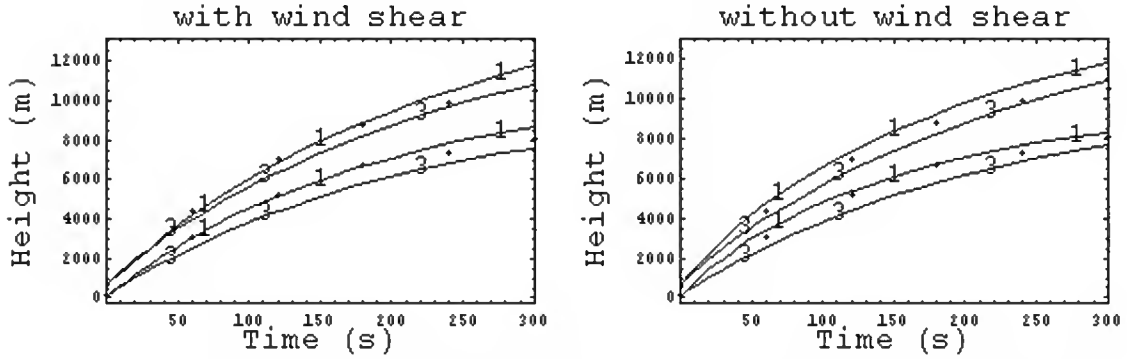

Figure 42. Cloud rise history plot for shot Simon, operation Upshot-Knothole

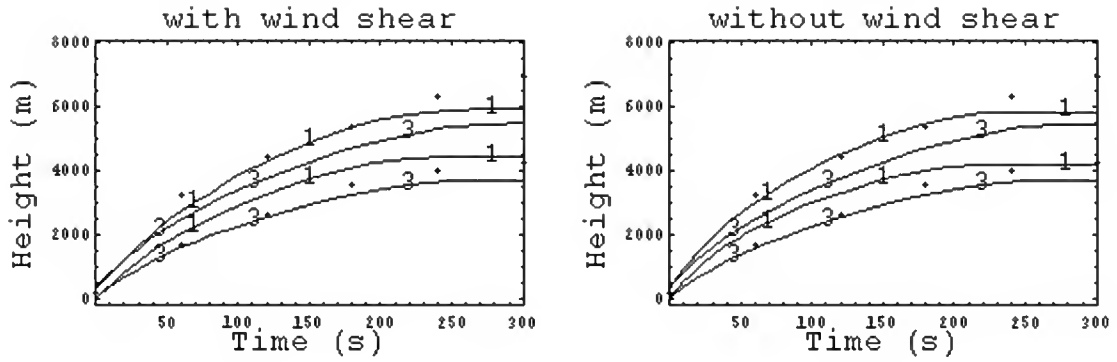

Figure 43. Cloud rise history plot for shot Tesla, operation Teapot

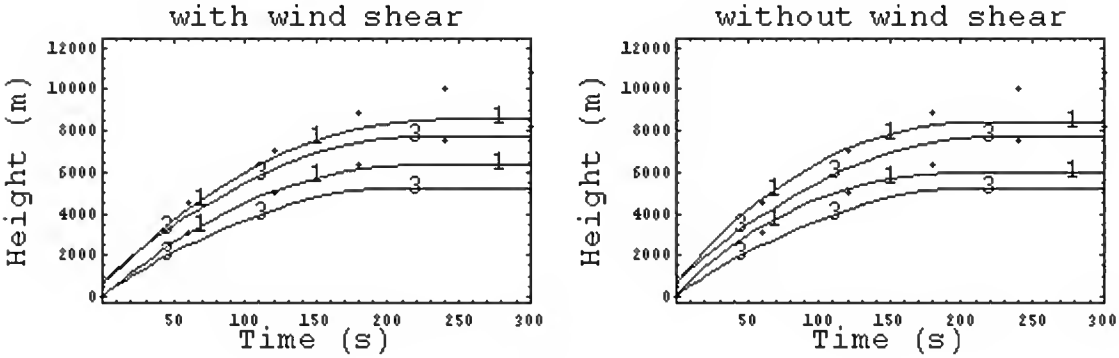

Figure 44. Cloud rise history plot for shot Turk, operation Teapot

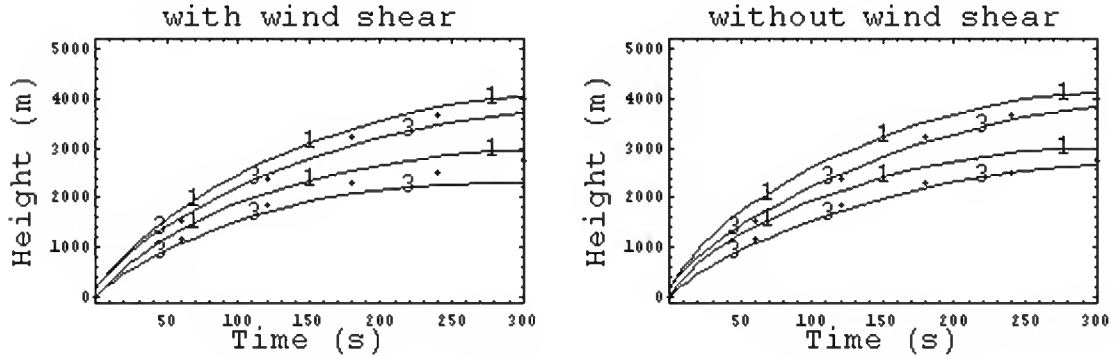

Figure 45. Cloud rise history plot for shot Wasp, operation Teapot

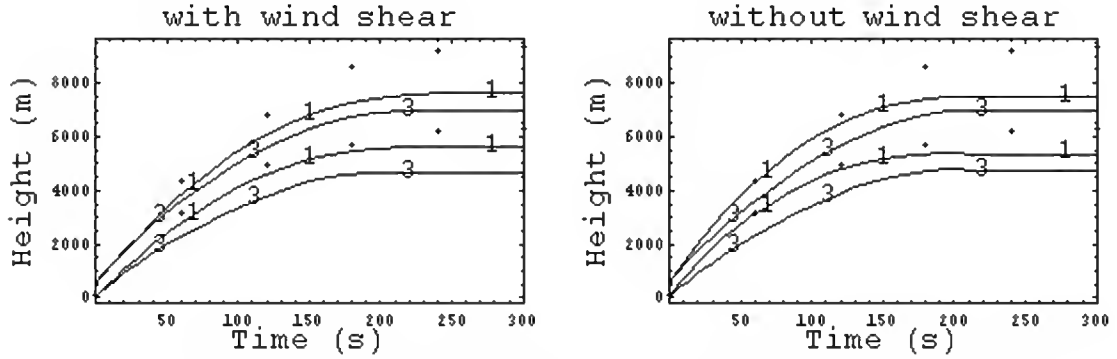

Figure 46. Cloud rise history plot for shot Zuchini, operation Teapot

Appendix F. Wind Shear Parameter, k6, Optimization

Table 23. Optimized wind shear parameter for each shot given the constant entrainment and eddy viscous drag parameters of Table 5

Shot	Yield	k6	FMD
Humboldt	0.008	1.00	-0.002
Catron	0.021	1.00	-0.077
Vesta	0.024	1.00	-0.294
Dona Ana	0.037	0.00	-0.434
Hidalgo	0.077	1.00	-0.120
Quay	0.079	1.00	-0.044
Eddy	0.083	1.00	-0.389
Rio Arriba	0.090	0.00	0.068
Wrangell	0.115	1.00	-0.139
Franklin	0.140	0.00	-0.108
Wheeler	0.197	1.00	-0.002
Ray	0.200	0.40	-0.001
Ruth	0.200	1.00	-0.087
Johnnie Boy	0.500	0.00	0.166
Laplace	1.000	1.00	-0.061
Wasp	1.000	0.00	0.192
Santa Fe	1.300	1.00	-0.152
Lea	1.400	1.00	-0.339
John	2.000	0.00	0.221
Mora	2.000	1.00	-0.178
Moth	2.000	0.00	0.239
Post	2.000	1.00	-0.393
Debaca	2.200	0.95	-0.399
Ha	3.000	1.00	-0.060
Wasp Prime	3.000	0.00	0.392
Hornet	4.000	0.00	0.432
Franklin Prime	4.700	0.00	0.259
Sanford	4.900	0.50	0.000
Socorro	6.000	1.00	-0.028
Tesla	7.000	0.00	0.263
Bee	8.000	0.00	0.413
Morgan	8.000	0.00	0.336
Owens	9.700	0.00	0.164
Kepler	10.000	1.00	-0.098
Wilson	10.000	0.00	0.102
Fizeau	11.000	0.00	0.255
Galileo	11.000	0.00	0.156
Doppler	11.000	0.00	0.217
Dixie	11.000	0.00	0.142

Boltzman	12.000	1.00	-0.160
Newton	12.000	1.00	-0.015
Charleston	12.000	0.00	0.137
Apple1	14.000	0.00	0.246
Grable	15.000	0.00	0.274
Annie	16.000	0.00	0.082
Shasta	17.000	1.00	-0.082
Diablo	17.000	1.00	-0.134
Whitney	19.000	1.00	-0.206
Stokes	19.000	0.00	0.044
Met	22.000	0.00	0.302
Badger	23.000	0.10	0.000
Nancy	24.000	0.00	0.150
Encore	27.000	0.00	0.141
Zuchini	28.000	0.00	0.315
Apple2	29.000	0.00	0.476
Harry	32.000	1.00	-0.104
Priscilla	37.000	0.00	0.028
Lacrosse	40.000	0.05	0.160
Simon	43.000	1.00	-0.026
Turk	43.000	0.00	0.320
Smokey	44.000	1.00	-0.131
Climax	61.000	1.00	-0.072
Hood	74.000	1.00	-0.047
Koon	110.000	0.00	0.024
Zuni	3500.000	0.95	-0.161
Tewa	5000.000	1.00	-0.012
Bravo	15000.000	1.00	-0.077

Appendix G. Cloud Top Comparison of Case 4 with and without Cloud Oscillations

Table 24. Cloud Top Comparison of Case 4 with and without Cloud Oscillations

Shot	Yield (kt)	Observed Cloud Top (m)	Calculated Cloud Top(m)		Fractional Deviation	
			No Cloud Oscillations	Cloud Oscillations	No Cloud Oscillations	Cloud Oscillations
Humboldt	0.0078	1050	1078	743	-0.027	0.292
Catron	0.021	1344	1436	1179	-0.069	0.123
Vesta	0.024	1760	2296	1850	-0.305	-0.051
Dona Ana	0.037	1940	2795	1788	-0.441	0.078
Hidalgo	0.077	2267	2542	2225	-0.122	0.018
Quay	0.079	1722	1817	1776	-0.055	-0.031
Eddy	0.083	1925	2537	2135	-0.318	-0.109
Rio Arriba	0.09	2870	2593	2131	0.097	0.258
Wrangell	0.115	1653	1892	1902	-0.145	-0.151
Franklin	0.14	3772	4195	3130	-0.112	0.170
Wheeler	0.197	3740	3735	3192	0.001	0.147
Ray	0.2	2644	2586	2530	0.022	0.043
Ruth	0.2	2833	3080	2935	-0.087	-0.036
Johnnie Boy	0.5	3612	2893	2923	0.199	0.191
Laplace	1	4592	4892	4837	-0.065	-0.053
Wasp	1	5042	4040	4022	0.199	0.202
Santa Fe	1.3	3753	4271	4562	-0.138	-0.215
Lea	1.4	3449	4570	4891	-0.325	-0.418
John	2	6008	4575	4838	0.239	0.195
Mora	2	3906	4601	4948	-0.178	-0.267
Moth	2	6057	4492	4618	0.258	0.238
Post	2	3341	4509	5122	-0.350	-0.533
Debaca	2.2	3601	5001	5186	-0.389	-0.440
Ha	3	5602	5905	6004	-0.054	-0.072
Wasp Prime	3	8250	4976	4825	0.397	0.415
Hornet	4	9965	5468	5507	0.451	0.447
Franklin Prime	4.7	8249	5915	6526	0.283	0.209
Sanford	4.9	6530	6171	7027	0.055	-0.076
Socorro	6	6207	6352	6781	-0.023	-0.092
Tesla	7	7827	5718	5538	0.269	0.292
Bee	8	10655	6207	5967	0.418	0.440
Morgan	8	10755	6877	7433	0.361	0.309
Owens	9.7	9231	7601	7808	0.177	0.154

Kepler	10	7090	7796	8195	-0.100	-0.156
Wilson	10	9226	7905	8800	0.143	0.046
Fizeau	11	10811	7967	7961	0.263	0.264
Galileo	11	9830	8024	8648	0.184	0.120
Doppler	11	9836	7450	8199	0.243	0.167
Dixie	11	10654	8920	9203	0.163	0.136
Boltzman	12	8615	9962	10091	-0.156	-0.171
Newton	12	8021	8129	8145	-0.014	-0.016
Charleston	12	8012	6876	6553	0.142	0.182
Apple1	14	8288	6175	6091	0.255	0.265
Grable	15	9570	6671	7905	0.303	0.174
Annie	16	11178	10083	10471	0.098	0.063
Shasta	17	8264	8881	9844	-0.075	-0.191
Diablo	17	8239	9180	9764	-0.114	-0.185
Whitney	19	7624	9040	9514	-0.186	-0.248
Stokes	19	9545	8922	9223	0.065	0.034
Met	22	11223	7778	7507	0.307	0.331
Badger	23	9513	9138	10048	0.039	-0.056
Nancy	24	11244	9275	9988	0.175	0.112
Encore	27	11125	9396	9690	0.155	0.129
Zuchini	28	10746	7278	7167	0.323	0.333
Apple2	29	14102	7287	7216	0.483	0.488
Harry	32	11642	13033	13521	-0.119	-0.161
Priscilla	37	11955	11098	12474	0.072	-0.043
Lacrosse	40	11582	9345	10323	0.193	0.109
Simon	43	12028	12260	12458	-0.019	-0.036
Turk	43	12104	8134	8011	0.328	0.338
Smokey	44	10004	11282	10950	-0.128	-0.095
Climax	61	11382	12191	11729	-0.071	-0.031
Hood	74	12884	13342	14017	-0.036	-0.088
Koon	110	16150	15233	16472	0.057	-0.020
Zuni	3500	24076	27933	26448	-0.160	-0.099
Tewa	5000	30171	30449	29449	-0.009	0.024
Bravo	15000	34745	37374	35368	-0.076	-0.018
				FMD	**0.044**	**0.050**
				FRMS	**0.217**	**0.218**

Appendix H. HPAC Comparison to the Recommended DELFIC Case

Table 25 provides a comparison of the HPAC software, the HPAC stand-alone source code, and the recommended DELFIC Case 4. Shots labeled N/A under the HPAC column did not meet the conditions to run the DELFIC rise option in the packaged software.

Table 25. Comparison of Cloud Top Heights for HPAC with recommended DELFIC "Case 4"

Shot	Obs	HPAC	HPAC Stand-Alone	Case 4
Humboldt	1050	N/A	485	1078
Catron[3]	1344	-474	903	1436
Vesta	1760	-773	1012	2296
Dona Ana[4]	1940	-67	1118	2795
Hidalgo[3]	2267	86	1427	2542
Quay[3]	1722	-157	1404	1817
Eddy[4]	1925	7	1907	2537
Rioarriba[3]	2870	244	1445	2593
Wrangell	1653	N/A	1522	1892
Franklin[3]	3772	167	1760	4195
Wheeler[3]	3740	1186	2304	3735
Ray[3]	2644	764	2040	2586
Ruth[3]	2833	410	2061	3080
Johnnie Boy	3612	N/A	2477	2893
Laplace[3]	4592	501	4554	4892
Wasp[3]	5042	2977	3694	4040
Santafe[4]	3753	2734	3543	4271
Lea[4]	3449	969	3907	4570
John	6008	N/A	3952	4575
Mora[4]	3906	2059	4405	4601
Moth[3]	6057	1820	3754	4492
Post[3]	3341	1405	4139	4509
Debaca[4]	3601	2389	3877	5001
Ha	5602	N/A	4832	5905
Wasp Prime[3]	8250	2696	4779	4976

[3] HPAC run resulted in the caution "HOB>180 Yield^0.4 ft weapon will not yield any fallout."
[4] HPAC run resulted in the cautions,
"HOB>180 Yield^0.4 ft weapon will not yield any fallout," and
"The SHOB exceeds PDCALC's limit for assessing personnel casualties. Therefore casualty for this weapon will not be assessed, however, effects radii for this weapon can be visualized from the "Show Effects Circles" option in SCIPUFF Plot."

Hornet	9965	3328	5070	5468
Franklin Prime[3]	8249	3923	5652	5915
Sanford[3]	6530	3585	5299	6171
Socorro[3]	6207	2926	6001	6352
Tesla	7827	3585	5169	5718
Bee[3]	10655	4359	5639	6207
Morgan[3]	10755	3953	6509	6877
Owens[3]	9231	8599	7798	7601
Kepler[3]	7090	6646	7749	7796
Wilson[3]	9226	4761	6519	7905
Fizeau[3]	10811	6980	7395	7967
Galileo[3]	9830	5239	7678	8024
Doppler[3]	9836	9838	8188	7450
Dixie	10654	N/A	8427	8920
Boltzman[3]	8615	8309	9664	9962
Newton[3]	8021	6653	7511	8129
Charleston[3]	8012	6531	6341	6876
Apple1	8288	4837	5444	6175
Grable	9570	5062	5709	6671
Annie	11178	6711	10142	10083
Shasta	8264	7551	9724	8881
Diablo	8239	6613	8650	9180
Whitney	7624	6053	8372	9040
Stokes[3]	9545	7732	8289	8922
Met	11223	7696	7272	7778
Badger	9513	5572	8162	9138
Nancy	11244	6873	8507	9275
Encore[3]	11125	7489	8252	9396
Zuchini	10746	6749	6688	7278
Apple2	14102	6551	6565	7287
Harry	11642	10059	13387	13033
Priscilla	11955	11585	10457	11098
Lacrosse	11582	11311	8833	9345
Simon	12028	12056	11385	12260
Turk	12104	6583	7457	8134
Smokey	10004	9479	10831	11282
Climax[3]	11382	10604	11407	12191
Hood[3]	12884	11797	11534	13342
Koon	16150	15310	14656	15233
Zuni	24076	21924	24956	27933
Tewa	30171	23485	26539	30449
Bravo	34745	N/A	21144	37374
FMD		**0.46**	**0.20**	**0.04**
FRMS		**0.57**	**0.28**	**0.22**

The atmospheric levels consisted of only those levels below the observed cloud top height for the given shot. When more than 25 levels existed, the number of levels would be divided by 25 to get the step fraction. The closest level to each step would then make up the atmospheric table.

Bibliography

[1] Grossman, B., et. al. *Operation Teapot, Project 9.4, Atomic Cloud Growth Study, WT-1152*. Boston: Air Force Cambridge Research Center, October 1955. (AD 426 840)

[2] McGahan, Joseph T. *Cloud Rise in NewFall and NWPN Draft*. Science Applications International Corporation, 15 September 2000.

[3] Eisenbud, Merril and Thomas Gesell. *Environmental Radioactivity From Natural, Industrial, and Military Sources, 4th Edition*. Academic Press, San Diego, CA, 1997.

[4] Glasstone, Samuel and Philip J. Dolan. *The Effects of Nuclear Weapons, Third Edition*. United States Department of Defense and the Energy Research and Development Administration, Washington DC, Government Printing Office, 1977. (ADA 087 568)

[5] Norment, H.G. *Validation and Refinement of the DELFIC Cloud Rise Module*. Atmospheric Science Associates, Bedford, MA, 15 January 1977. (AD A047 372)

[6] Huebsch I. O. *The Development of a Water-Surface-Burst Fallout Model: The Rise and Expansion of the Atomic Cloud*. U. S. Naval Radiological Defense Laboratory, San Francisco, CA, 23 April 1964. (AD 441 983)

[7] Norment, H.G. and S. Woolf. *Department of Defense Land Fallout Prediction System. Volume III. Cloud Rise. Revised*. ARCON Corporation, Wakefield, MA, 1 September 1970. (AD 879 890)

[8] Huebsch I.O. *Analysis and Revision of the Cloud Rise Module of the Department of Defense Land Fallout Prediction System (DELFIC)*. Euclid Research Group, Berkeley, CA, August 1975. (AD B007 607)

[9] Jodoin, Vincent J. *Nuclear Cloud Rise and Growth*, Air Force Institute of Technology, Wright-Patterson AFB, OH, June 1994. (AD A280 688)

[10] Huebsch, I. O. *Wind Shear, Turbulence and Interface Criteria for Nuclear-Explosion Cloud, Debris and Fallout Models*, Naval Radiological Defense Laboratory, San Francisco, CA, July 1969. (AD 856 228)

[11] D. Randerson, editor. *Atmospheric Science and Power Production*, Office of Scientific and Technical Information, U.S. Dept. of Energy, DOE/TIC-27601, Oak Ridge, TN, 1984

[12] Telegadas, Kosta. *Fallout Patterns from Operation Hardtack, Phase II*. U.S. Weather Bureau, Washington DC, May 1960. (ADA 078 562)

[13] Norment, Hillyer G. *DELFIC: Department of Defense Fallout Prediction System. Volume I – Fundamentals*. Atmospheric Science Associates, Bedford, MA, 31 December 1979. (ADA 088 512)

[14] Lamarche, Craig F. *Performance Evaluation of the Nuclear Weapon (NWPN Source Model for the Hazard Prediction and Assessment Capability (HPAC) Code*, Air Force Institute of Technology, Wright-Patterson AFB, OH, September 1999.

[15] Jodoin, Vincent J. *Critique of DELFIC's Cloud Rise Module*, Air Force Institute of Technology, Wright-Patterson AFB, OH, May 1993. (ADA 265 587)

[16] Hawthorne, Howard A. *Compilation of Local Fallout Data From Test Detonations 1945-1962 Extracted From DASA1251. Volume I – Continental US Tests.* General Electric Co., Santa Barbara, CA, DASIAC, 01 May 1979. (ADA 079310)

Vita

Daniel E. Zalewski was born on 12 October 1965 in Silver Spring, Maryland to Elizabeth and Robert Zalewski. He graduated from Archbishop Carroll High School in 1984 and went on to the Virginia Military Institute in Lexington, Virginia. He graduated with a Bachelor or Science degree in mathematics in 1988 and accepted a commission as a second lieutenant in the US Army Military Police Corps. After completion of the Officer Basic Course he was assigned as a platoon leader to the 165th Military Police (MP) Company in Fischbach, FRG from March 1989 to June 1991. He then became the Battalion Security Officer for the 197th Ordnance Battalion, Pirmasens, FRG from June 1991 to February 1992. Upon completion of this assignment he attended the Advanced Officers Course with a follow-on assignment as Assistant S-3, Law Enforcement Command, Fort Ord, Ca from August 1992 to December 1992 and then as the Company Commander, 7th MP Company (Light), 7th Infantry Division (Light) from December 1992 to August 1993. After the inactivation of the 7th Infantry Division (Light) he took command of the Headquarters, Headquarter Company and later the Alpha Company of the 705th MP Battalion, Fort Leavenworth, KS from August 1993 to August 1995. He then went on to be the assistant professor of military science for Bucknell University Army ROTC from August 1995 to August 1998. While assigned, he completed his Master of Science degree in Instructional Technology from Bloomsburg University. He was then selected to attend the Air Force Institute of Technology where he is a candidate for a Master of Science degree. His next assignment will be with the Defense Threat Reduction Agency in Alexandria, VA.

REPORT DOCUMENTATION PAGE	Form Approved OMB No. 074-0188

1. REPORT DATE *(DD-MM-YYYY)*	2. REPORT TYPE	3. DATES COVERED *(From – To)*
02-24-2001	Master's Thesis	Jun 2000 – Sep 2001

4. TITLE AND SUBTITLE

Assessment of the Effects of Entrainment and Wind Shear on Nuclear Cloud Rise Modeling

5a. CONTRACT NUMBER

5b. GRANT NUMBER

5c. PROGRAM ELEMENT NUMBER

6. AUTHOR(S)

Zalewski, Daniel E., Major, U.S. Army

5d. PROJECT NUMBER

5e. TASK NUMBER

5f. WORK UNIT NUMBER

7. PERFORMING ORGANIZATION NAMES(S) AND ADDRESS(S)
Air Force Institute of Technology
Graduate School of Engineering and Management (AFIT/EN)
2950 P Street, Building 640
WPAFB OH 45433-7765

8. PERFORMING ORGANIZATION REPORT NUMBER

AFIT/GNE/ENP/01M-06

9. SPONSORING/MONITORING AGENCY NAME(S) AND ADDRESS(ES)
Defense Threat Reduction Agency (DTRA)
Collateral Effects Branch (CPWE)
6801 Telegraph Road
Alexandria, VA 22310-3398

10. SPONSOR/MONITOR'S ACRONYM(S)

11. SPONSOR/MONITOR'S REPORT NUMBER(S) QAF-185005203215

12. DISTRIBUTION/AVAILABILITY STATEMENT
APPROVED FOR PUBLIC RELEASE; DISTRIBUTION UNLIMITED.

13. SUPPLEMENTARY NOTES
Effort sponsored by the Air Force Office of Scientific Research, Air Force Materiel Command, USAF. The U. S. Government is authorized to reroduce and distribute reprints for Governmental purposes notwithstanding any copyright notation thereon.

14. ABSTRACT

Accurate modeling of nuclear cloud rise is critical in hazard prediction following a nuclear detonation. This thesis recommends improvements to the model currently used by DOD. It considers a single-term versus a three-term entrainment equation, the value of the entrainment and eddy viscous drag parameters, as well as the effect of wind shear in the cloud rise following a nuclear detonation. It examines departures from the 1979 version of the Department of Defense Land Fallout Interpretive Code (DELFIC) with the current code used in the Hazard Prediction and Assessment Capability (HPAC) code version 3.2.

The recommendation for a single-term entrainment equation, with constant value parameters, without wind shear corrections, and without cloud oscillations is based on both a statistical analysis using 67 U.S. nuclear atmospheric test shots and the physical representation of the modeling. The statistical analysis optimized the parameter values of interest for four cases: the three-term entrainment equation with wind shear and without wind shear as well as the single-term entrainment equation with and without wind shear. The thesis then examines the effect of cloud oscillations as a significant departure in the code. Modifications to user input atmospheric tables are identified as a potential problem in the calculation of stabilized cloud dimensions in HPAC.

15. SUBJECT TERMS
Nuclear Cloud Rise, Wind Shear, Entrainment, Eddy Viscous Drag, Hazard Prediction and Assessment Capability, HPAC, Nuclear Detonation Modeling, Department of Defense Land Fallout Interpretive Code, DELFIC

16. SECURITY CLASSIFICATION OF:			17. LIMITATION OF ABSTRACT	18. NUMBER OF PAGES	19a. NAME OF RESPONSIBLE PERSON
a. REPORT	b. ABSTRACT	c. THIS PAGE			MAJ Vincent J. Jodoin, ENP
U	U	U	UU	134	19b. TELEPHONE NUMBER *(Include area code)* (937) 255-3636, ext 4506

Standard Form 298 (Rev. 8-98)
Prescribed by ANSI Std. Z39-18

	Form Approved OMB No. 074-0188